

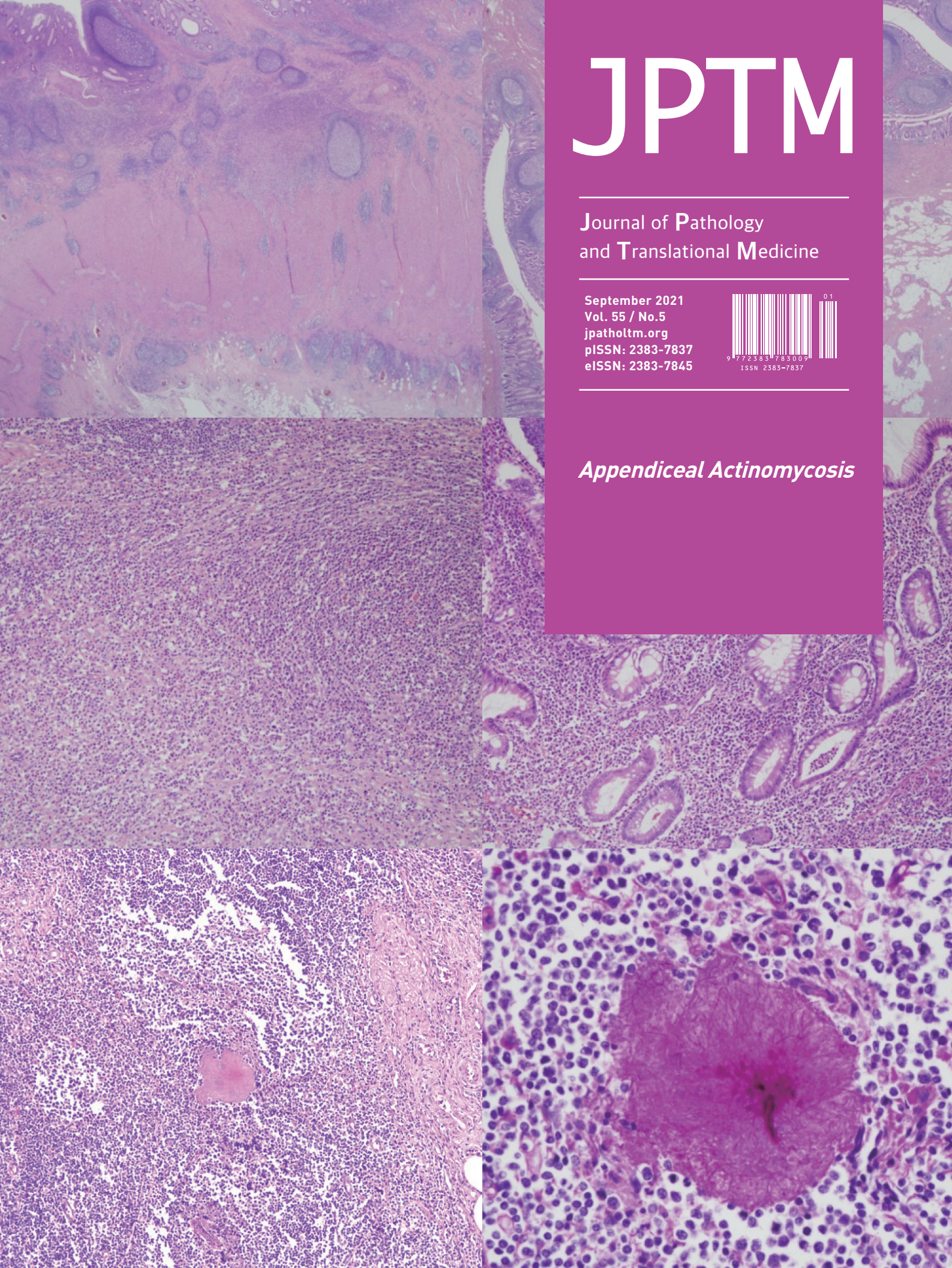
JPTM

Journal of Pathology
and Translational Medicine

September 2021
Vol. 55 / No.5
jpatholtm.org
pISSN: 2383-7837
eISSN: 2383-7845



Appendiceal Actinomycosis



Aims & Scope

The *Journal of Pathology and Translational Medicine* is an open venue for the rapid publication of major achievements in various fields of pathology, cytopathology, and biomedical and translational research. The Journal aims to share new insights into the molecular and cellular mechanisms of human diseases and to report major advances in both experimental and clinical medicine, with a particular emphasis on translational research. The investigations of human cells and tissues using high-dimensional biology techniques such as genomics and proteomics will be given a high priority. Articles on stem cell biology are also welcome. The categories of manuscript include original articles, review and perspective articles, case studies, brief case reports, and letters to the editor.

Subscription Information

To subscribe to this journal, please contact the Korean Society of Pathologists/the Korean Society for Cytopathology. Full text PDF files are also available at the official website (<https://jpatholtm.org>). *Journal of Pathology and Translational Medicine* is indexed by Emerging Sources Citation Index (ESCI), PubMed, PubMed Central, Scopus, KoreaMed, KoMCI, WPRIM, Directory of Open Access Journals (DOAJ), and CrossRef. Circulation number per issue is 50.

Editors-in-Chief

Jung, Chan Kwon, MD (*The Catholic University of Korea, Korea*) <https://orcid.org/0000-0001-6843-3708>

Park, So Yeon, MD (*Seoul National University, Korea*) <https://orcid.org/0000-0002-0299-7268>

Associate Editors

Shin, Eunah, MD (*Yongin Severance Hospital, Yonsei University, Korea*) <https://orcid.org/0000-0001-5961-3563>

Kim, Haeryoung, MD (*Seoul National University, Korea*) <https://orcid.org/0000-0002-4205-9081>

Bychkov, Andrey, MD (*Kameda Medical Center, Japan; Nagasaki University Hospital, Japan*) <https://orcid.org/0000-0002-4203-5696>

Editorial Board

Avila-Casado, Maria del Carmen, MD (*University of Toronto, Toronto General Hospital UHN, Canada*)

Bae, Young Kyung, MD (*Yeungnam University, Korea*)

Bongiovanni, Massimo, MD (*Lausanne University Hospital, Switzerland*)

Bova, G. Steven, MD (*University of Tampere, Finland*)

Choi, Joon Hyuk, MD (*Yeungnam University, Korea*)

Chong, Yo Sep, MD (*The Catholic University of Korea, Korea*)

Chung, Jin-Haeng, MD (*Seoul National University, Korea*)

Fadda, Guido, MD (*Catholic University of Rome-Foundation Agostino Gemelli University Hospital, Italy*)

Fukushima, Noriyoshi, MD (*Ichii Medical University, Japan*)

Go, Heunjeong, MD (*University of Ulsan, Korea*)

Hong, Soon Won, MD (*Yonsei University, Korea*)

Jain, Deepali, MD (*All India Institute of Medical Sciences, India*)

Kakudo, Kennichi, MD (*Izumi City General Hospital, Japan*)

Kim, Jang-Hee, MD (*Ajou University, Korea*)

Kim, Jung Ho, MD (*Seoul National University, Korea*)

Kim, Se Hoon, MD (*Yonsei University, Korea*)

Komuta, Mina, MD (*Keio University, Tokyo, Japan*)

Kwon, Ji Eun, MD (*Ajou University, Korea*)

Lai, Chiung-Ru, MD (*Taipei Veterans General Hospital, Taiwan*)

Lee, C. Soon, MD (*University of Western Sydney, Australia*)

Lee, Hye Seung, MD (*Seoul National University, Korea*)

Lee, Sung Hak (*The Catholic University, Korea*)

Liu, Zhiyan, MD (*Shanghai Jiao Tong University, China*)

Lkhagvadorj, Sayamaa, MD (*Mongolian National University of Medical Sciences, Mongolia*)

Moran, Cesar, MD (*MD Anderson Cancer Center, U.S.A.*)

Paik, Jin Ho, MD (*Seoul National University, Korea*)

Park, Jeong Hwan (*Seoul National University, Korea*)

Ro, Jae Y., MD (*Cornell University, The Methodist Hospital, U.S.A.*)

Sakhuja, Puja, MD (*Govind Ballabh Pant Hospital, India*)

Shahid, Pervez, MD (*Agu Khan University, Pakistan*)

Song, Joon Seon, MD (*University of Ulsan, Korea*)

Tan, Puay Hoon, MD (*National University of Singapore, Singapore*)

Than, Nandor Gabor, MD (*Semmelweis University, Hungary*)

Tse, Gary M., MD (*The Chinese University of Hong Kong, Hong Kong*)

Yatabe, Yasushi, MD (*Aichi Cancer Center, Japan*)

Zhu, Yun, MD (*Jiangsu Institution of Nuclear Medicine, China*)

Ethic Editor

Choi, In-Hong, MD (*Yonsei University, Korea*)

Huh, Sun, MD (*Hallym University, Korea*)

Statistics Editors

Kim, Dong Wook (*National Health Insurance Service Ilsan Hospital, Korea*)

Lee, Hye Sun (*Yonsei University, Korea*)

Manuscript Editor

Chang, Soo-Hee (*InfoLumi Co., Korea*)

Layout Editor

Kim, Haeja (*iMiS Company Co., Ltd., Korea*)

Website and JATS XML File Producers

Cho, Yoosang (*M2Community Co., Korea*)

Im, Jeonghee (*M2Community Co., Korea*)

Administrative Assistants

Jung, Ji Young (*The Korean Society of Pathologists*)

Jeon, Anmi (*The Korean Society for Cytopathology*)

Contact the Korean Society of Pathologists/the Korean Society for Cytopathology

Publishers: Cho, Nam Hoon, MD, Gong, Gyungyub, MD

Editors-in-Chief: Jung, Chan Kwon, MD, Park, So Yeon, MD

Published by the Korean Society of Pathologists/the Korean Society for Cytopathology

Editorial Office

Room 1209 Gwanghwamun Officia, 92 Saemunan-ro, Jongno-gu, Seoul 03186, Korea

Tel: +82-2-795-3094 Fax: +82-2-790-6635 E-mail: office@jpatholtm.org

#1508 Renaissancetower, 14 Mallijae-ro, Mapo-gu, Seoul 04195, Korea

Tel: +82-2-593-6943 Fax: +82-2-593-6944 E-mail: office@jpatholtm.org

Printed by iMiS Company Co., Ltd. (JMC)

Jungang Bldg. 18-8 Wonhyo-ro 89-gil, Yongsan-gu, Seoul 04314, Korea

Tel: +82-2-717-5511 Fax: +82-2-717-5515 E-mail: ml@smileml.com

Manuscript Editing by InfoLumi Co.

210-202, 421 Pangyo-ro, Bundang-gu, Seongnam 13522, Korea

Tel: +82-70-8839-8800 E-mail: infolumi.chang@gmail.com

Front cover image: Representative histologic features of appendiceal actinomycosis (p351).

© Copyright 2021 by the Korean Society of Pathologists/the Korean Society for Cytopathology

© Journal of Pathology and Translational Medicine is an Open Access journal under the terms of the Creative Commons Attribution Non-Commercial License (<https://creativecommons.org/licenses/by-nc/4.0>).

© This paper meets the requirements of KS X ISO 9706, ISO 9706-1994 and ANSI/NISO Z.39.48-1992 (Permanence of Paper).

CONTENTS

ORIGINAL ARTICLES

- 307 SMARCA4/BRG1 protein-deficient thoracic tumors dictate re-examination of small biopsy reporting in non-small cell lung cancer
Anurag Mehta, Divya Bansal, Rupal Tripathi, Ankush Jajodia
- 317 Proto-oncogene *Pokemon* in thyroid cancer: a potential promoter of tumorigenesis in papillary thyroid carcinoma
Kyungseek Chang, Sung-Im Do, Kyungeun Kim, Seoung Wan Chae, In-gu Do, Hyun Joo Lee, Dong Hoon Kim, Jin Hee Sohn
- 324 Robust home brew fragment sizing assay for detection of *MET* exon 14 skipping mutation in non-small cell lung cancer patients in resource constrained community hospitals
Anurag Mehta, Shrinidhi Nathany, Aanchal Chopra, Sakshi Mattoo, Dushyant Kumar, Manoj Kumar Panigrahi
- 330 Upward trend in follicular lymphoma among the Korean population: 10-year experience at a large tertiary institution
Meejeong Kim, Hee Sang Hwang, Hyungwoo Cho, Dok Hyun Yoon, Cheolwon Suh, Chan Sik Park, Heounjeong Go, Jooryung Huh
- 338 Prognostic significance of viable tumor size measurement in hepatocellular carcinomas after preoperative locoregional treatment
Yoon Jung Hwang, Youngeun Lee, Hyunjin Park, Yangkyu Lee, Kyoungbun Lee, Haeryoung Kim

CASE REPORTS

- 349 Appendiceal actinomycosis mimicking appendiceal tumor, appendicitis or inflammatory bowel disease
You-Na Sung, Jihun Kim
- 355 Primary hepatic mixed germ cell tumor in an adult
Hyun-Jung Sung, Jihun Kim, Kyu-rae Kim, Shinkyu Yoon, Jae Hoon Lee, Hyo Jeong Kang
- 360 Metastatic leiomyosarcoma of the thyroid gland: cytologic findings and differential diagnosis
Jiyeon Lee, Yunjoo Cho, Kyue Hee Choi, Inwoo Hwang, Young Lyun Oh

NEWSLETTER

366 What's new in gynecologic pathology 2021: ovary and fallopian tube
Gulisa Turashvili, Ricardo Lastra

Instructions for Authors for *Journal of Pathology and Translational Medicine* are available at <http://jpatholm.org/authors/authors.php>

SMARCA4/BRG1 protein-deficient thoracic tumors dictate re-examination of small biopsy reporting in non-small cell lung cancer

Anurag Mehta¹, Divya Bansal², Rupal Tripathi³, Ankush Jajodia⁴

¹Department of Laboratory, Molecular and Transfusion Services, Rajiv Gandhi Cancer Institute and Research Centre (RGCIRC), New Delhi; Departments of ²Pathology, ³Research, and ⁴Radiology, Rajiv Gandhi Cancer Institute and Research Centre (RGCIRC), New Delhi, India

Background: SMARCA4/BRG1 protein-deficient lung adenocarcinomas and thoracic sarcoma are recently described entities that lack distinctive histological features, transcription termination factor 1 (TTF1) reactivity, and actionable driver mutations. The current diagnostic path for small lung biopsies as recommended by the World Health Organization (WHO, 2015) is likely to categorize these as non-small cell carcinoma-not otherwise specified (NSCC-NOS). The present study attempts to define the subtle but distinctive clinicopathologic features of SMARCA4/BRG1 protein-deficient thoracic tumors; highlight their unique biology; and addresses the unmet need to segregate these using a new, tissue-proficient diagnostic pathway. **Methods:** All lung biopsies and those from metastatic sites in patients with suspected advanced lung cancer and classified as NSCC-NOS as per WHO (2015) guidelines were subjected to BRG1 testing by immunohistochemistry. SMARCA4/BRG1 protein-deficient thoracic tumors were evaluated by an extended immunohistochemistry panel. Predictive biomarker and programmed death-ligand 1 testing was conducted in all cases. **Results:** Of 110 cases, nine were found to be SMARCA4/BRG1 protein-deficient; six were identified as SMARCA4/BRG1 protein-deficient lung adenocarcinomas, and three were SMARCA4/BRG1 protein-deficient thoracic sarcomas. The histology ranged from poorly differentiated to undifferentiated to rhabdoid. None of the cases showed significant expression of TTF1 or p40, and no actionable mutation was identified. **Conclusions:** It is difficult to separate BRG1-deficient lung adenocarcinomas and thoracic sarcomas based on morphology alone. We propose a diagnostic pathway for small biopsies of thoracic tumors to segregate these distinct entities so that they can be studied more efficaciously for new biomarkers and therapeutic options.

Key Words: Adenocarcinoma; BRG1 protein; Lung; Non-small cell lung carcinoma; SMARCA4

Received: February 8, 2021 **Revised:** May 6, 2021 **Accepted:** May 10, 2021

Corresponding Author: Divya Bansal, MD, Department of Pathology, Rajiv Gandhi Cancer Institute and Research Centre (RGCIRC), New Delhi 110085, India
 Tel: +91-9971869669, Fax: +91-11-27051037, E-mail: divyabansalrgci@gmail.com

Switch/Sucrose non-fermenter (SWI/SNF) multiprotein complex is an ATP-dependent chromatin remodeling factor. One important and core constituent of this multiprotein complex is the brahma related gene 1 (BRG1) protein encoded by the *SMARCA4* gene. The SMARCA4/BRG1 protein hydrolyzes ATP and provides energy for unspooling DNA from the histone octamer, allowing transcription to proceed [1-3]. The chromatin remodeling complex also plays an essential role in maintenance of stemness [4]. The pathogenesis and dedifferentiation of neoplasms in various organs are linked increasingly to chromatin remodeling by the SWI/SNF complex [5-7].

SMARCA4-inactivating mutations and consequent loss of functional SMARCA4/BRG1 protein are observed in many tu-

mor types [6-8] and are observed in 8.43% of non-small cell lung cancers (NSCLC) [9-12]. Furthermore, SMARCA4/BRG1 protein-deficient thoracic sarcoma (SD-TS) is also recognized more frequently, primarily due to rising awareness of its existence [13-15]. There is uncertainty as to whether the histogenesis of SD-TS represents undifferentiated/dedifferentiated carcinomas or de novo genesis [16,17]. Overlapping histomorphology of SMARCA4/BRG1 protein-deficient lung adenocarcinoma (SD-LUAD), SD-TS, and other lung adenocarcinomas necessitates more exhaustive immunophenotyping than allowed with the current diagnostic pathway for small lung biopsy [18]. SMARCA4/BRG1 protein-deficient thoracic tumors (SD-TT) constitute a significant percentage of thoracic malignancies with rea-

sonable fear of being inappropriately classified as non-small cell carcinoma—not otherwise specified (NSCC-NOS) and subjected to molecular testing. SD-TT are devoid of actionable molecular targets and need to be distinguished and studied separately to determine the best standard of care for these highly aggressive and rapidly lethal tumors and to save resources on unjustifiable predictive biomarker testing for NSCC-NOS. Moreover, SD-LUAD and SD-TS must be separated properly to retain histogenetic fidelity and to develop suitable therapeutic modalities.

Here, we describe a series of SD-TT and share a new diagnostic pathway to effectively segregate this distinct subset with proficient use of biopsied tissue and immunohistochemistry (IHC).

MATERIALS AND METHODS

Study place and study duration

The present study is an analysis of nine cases of SD-TT diagnosed at Rajiv Gandhi Cancer Institute and Research Center, New Delhi, from 1 September 2020 to 15 January 2021. Clinicoradiological details were obtained from the electronic medical records (EMR), and follow-up information was gathered either through EMR or via telephone.

Study population

The current World Health Organization (WHO) guidelines do not advocate extensive immunophenotyping beyond transcription termination factor 1 (TTF1) and p40 for classifying small biopsy specimens from suspected lung cancers and classify lung carcinomas as NSCC-NOS in the absence of both TTF1 and p40 [18]. SD-TT have been shown to be confined largely to TTF1-negative/low expression NSCC [10,11,19]. We reaffirmed these findings using two tissue microarrays of 25 samples of TTF1-negative and TTF1-positive NSCC subjected to BRG1 IHC testing. None of the TTF1-positive (moderate to strong nuclear expression) NSCCs showed loss of BRG1 expression, while eight of 25 cases of TTF1-negative NSCC showed loss of BRG1 expression. With similar findings noted in the literature, we applied additional IHC for BRG1 expression for this subset of lung cancers to identify SD-TT starting in September 2020. Nine such cases were identified to be BRG1 deficient. Of these, eight were newly diagnosed, and one (case number 4) underwent repeat biopsy for programmed death–ligand 1 (PD-L1) tumor proportion scoring after failure of multiple lines of cytotoxic therapy.

Immunohistochemistry

All lung biopsies and those from metastatic sites in patients with suspected advanced lung cancers were classified per WHO (2015) guidelines [18] into NSCC-Adenocarcinoma (Ad Ca)/favor adenocarcinoma, NSCC–squamous cell carcinoma (SCC)/favor SCC, and NSCC-NOS using only p40 (clone BC28, ready-to-use [RTU], Zytomed Systems, Berlin, Germany) and TTF1 (clone-SP141, RTU, Ventana, Tucson, AZ, USA) IHC. Those classified as NSCC-NOS were tested for expression of SMARCA4/BRG1 protein (1:100, EPNCIR111A, Abcam, Cambridge, UK). Cases with loss of BRG1 protein were classified as SD-TT and further evaluated using an extended IHC panel of panCK (1:200, AE1, AE3, 5D3, Zytomed), cytokeratin 7 (CK7; 1:200, OV-TL 12/30, Thermo Fisher Scientific, Waltham, MA, USA), epithelial membrane antigen (EMA; 1:50, E29, Dako, Santa Clara, CA, USA), Hep Par 1 (OCHIE5, RTU, PathnSitu, Pleasanton, CA, USA), SALL4 (EP299, RTU, PathnSitu), SOX2 (1:100, SP76, Cell Marque, Darmstadt, Germany), CD34 (QBEnd10, RTU, Dako), synaptophysin (1:100, MRQ-40, Cell Marque), SMARCB1/INI1 (MRQ-27, RTU, Cell Marque), and E-cadherin (NCH-38, 1:100, Dako). Tissues were formalin-fixed, paraffin-embedded, sectioned to 4 µm thickness, and then fixed for 6–48 hours in neutral buffered formalin before conventional tissue processing and staining by IHC. Antigen retrieval at alkaline pH of 8.6 in Tris-EDTA buffer and further staining steps were performed on an automated IHC staining instrument (Benchmark XT, Ventana Medical Systems, Inc. [F. Hoffmann-La Roche Ltd.]). The chromogenic signal was generated using the Ventana UltraView universal 3,3'-diaminobenzidine (DAB) detection kit (Ventana Medical Systems, Inc. [F. Hoffmann-La Roche Ltd.]). All IHC stains were applied with appropriate positive controls. For IHC analysis, moderate to strong staining intensity in > 5% of tumor cells with nuclear (TTF-1, p40, SOX2, and SALL4), cytoplasmic (panCK, CK7, CD34, Hep Par 1, and synaptophysin), or membranous (EMA and E-cadherin) pattern was considered positive. BRG1 immunostaining that exhibited a null phenotype in tumor cells with strong nuclear staining in the stromal fibroblasts as well as the endothelial and inflammatory cells was deemed as lost and defined the SD-TT cohort.

Anaplastic lymphoma kinase 1 (ALK-1) protein expression was assessed using a U.S. Food and Drug Administration (FDA)–approved IHC assay employing anti-ALK (D5F3) rabbit monoclonal primary antibody with other proprietary components of the Ventana ALK assay on the Ventana Benchmark XT Autostainer (using the Ventana Optiview DAB and amplification kit).

PD-L1 expression testing was performed using rabbit Anti-Human PD-L1 monoclonal antibody (clone SP263) on the Ventana Benchmark XT, and partial or complete membranous expression of any intensity in $\geq 1\%$ of tumor cells was considered significant.

DNA extraction and polymerase chain reaction

A predictive biomarker search was performed for epidermal growth factor receptor (EGFR) using the Qiagen EGFR Therascreen RGQ polymerase chain reaction (PCR) kit, an FDA-approved amplification refractory mutation system. Five sections of 4 μM each were collected in Eppendorf tubes by manual macrodissection to enrich tumor fraction wherever necessary. DNA was extracted using the Qiagen DNeasy blood and tissue kit (Hilden, Germany). The DNA was quality checked on the Qubit fluorometer. Multiplexed reverse transcription PCR was carried out on a ROTORGENE thermal cycler (Qiagen) in eight tubes along with positive and no template controls. Interpretation was conducted per the manufacturer's instructions.

Fluorescence in situ hybridization

Fluorescence in situ hybridization (FISH) analysis was performed on 4 μM formalin-fixed and paraffin-embedded tissue sections following a standardized protocol that included pretreatment (dewax/proteolysis), denaturation, probe application, and hybridization; application of 4',6-diamidino-2-phenylindole (DAPI)/antifade solution; and analysis of slides using Leica fluorescent microscopy (DM6000B). *ROS1* (ROS proto-oncogene 1, receptor tyrosine kinase) rearrangement was tested by FISH using a dual-color break-apart probe (ZytoLight Spec ROS1, ZytoVision, Germany) as previously described [20].

One case (case No. 1) was subjected to a targeted panel for multigene profiling using the OncoPrint focus assay on the Ion

Torrent Personal Genome Machine (Ion PGM, Thermo Fisher Scientific). Reaffirmation of the next-generation sequencing findings for copy number gain used FISH for *c-MYC*. The XL MYC BA spectral orange-labeled probe hybridizing proximal to the MYC gene region at 8q24.21 and a green-labeled probe hybridizing distal to the MYC gene region at 8q24.21 were applied (Metasystems Probes GmbH, Altlußheim, Germany). No centromeric probe was used. The number of *c-MYC* signals per cell was counted in 100 tumor cells and averaged. *c-MYC* copy number gain was defined as average copy number ≥ 3.0 .

RESULTS

Clinical findings

A total of 110 cases of thoracic tumors was identified during this period, of which nine (8.1%) were found to be *SMARCA4* deficient. Six cases (case Nos. 1–6) were SD-LUAD, and three (case Nos. 7–9) were SD-TS. Patient age ranged from 45–73 years, with a male to female ratio of 3.5:1. All cases of SD-LUAD had history of smoking, lung mass, bulky lymphadenopathy, and bony involvement. All cases of SD-TS had a significant history of smoking; two (case No. 7, case No. 9) had massive lung disease (Fig. 1A), while one had mediastinal disease (case No. 8) (Fig. 1B). All cases of SD-TS also had bulky lymphadenopathy. However, no bony involvement was noted in any SD-TS patients. The clinical features of SD-TT are summarized in Table 1.

Pathological findings in SD-LUAD

The histopathologic characteristics of SD-LUAD are summarized in Table 2 (case Nos. 1–6) and shown in Fig. 2A–D. All six cases of SD-LUAD had a solid pattern of growth in the biopsied material, while case No. 2 also showed a vague acinar pattern focally. One case (case No. 2) had an Indian file pattern of

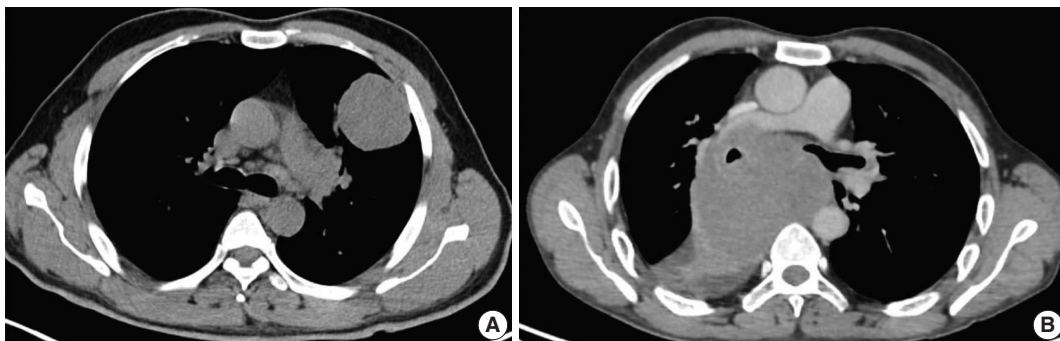


Fig. 1. Axial computed tomography images of *SMARCA4/BRG1* protein-deficient thoracic sarcoma (SD-TS). (A) Case No. 7 showed well defined intra-pulmonary mass on the left side, abutting the pleural margin. (B) Case No. 8 showed a well defined heterogeneously enhancing mediastinal-based mass splaying the carina and abutting the right pulmonary artery, encasing the right main bronchus without invasion.

Table 1. Clinical features of SMARCA4/BRG1 protein-deficient thoracic tumors

Case No.	Age/Sex	Smoking	Biopsy site	Metastasis	TNM stage	Radiological findings	Treatment	Present status
1	67/M	Present	Cervical lymph node	Present	IV	Bilateral lung nodules, mediastinal and cervical lymph nodes, skeletal and adrenal metastasis	Supportive care	Died, 7 days
2	47/M	Present	Pleura	Present	IV	Pleura based mass, supraclavicular LAP, rib and vertebral body	Supportive care	Died, 15 days
3	65/F	Present	Left upper lobe lung	Present	IV	Left lung mass, pleural effusion, mediastinal LAP, multiple bones	1st cycle of platinum doublet	Alive
4	45/M	Present	Left upper lobe lung (second biopsy after treatment failure)	Present	IV	Centrally non-enhancing lung mass (necrotic), mediastinal LAP, vertebral body	Multiple lines of chemotherapy	Died a month after 2nd biopsy (OS, 23 mo)
5	73/F	Present	Right iliac blade	Present	IV	Left lung mass, mediastinal LAP, multiple bone, brain and liver metastasis	Supportive care	Died, 15 days
6	66/M	Present	Left scapular soft tissue deposit	Present	IV	Right lung mass, mediastinal and cervical LAP, skeletal, adrenal	1st cycle of Platinum doublet	Alive
7	49/M	Present	Left upper lobe lung	Absent	IIIC	Left lung mass, mediastinal LAP, supraclavicular LN	Platinum doublet at another centre	Alive
8	46/M	Present	Right parahilar region	Present	IV	Right mediastinal mass, pleural effusion and mediastinal LAP	Platinum doublet at another centre	Alive
9	60/M	Present	Right supraclavicular LN	Absent	IIIC	Right lung mass mediastinal LAP, supraclavicular LN	Platinum doublet at another centre	Alive

M, male; LAP, lymphadenopathy; F, female; OS, overall survival; LN, lymph node.

growth that resembled lobular carcinoma of breast (Fig. 2C); however, E-cadherin expression was intact, and none of the IHC markers for breast cancer (GATA3, estrogen receptor, and progesterone receptor) were positive. Case Nos. 4 and 6 showed multicell trabecular patterns (3–4 cell layer thick) reminiscent of hepatocellular carcinoma. All tumors were characterized by large constituent cells possessing eosinophilic to clear cytoplasm (Fig. 2A, B). Scattered populations of rhabdoid cells were seen in two cases (case Nos. 3 and 5) (Fig. 2D). Four cases (case Nos. 1, 2, 4, and 6) exhibited scattered cells with blue intracytoplasmic mucin, which were mucicarmine positive (Fig. 2E).

The cytoplasmic margins of large polygonal cells were sharp and mimicked squamous morphology. The nuclei were large and irregularly contoured with cloudy chromatin. The rhabdoid population of tumor cells showed well-described, eccentric nuclei with prominent eosinophilic nucleoli and a cytoplasmic globule filled with hyaline content (Fig. 2D). Mitosis was intense. Apoptosis and wide swaths of necrosis were common. All our cases revealed inflamed stroma rich in lymphocytes and neutrophils (Fig. 2D). Neutrophilic emperipolesis was observed in three cases (Table 2).

The IHC profile of SD-LUAD is summarized in Table 3 and shown in Fig. 2F–L. Cases Nos. 1, 2, 4, and 6 exhibited diffuse positivity for CK, CK7, and BerEp4 (Fig. 2F–H) and variably intense positivity for Hep Par 1 (Fig. 2I), but none of the cases was positive for SOX2, CD34, or SALL4. Diffuse positivity for

CK7 and BerEp4 was consistent with adenocarcinoma appellation. Case Nos. 3 and 5 had strong CK and Hep Par 1 positivity along with focal positivity for two of three markers of stemness (SOX2, CD34, and SALL4), while both of them were negative for CK7 and BerEp4. Cases that showed focal expression of markers of stemness also had focal rhabdoid morphology.

Pathological findings in SD-TS

The histopathologic characteristics of SD-TS are summarized in Table 2 (case Nos. 7–9) and shown in Fig. 3A–F. All three cases had a solid pattern of growth with pure rhabdoid morphology seen in two cases (case Nos. 7 and 9) (Fig. 3D–F). One case (case No. 8) had morphology similar to the features described in SD-LUAD (Fig. 3A–C). None of these cases showed areas of spindling, myxoid change, or any other feature that raised suspicion of sarcomatous histogenesis. Additional features noted in SD-LUAD such as inflamed stroma, neutrophilic emperipolesis, necrosis, brisk mitoses, and apoptosis were seen in these tumors (Table 2, Fig. 3D, E). On IHC, all cases had weak focal positivity for CK (Fig. 4A); two cases exhibited focal expression of CK7 (case Nos. 7 and 8) (Fig. 4B, C), and one case (case No. 9) showed weak focal expression for EMA. Hep Par 1 (Fig. 4D) and synaptophysin (Fig. 4H) were focally expressed in case No. 7, and p40 was focally expressed in case No. 8. Case Nos. 7 and 8 showed diffuse positivity for stem cell markers SALL4, SOX2, and CD34 (Fig. 4E–G) along with BRG1 loss (Fig. 4I), while case No. 9 had

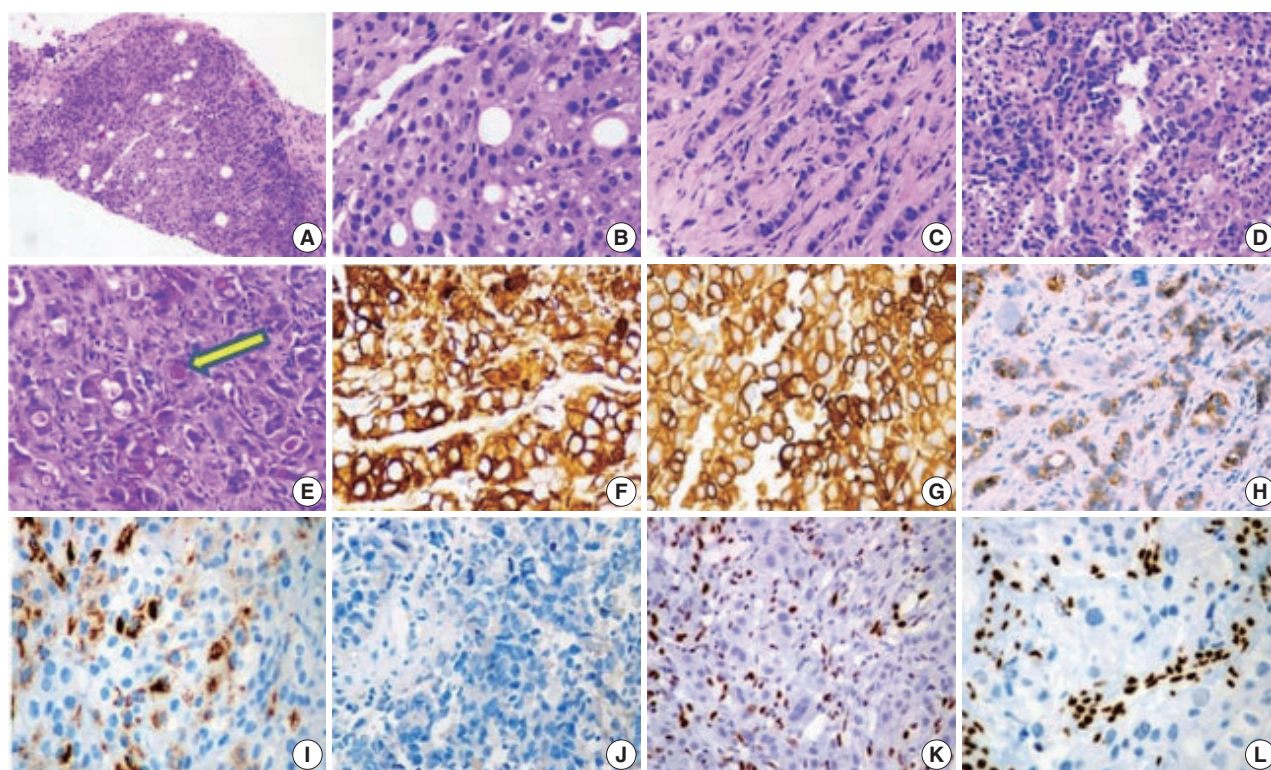


Fig. 2. Histology and immunohistochemistry images of SMARCA4/BRG1 protein-deficient lung adenocarcinoma (SD-LUAD). (A) Scanner view of SD-LUAD. Note the solid pattern of growth with a sieved appearance. (B) The dry high-power view exhibits large cells with sharp margins and scattered large signet ring cells that are regularly observed in this tumor type. Also note the bubbly cytoplasm of many cells with indented nuclei. (C) The second case of SD-LUAD exhibited tumor cells arranged in an Indian file pattern. (D) The third case of SD-LUAD showed with highly inflamed background and a solid growth pattern comprised of large rhabdoid cells. (E) Tumor cells showed intracytoplasmic mucin (arrow) highlighted by mucicarmine. (F, G) Tumor cells showed strong cytokeratin (CK) and CK7 immunoreactivity, respectively. (H) SD-LUAD expressed BerEp4, supporting the adenocarcinomatous histogenesis. (I) All SD-LUAD expressed varying degrees of Hep Par 1. (J) Transcription termination factor 1 was universally absent. (K, L) No SD-LUAD exhibited BRG1 nuclear expression. Note the strong nuclear reactivity for BRG1 in the inflammatory cells.

focal CD34 positivity in combination with BRG1 loss. SMARCB1/INI1 was intact in all cases. Table 3 and Fig. 4 show the IHC of SD-TS.

Molecular analysis

On molecular analysis, no actionable mutation in *EGFR*, *ALK-1*, or *ROS1* gene was identified in SD-TT (Table 3). The targeted panel for biomarker detection in case No. 1 showed a copy number gain of *c-MYC* gene to 7.46 against the normal ploidy of 2, which was confirmed by FISH (copy number gain of 8.2 signals per cell). Significant PD-L1 ($\geq 1\%$) expression was seen in two cases (case Nos. 4 and 6) (Table 3).

Clinical outcome

Follow-up information was available for all cases of SD-LUAD (Table 1). Three cases of SD-LUAD (case Nos. 1, 2, and 5) were on supportive care and died within two weeks of diagnosis. One

case (case No. 4), which was reclassified as SD-LUAD and had received multiple lines of chemotherapy, died 23 months after initial diagnosis and within one month of repeat biopsy. All cases of SD-TS opted for further treatment in their respective cities and are alive, as learned telephonically. The duration of observation in this subgroup was 3–4 months, but the status of objective response and nature of therapy are not known.

DISCUSSION

Mammalian SWI/SNF chromatin remodeling is dependent on ATPase activity that resides in BRG1 or its ortholog brahma [1,3,4]. Two thoracic tumors are caused by somatic loss of heterozygosity resulting from biallelic loss of *SMARCA4*, namely SD-LUAD and SD-TS. The existing literature on these tumors has brought greater awareness about clinicopathologic characteristics, prognosis, and therapeutic consequences [10-17].

Table 2. Histopathological profile of SMARCA4/BRG1 protein-deficient thoracic tumors

Case No.	Architectural pattern	Cell type	Cytoplasm	Nuclear features	Stroma	Emperipolesis	Necrosis	Mitoses (/10 hpf)
1	Diffuse with sieve like appearance	Large polygonal with scattered clear cells	Eosinophilic with mucin	Cloudy chromatin	Inflamed	Present	Present, extensive	24
2	Indian file pattern mimicking lobular carcinoma breast with few nests and tubules	Large polygonal with scattered clear cells	Eosinophilic with mucin	Fragile looking chromatin with indented nuclei	Desmoplasia with moderate inflammation	Absent	Focal	12
3	Solid	Large polygonal with scattered clear cells scattered rhabdoid cells	Eosinophilic with globular inclusions	Indented nuclei, and prominent eosinophilic nucleoli	Inflamed	Absent	Present	>50
4	Solid, trabecular	Large polygonal with scattered clear cells	Eosinophilic with mucin	Cloudy chromatin	Inflamed	Present	Present, extensive	30
5	Solid	Large polygonal with scattered clear cells, scattered rhabdoid cells	Eosinophilic with globular inclusions	Fragile looking chromatin with indented nuclei	Inflamed	Present	Present, extensive	30
6	Solid, trabecular	Large polygonal with scattered clear cells	Eosinophilic with mucin	Cloudy chromatin	Desmoplasia with mild inflammation	Absent	Focal	15
7	Solid	Pure rhabdoid	Globular inclusions	Cloudy chromatin	Markedly inflamed	Present	Absent	30
8	Solid	Large polygonal with scattered clear cells	Eosinophilic with globular inclusions	Fragile looking chromatin with indented nuclei	Inflamed	Absent	Present, extensive	>50
9	Solid	Pure rhabdoid	Globular inclusions	Cloudy chromatin	Inflamed	Absent	Present, extensive	>50

hpf, high-power field.

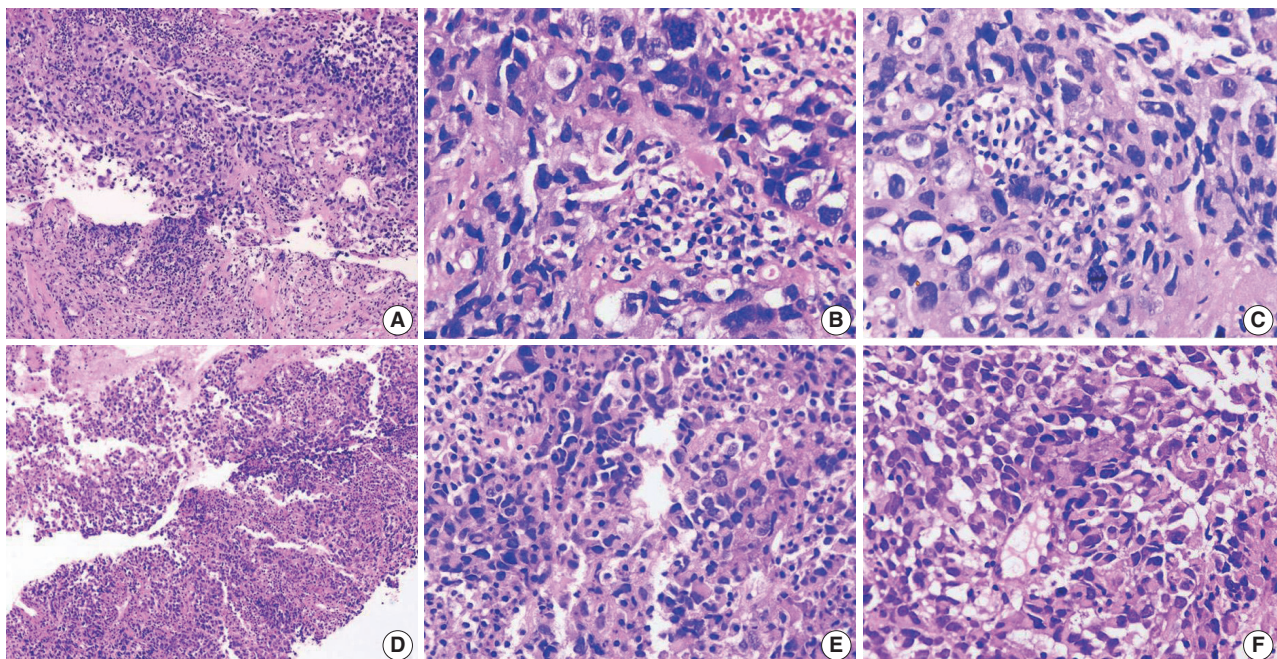


Fig. 3. Histology images of cases. (A–C) Case No. 8 of SMARCA4/BRG1 protein-deficient thoracic sarcoma (SD-TS) showed a diffuse growth pattern. The constituent cells are large, and some have clear cytoplasm. Nuclei are irregular. (D, E) The stroma is inflamed in SD-TS. (E, F) Two cases (cases No. 7 and 9) revealed tumors with diffuse growth but obvious rhabdoid morphology of spheroidal cytoplasm, eccentric nuclei, and globoid inclusions.

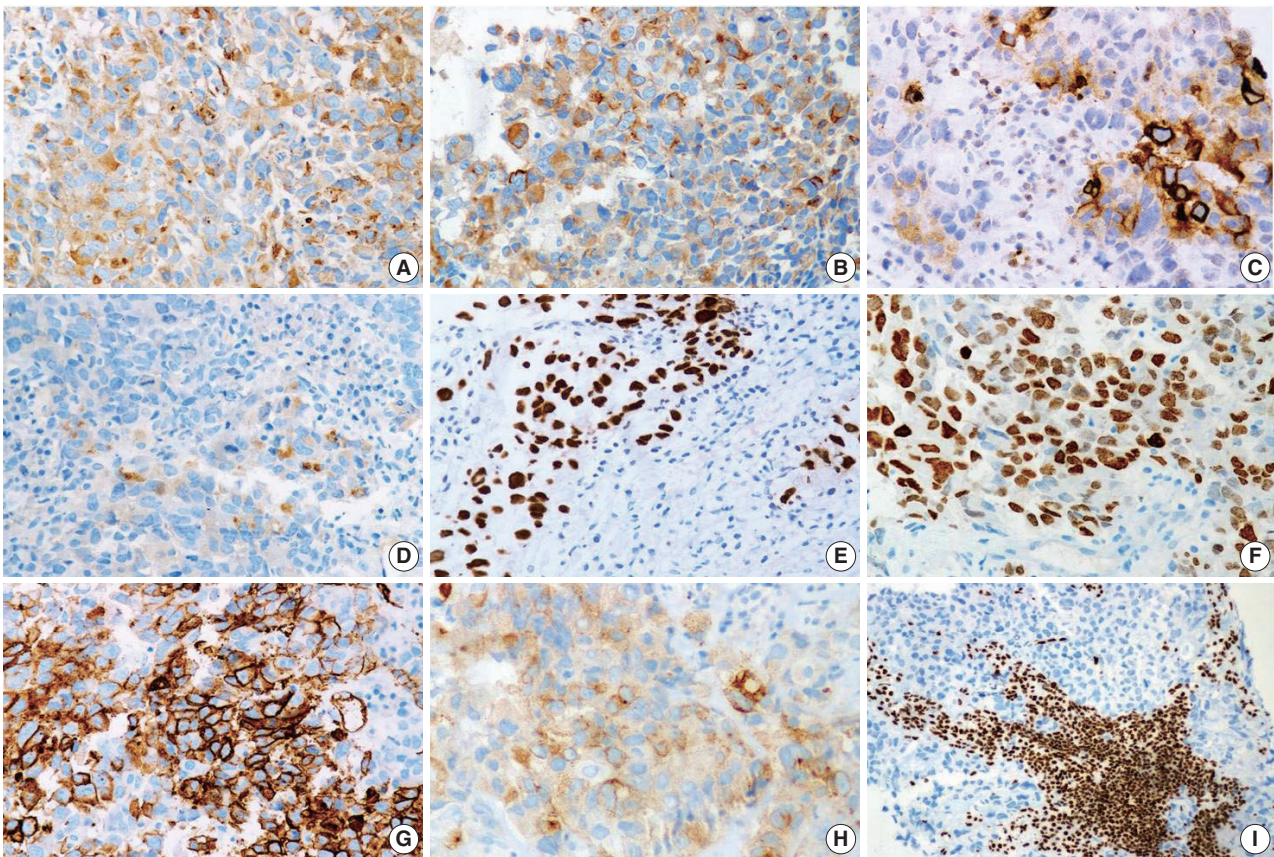


Fig. 4. Immunophenotype of SMARCA4/BRG1 protein-deficient thoracic sarcoma (SD-TS). (A) Weak expression of pan-cytokeratin (CK) was observed in all cases of SD-TS. (B) Weak CK7 immunoreactivity was noted in case No. 7. (C) Focal strong CK7 staining is seen in case No. 8. (D) Case No. 7 expressed weak and focal Hep Par 1. (E–G) Expression of stemness markers of SALL4, SOX2, and CD34, respectively. (H) Expression of synaptophysin in case No. 7 of SD-TS. (I) Lack of nuclear expression of BRG1 defining BRG1 loss. Note the intense staining of stromal and inflammatory cells.

Table 3. Ancillary testing results of SMARCA4/BRG1 protein-deficient thoracic tumors

Case No.	CK	CK7	EMA	TTF1	Hep Par 1	SALL4	SOX2	CD34	p40	BRG1	Status of predictive biomarker (EGFR, ALK-1, ROS1)	PD-L1 membranous expression (% positivity in tumor cells and intensity)
1	Pos	Pos	Pos	Neg	Pos	Neg	Neg	Neg	Neg	Loss	Negative c-MYC-copy number gain 7.46	<1
2	Pos	Pos	Pos	Neg	Pos	Neg	Neg	Neg	Neg	Loss	Negative	<1
3	Pos	Neg	Focal Pos	Neg	Pos	Neg	Pos	Focal Pos	Neg	Loss	Negative	<1
4	Pos	Pos	Pos	Neg	Pos	Neg	Neg	Neg	Neg	Loss	Negative	60
5	Pos	Neg	Focal Pos	Neg	Pos	Neg	Focal Pos	Pos	Neg	Loss	Negative	<1
6	Pos	Pos	Pos	Neg	Pos	Neg	Neg	Neg	Neg	Loss	Negative	70
7	Weak, focal Pos	Weak, focal Pos	Neg	Neg	Focal Pos	Pos	Pos	Pos	Neg	Loss	Negative	<1
8	Weak, focal Pos	Strong, focal Pos	Neg	Neg	Neg	Pos	Pos	Pos	Focal Pos	Loss	Negative	<1
9	Weak, focal Pos	Neg	Weak, focal Pos	Neg	Neg	Neg	Neg	Focal Pos	Neg	Loss	Negative	<1

CK, cytokeratin; EMA, epithelial membrane antigen; TTF1, transcription termination factor 1; EGFR, epidermal growth factor receptor; ALK-1, anaplastic lymphoma kinase 1; PD-L1, programmed death-ligand 1; Pos, positive; Neg, negative.

In a recently published, large series on SD-TT, the majority of cases was male, chronic smokers, and ranged in age from 30–80 years (mean, 58 years). Most had large thoracic mass with bulky lymphadenopathy, and nearly all patients had stage IV disease with bone metastasis [17]. Seven of our nine cases of SD-TT were also male, middle aged to elderly, and chronic smokers. Similarly, all our SD-LUAD cases had significant lung mass and stage IV disease with bony metastasis. A surprising observation in our cohort was lack of bone metastasis in SD-TS, whereas all cases of SD-LUAD had extensive bone involvement. This observation contradicts the dedifferentiation hypothesis [14,16] for emergence of SD-TS from SD-LUAD, though weak expression of epithelial markers in SD-TS and stem cell markers in SD-LUAD suggest the possibility of transition from SD-LUAD to SD-TS.

Morphological patterns of SD-LUAD have been recognized, from less common, well-differentiated to more common, poorly-differentiated malignant tumors [11]. All our cases had a predominant solid growth pattern with scattered clear to signet ring cells and inflamed stroma, similar to the findings seen in other studies [11,12]. Scattered cells with intracytoplasmic mucin were noted in four of six cases. This observation replicates the findings of Agaimy et al. [11]. Two cases with trabecular pattern of TTF1 negativity and Hep Par 1 expression, could easily be misinterpreted as hepatoid adenocarcinomas or hepatocellular carcinomas without BRG1 testing. We contend that all cases of malignancy of unknown origin (MUO) with hepatoid immunophenotype be tested for lack of BRG1 expression to correctly diagnose SD-TT. However, the aberrant expression of Hep Par 1 has not been explained well in the existing literature and is possibly a result of extensive chromatin remodeling associated with *SMARCA4* loss. SD-LUAD tumors were negative for p40, TTF1, Napsin A, neuroendocrine markers, and CK5/6 but expressed CK7 in four of the six cases and Hep Par 1 and EMA in all cases, which was in line with observation from other studies [10–12]. Two cases of SD-LUAD (case Nos. 3 and 5) with scattered rhabdoid cells, despite showing diffuse positivity for CK, were negative for CK7 and had weak and focal Hep Par 1 expression and weak SOX2 and CD34, which placed them between SD-LUAD and SD-TS. These cases represent a possible transition toward SD-TS and support the concept of a biologic continuum between these tumors [17,19]. Notably, CK and EMA expression levels were strong in these two cases, unlike the other SD-TS, allowing us to categorize them as SD-LUAD.

The prevailing literature remains controversial as to whether SD-TS represent a distinct entity and, if so, whether there is an

evolutionary relation between SD-LUAD and SD-TS [14,16,17]. There are no unambiguous clinico-radiological or histopathological findings to differentiate between them [10–17]. Perret et al. [14] proposed criteria for SD-TS of (1) rhabdoid or poorly differentiated phenotype; (2) complete loss of expression of *SMARCA4* and *SMARCA2*; and (3) focal or diffuse expression of at least two of the following markers: SOX2, CD34, or SALL4.

SD-TS patients in our case series had dominance of rhabdoid tumor cells, but the overall morphology was indistinguishable from that of SD-LUAD. No spindle cell cytology, myxoid alterations, or a known growth pattern exclusive to sarcomatous histogenesis was observed. Separation from the latter was achieved solely by immunophenotyping, which revealed diffuse and strong staining for stem cell markers CD34, SOX2, and SALL4 and focal staining for keratin and Hep Par 1 in SD-TS in two of the three cases. Also, these two cases had no expression of EMA. The third case had undifferentiated round cell to rhabdoid morphology with BRG1 loss but focal staining for CD34 and CK and weak, focal staining for EMA. In such cases, other tumors like epithelioid mesotheliomas, which can show BRG1 loss, must be excluded by clinico-radiological features and negativity for other mesothelial markers (CK5/6, calretinin, and WT1) [14]. Further, complete absence or weak focal presence of EMA with focal positivity for CK helps to exclude sarcomatoid/undifferentiated carcinomas.

Predictive biomarker testing for sensitizing *EGFR* mutation and *ALK-1* and *ROS1* rearrangement was negative in all SD-TT cases in this cohort. Case No. 1, which was tested by massively parallel sequencing for broad predictive biomarkers, showed copy number gain for *c-MYC* but none of the actionable genetic alterations. Lack of currently druggable genetic alterations is the hallmark of SD-LUAD. This finding in our series is a reiteration of similar findings in previous studies [19,21]. This confirms the futility of expensive biomarker testing in this subset of lung adenocarcinoma and highlights the need to filter such cases upfront to avoid wasting effort and resources. Furthermore, for these tumors with a different biology and an aggressive course with no actionable drivers yet, a better understanding of their mechanistic nuances with new and efficacious therapeutic options are needed [22], some of which such as EZH2 inhibitors [23] and immune check point inhibitors [24,25] have started emerging. To fulfill the referred objective of differentiating SD-TT from NSCC-NOS, we followed a simple tissue proficient diagnostic schema as shown in Fig. 5.

There are certain limitations in the present study. First, the number of cases studied is small. Second, the study only confirmed that BRG1 loss is confined to TTF1-negative NSCLC based on small

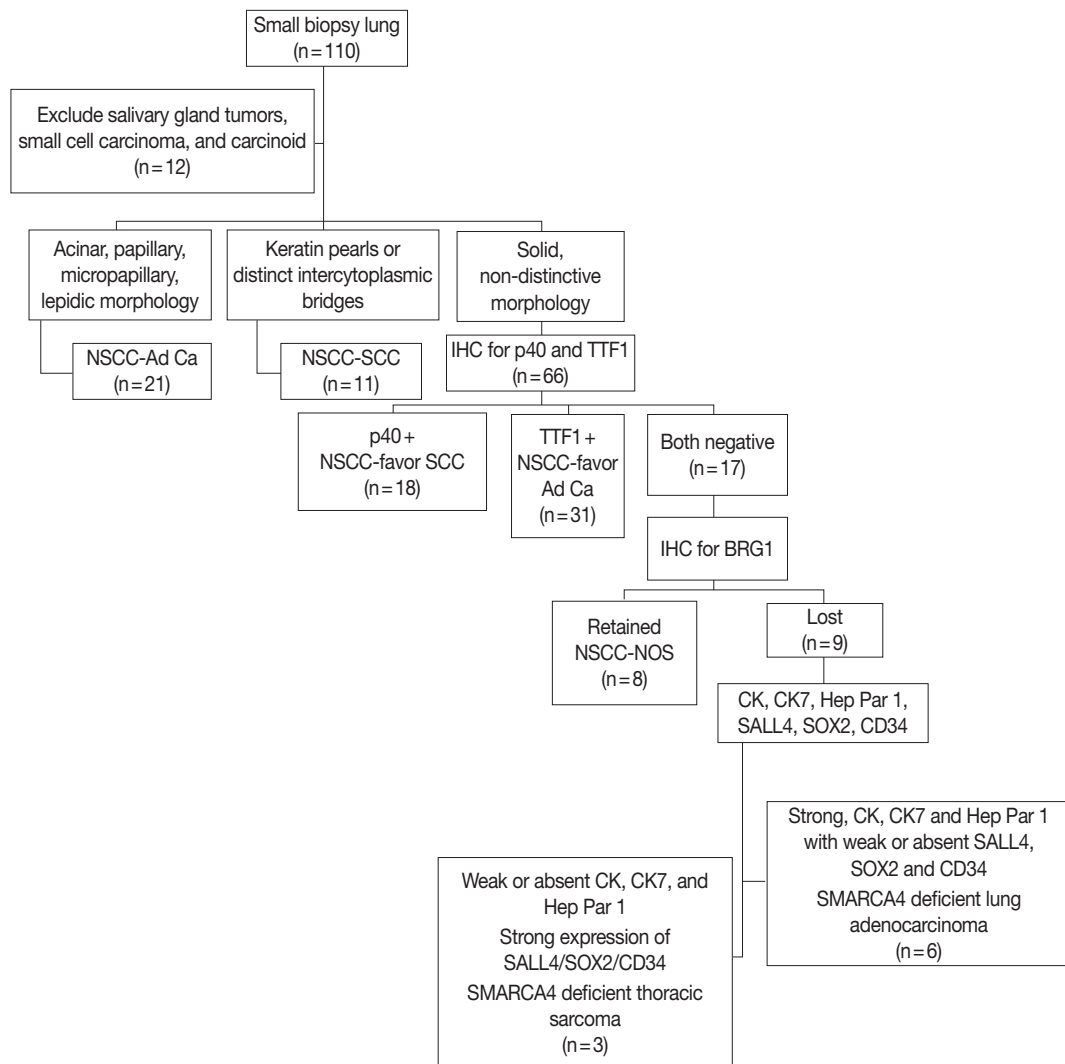


Fig. 5. Diagnostic schema for SMARCA4/BRG1 protein-deficient thoracic tumors. NSCC-Ad Ca, non-small cell carcinoma adenocarcinoma; SCC, squamous cell carcinoma; IHC, immunohistochemistry; TTF1, transcription termination factor 1; CK, cytokeratin.

tissue microarray and might not agree with all existing literature [10]. Third, no confirmatory molecular testing targeting *SMARCA4* gene mutation was performed. Fourth, the diagnostic pathway requires extensive use of IHC to separate SD-TT into SD- LUAD and SD-TS once BRG1 loss is established. However, such extension of IHC is acceptable in the BRG1-deficient subset that lacks actionable biomarkers and omits biomarker testing without therapeutic impact.

To conclude, SD-LUAD and SD-TS are difficult to differentiate from each other and from other NSCLC based on morphology alone. They are likely to be reported as NSCC-NOS with immunonegativity to p40 and TTF1, necessitating biomarker testing with a waste of time and resources. We argue that the diagnostic pathway presented here can help to diagnose such cases so that they can be studied more effectively for new biomarkers and ther-

apeutic techniques. Overall, this study highlights the need and method of delineating SD-TT in reporting of small biopsy for NSCLC and shares a useable workflow to clarify tumor type. Finally, awareness of this entity can help prevent misdiagnosis of MUO as hepatic or hepatoid carcinomas with consequent negative effects.

Ethics Statement

All procedures performed in the current study were approved by Institutional Review Board (vide letter no: RGCIRC/IRB-BHR/33/2021 dated 6th January 2021) in accordance with the 1964 Helsinki declaration and its later amendments. Informed consent was obtained from all individual participants included in the study.

Availability of Data and Material

The datasets generated or analyzed during the study are available from the corresponding author on reasonable request.

Code Availability

Not applicable.

ORCID

Anurag Mehta <https://orcid.org/0000-0001-6517-3664>
 Divya Bansal <https://orcid.org/0000-0001-9445-4086>
 Rupal Tripathi <https://orcid.org/0000-0003-2007-2450>
 Ankush Jajodia <https://orcid.org/0000-0002-7689-9484>

Author Contributions

Conceptualization: AM. Data curation: DB, RT. Formal analysis: AM, DB. Investigation: AM, DB, AJ. Methodology: AM, DB. Resources: RT, AJ. Supervision: AM. Visualization: AM, DB. Writing—original draft: DB, AM, RT. Writing—review & editing: AM, DB. Approval of final manuscript: all authors.

Conflicts of Interest

The authors declare that they have no potential conflicts of interest.

Funding Statement

No funding to declare.

References

- Oike T, Ogiwara H, Nakano T, Yokota J, Kohno T. Inactivating mutations in SWI/SNF chromatin remodeling genes in human cancer. *Jpn J Clin Oncol* 2013; 43: 849-55.
- Shain AH, Pollack JR. The spectrum of SWI/SNF mutations, ubiquitous in human cancers. *PLoS One* 2013; 8: e51119.
- Wang X, Haswell JR, Roberts CW. Molecular pathways: SWI/SNF (BAF) complexes are frequently mutated in cancer: mechanisms and potential therapeutic insights. *Clin Cancer Res* 2014; 20: 21-7.
- Ganguly D, Sims M, Cai C, Fan M, Pfeiffer LM. Chromatin remodeling factor BRG1 regulates stemness and chemosensitivity of glioma initiating cells. *Stem Cells* 2018; 36: 1804-15.
- Agaimy A. The expanding family of SMARCB1(INI1)-deficient neoplasia: implications of phenotypic, biological, and molecular heterogeneity. *Adv Anat Pathol* 2014; 21: 394-410.
- Jelinic P, Mueller JJ, Olvera N, et al. Recurrent SMARCA4 mutations in small cell carcinoma of the ovary. *Nat Genet* 2014; 46: 424-6.
- Stewart CJ, Crook ML. SWI/SNF complex deficiency and mismatch repair protein expression in undifferentiated and dedifferentiated endometrial carcinoma. *Pathol* 2015; 47: 439-45.
- Agaimy A, Daum O, Markl B, Lichtmannegger I, Michal M, Hartmann A. SWI/SNF Complex-deficient undifferentiated/rhabdoid carcinomas of the gastrointestinal tract: a series of 13 cases highlighting mutually exclusive loss of SMARCA4 and SMARCA2 and frequent co-inactivation of SMARCB1 and SMARCA2. *Am J Surg Pathol* 2016; 40: 544-53.
- AACR Project GENIE Consortium. AACR Project GENIE: powering precision medicine through an international consortium. *Cancer Discov* 2017; 7: 818-31.
- Herpel E, Rieker RJ, Dienemann H, et al. SMARCA4 and SMARCA2 deficiency in non-small cell lung cancer: immunohistochemical survey of 316 consecutive specimens. *Ann Diagn Pathol* 2017; 26: 47-51.
- Agaimy A, Fuchs F, Moskalev EA, Sirbu H, Hartmann A, Haller F. SMARCA4-deficient pulmonary adenocarcinoma: clinicopathological, immunohistochemical, and molecular characteristics of a novel aggressive neoplasm with a consistent TTF1(neg)/CK7(pos)/Hep-Par-1(pos) immunophenotype. *Virchows Arch* 2017; 471: 599-609.
- Nambirajan A, Singh V, Bhardwaj N, Mittal S, Kumar S, Jain D. SMARCA4/BRG1-deficient non-small cell lung carcinomas: a case series and review of the literature. *Arch Pathol Lab Med* 2021; 145: 90-8.
- Le Loarer F, Watson S, Pierron G, et al. SMARCA4 inactivation defines a group of undifferentiated thoracic malignancies transcriptionally related to BAF-deficient sarcomas. *Nat Genet* 2015; 47: 1200-5.
- Perret R, Chalabreysse L, Watson S, et al. SMARCA4-deficient thoracic sarcomas: clinicopathologic study of 30 cases with an emphasis on their nosology and differential diagnoses. *Am J Surg Pathol* 2019; 43: 455-65.
- Yoshida A, Kobayashi E, Kubo T, et al. Clinicopathological and molecular characterization of SMARCA4-deficient thoracic sarcomas with comparison to potentially related entities. *Mod Pathol* 2017; 30: 797-809.
- Sauter JL, Graham RP, Larsen BT, Jenkins SM, Roden AC, Boland JM. SMARCA4-deficient thoracic sarcoma: a distinctive clinicopathological entity with undifferentiated rhabdoid morphology and aggressive behavior. *Mod Pathol* 2017; 30: 1422-32.
- Rekhtman N, Montecalvo J, Chang JC, et al. SMARCA4-deficient thoracic sarcomatoid tumors represent primarily smoking-related undifferentiated carcinomas rather than primary thoracic sarcomas. *J Thorac Oncol* 2020; 15: 231-47.
- Nicholsan AG, Geisinger K, Aisner SC, et al. Terminology and criteria in non-resection specimens. In: Travis WD, Brambilla E, Burke AP, Marx A, Nicholson AG, eds. WHO classification of tumors of the lung, pleura, thymus and heart. 4th ed. Lyon: IARC Press, 2015; 26-37.
- Matsubara D, Kishaba Y, Ishikawa S, et al. Lung cancer with loss of BRG1/BRM, shows epithelial mesenchymal transition phenotype and distinct histologic and genetic features. *Cancer Sci* 2013; 104: 266-73.
- Mehta A, Saifi M, Batra U, Suryavanshi M, Gupta K. Incidence of ROS1-rearranged non-small-cell lung carcinoma in India and efficacy of crizotinib in lung adenocarcinoma patients. *Lung Cancer (Auckl)* 2020; 11: 19-25.
- Cancer Genome Atlas Research Network. Comprehensive molecular profiling of lung adenocarcinoma. *Nature* 2014; 511: 543-50.
- Bell EH, Chakraborty AR, Mo X, et al. SMARCA4/BRG1 is a novel prognostic biomarker predictive of cisplatin-based chemotherapy outcomes in resected non-small cell lung cancer. *Clin Cancer Res* 2016; 22: 2396-404.
- Chan-Penebre E, Armstrong K, Drew A, et al. Selective killing of SMARCA2- and SMARCA4-deficient small cell carcinoma of the ovary, hypercalcemic type cells by inhibition of EZH2: in vitro and in vivo preclinical models. *Mol Cancer Ther* 2017; 16: 850-60.
- Naito T, Udagawa H, Umemura S, et al. Non-small cell lung cancer with loss of expression of the SWI/SNF complex is associated with aggressive clinicopathological features, PD-L1-positive status, and high tumor mutation burden. *Lung Cancer* 2019; 138: 35-42.
- Takada K, Sugita S, Murase K, et al. Exceptionally rapid response to pembrolizumab in a SMARCA4-deficient thoracic sarcoma overexpressing PD-L1: a case report. *Thorac Cancer* 2019; 10: 2312-5.

Proto-oncogene Pokemon in thyroid cancer: a potential promoter of tumorigenesis in papillary thyroid carcinoma

Kyungseek Chang, Sung-Im Do, Kyungeun Kim, Seoung Wan Chae, In-gu Do, Hyun Joo Lee, Dong Hoon Kim, Jin Hee Sohn

Department of Pathology, Kangbuk Samsung Hospital, Sungkyunkwan University School of Medicine, Seoul, Korea

Background: Pokemon is an oncogenic transcription regulator that plays a critical role in cellular differentiation. Although it has been found to be overexpressed in several types of cancer involving different organs, its role in thyroid gland has yet to be reported. The objective of this study was to evaluate the expression of Pokemon in papillary thyroid carcinoma (PTC) based on clinicopathological parameters. **Methods:** Tissue microarray samples derived from patients with PTC or benign thyroid disease were used to evaluate Pokemon expression based on immunohistochemical analysis. Correlations of its expression with various clinicopathological parameters were then analyzed. **Results:** Pokemon expression was observed in 22.0% of thyroid follicular cells from the normal group, 44.0% from the group with benign thyroid diseases, and 92.1% from the group with PTC ($p < .001$). The intensity of Pokemon expression was markedly higher in the PTC group. Pokemon expression level and PTC tumor size showed an inverse correlation. T1a tumors showed strong expression levels of Pokemon. However, larger tumors showed weak expression ($p = .006$). **Conclusions:** Pokemon expression is associated with tumorigenesis of PTC, with expression showing an inverse correlation with PTC tumor size. This might be related to the negative regulation of aerobic glycolysis by Pokemon.

Key Words: Pokemon; ZBTB7A; Papillary thyroid carcinoma; Thyroid neoplasms

Received: April 6, 2021 Revised: June 17, 2021 Accepted: June 28, 2021

Corresponding Author: Sung-Im Do, MD, PhD, Department of Pathology, Kangbuk Samsung Hospital, Sungkyunkwan University School of Medicine, 29 Saemunan-ro, Jongno-gu, Seoul 03181, Korea

Tel: +82-2-2001-2389, Fax: +82-2-2001-2398, E-mail: sungim.do@samsung.com

Thyroid cancer is the most common endocrine malignancy. It represents 1% of all malignancies [1]. Papillary thyroid carcinoma (PTC) is the most common cancer among these malignant tumors, accounting for about 85% of thyroid cancers. Patients with PTC have an excellent prognosis with a 10-year survival rate greater than 90% [1]. One single institutional long-term follow-up study in 2018 reported that 10-, 15-, and 20-year overall survival rates of PTC patients were 97%, 95%, and 90%, respectively [2]. However, some PTCs display aggressive features. Several clinicopathological parameters such as old age, large tumor size, presence of extrathyroidal extension, and cervical lymph node metastasis have been suggested as poor prognostic factors [3,4].

Recent studies have identified specific molecular alterations involved in the formation of PTC [5], including *BRAF* V600E mutations and changes in mitogen-activated protein kinase pathway, *RAS* mutations and changes in phosphoinositide 3 kinase-AKT (PI3K-AKT) pathway, *RET/PTC* rearrangement,

PAX8/PPAR γ rearrangement and changes in *PTEN*-activated PI3K-AKT pathway, and TRK rearrangements [5]. Pokemon (POK erythroid myeloid ontogenic factor), also known as ZBTB7a (zinc finger and BTB domain-containing protein 7a) or FBI-1 (factor binding inducer of short transcripts of human immunodeficiency virus type 1), is a transcriptional regulator that belongs to the POK protein family. It plays a critical role in cellular differentiation [6,7]. Pokemon protein is a transcriptional regulator of several genes. Pokemon can specifically repress the transcription of the tumor suppressor gene *ARF* via direct binding [6]. Genes such as *RBI* [8], *CDKN1A* [9], nuclear factor- κ B responsive genes [10], survivin [11], *CDK2* and *E2F4* [12], *ADH5/FDH* [13], and *FASN* [14] are also regulated by Pokemon. Dysfunctional POK proteins can cause disorders in cellular development and trigger oncogenic processes [6]. Overexpression of Pokemon has been detected in several types of cancer, such as breast cancer, liver cancer, prostate cancer, and malig-

nant glioma [6,11,15-17]. However, the carcinogenic effect of Pokemon overexpression in thyroid gland has yet to be reported. Thus, the objective of this study was to analyze the expression of Pokemon in PTC and evaluate correlations between Pokemon expression and clinicopathological parameters of PTC using tissue samples obtained from 90 cases of PTC and 25 cases of benign thyroid disease.

MATERIALS AND METHODS

Tissue specimens

We selected 90 cases of PTC and 25 cases of benign thyroid diseases such as nodular hyperplasia, follicular adenoma, Hashimoto's thyroiditis, and Graves' disease from archival cases in Kangbuk Samsung Hospital (Seoul, Republic of Korea). Controls included 68 normal thyroid tissues identified from selected cases. Tissues resected by surgeons were examined by pathologists before fixation in 10% neutral-buffered formalin for 12–24 hours, followed by thorough macroscopic evaluation and sectioning. After automatic tissue processing, sections were embedded in paraffin blocks. Four-micrometer-thick sections were cut from each formalin-fixed, paraffin-embedded (FFPE) tissue block using a rotary microtome, stained with hematoxylin and eosin, covered with a glass coverslip, followed by analysis and diagnosis by two board-certified pathologists. Clinical and pathological information were obtained from pathology reports and electrical medical information systems. Information collected included age, sex, multifocality, the greatest dimension of the tumor, presence of lymphovascular invasion, extrathyroidal extension, lymph node metastasis, number of metastatic lymph nodes, *BRAF* mutational status, and presence of background thyroiditis. One out of these 90 PTC patients was excluded from statistical analysis due to insufficient data (Table 1).

Tissue microarray construction

Tissue microarray (TMA) blocks were constructed in following orders. Briefly, all hematoxylin and eosin-stained slides were reviewed and the two most representative tumor areas were marked on the corresponding FFPE tissue blocks. Two 2-mm-diameter tissue cores were obtained from each block and manually arrayed into recipient TMA blocks. Only one 2-mm-diameter tissue cores were obtained from blocks with largest tumor size less than 5 mm. The assembly was held in an X-Y position with a 1-mm increment between individual cores. Modified biopsy needle was used to bore holes in a recipient block with defined array cores and to transfer the cores into the recipient block.

Table 1. Clinicopathological parameters of subjects in the PTC group

	Value (n=89)
Age (yr)	43.41 ± 12.14
Sex	
Female	61 (68.5)
Male	28 (31.5)
Tumor size (cm)	1.08 ± 0.94
≤ 1	61 (68.5)
> 1	28 (31.5)
Lymph node metastasis	
0 (absent)	36 (40.4)
≥ 1 (present)	53 (59.6)
Lymphovascular invasion	
Absent	87 (97.8)
Present	2 (2.2)
Extrathyroidal invasion	
Absent	40 (44.9)
Present	49 (55.1)
No. of tumors	
1 (single)	68 (76.4)
≥ 2 (multiple)	21 (23.6)
<i>BRAF</i> V600E mutation	
Wild type	8 (8.9)
Mutant	49 (55.1)
Not obtained	32 (36.0)
Background thyroiditis	
None	61 (68.5)
Thyroiditis	28 (31.5)

Values are presented as mean ± SD or number (%).
PTC, papillary thyroid carcinoma.

The percentage of tumor volume in each core was > 70%. Two TMA blocks were prepared for each case.

Immunohistochemistry

Immunohistochemical staining was performed using the Bond Polymer Refine Detection kit (Leica Biosystems, Newcastle upon Tyne, UK) in the Bond-Max automatic immunostainer (Leica Biosystems). ZBTB7A/Pokemon antibody (1:200, clone, Novus Biologicals, Littleton, CO, USA) was used as the primary antibody. Immunohistochemical slides were independently evaluated by two pathologists (SID and SWC). Discrepant cases were reviewed. Pokemon expression was interpreted as positive if the cell showed positivity in either the nucleus or the cytoplasm. The intensity of expression was defined as negative, weakly positive, or strongly positive (Fig. 1). Immunohistochemical expression (× 200) of Pokemon in thyroid tissues from normal (Fig. 1A–C), benign thyroid disease (Fig. 1D–F), and PTC (Fig. 1G–I) groups. Pokemon expression intensity is interpreted as negative (Fig. 1A, D, G), weakly positive (Fig. 1B,

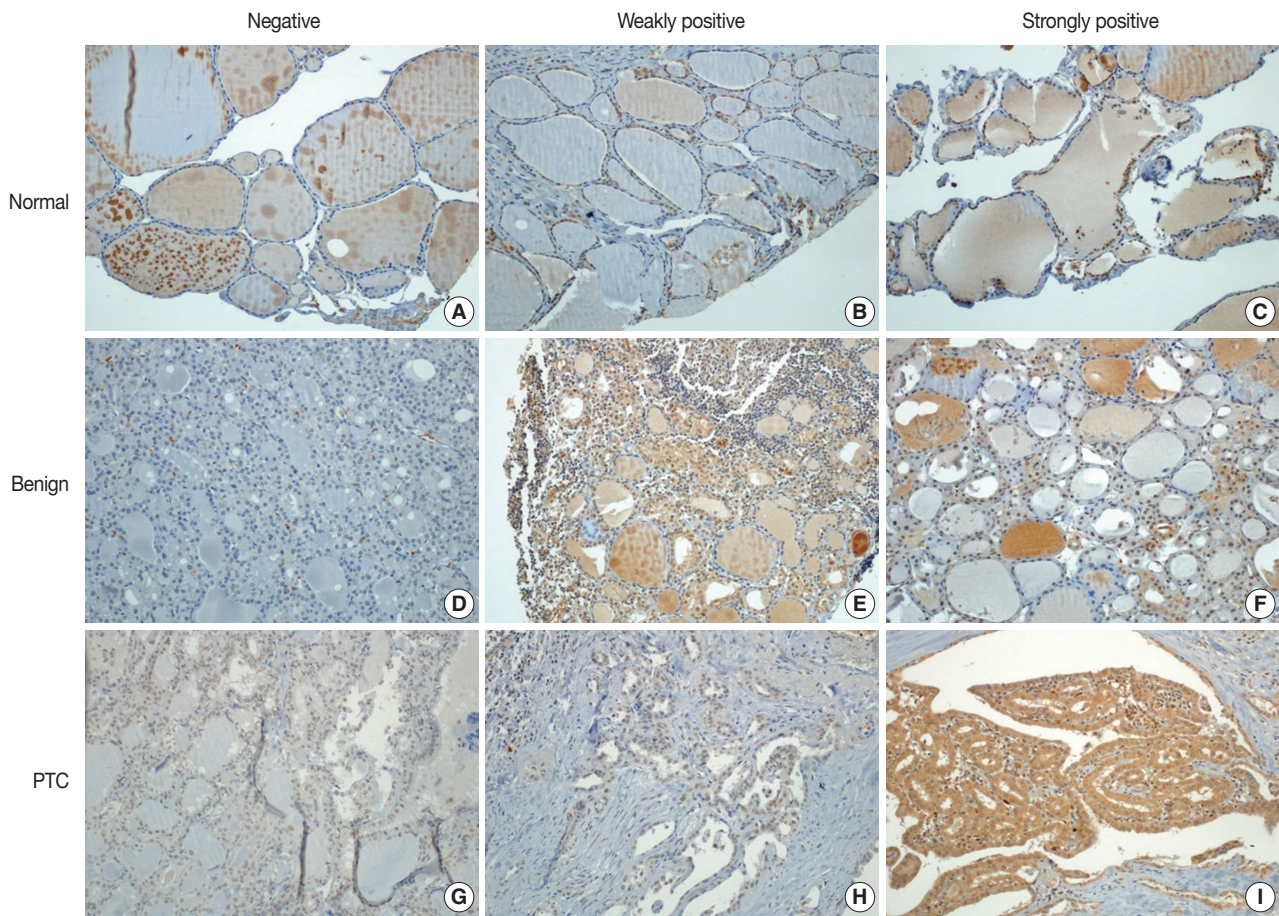


Fig. 1. Immunohistochemical expression of Pokemon in thyroid tissues of normal (A–C), benign thyroid disease (D–F), and PTC (G–I) groups. Pokemon expression intensity is interpreted as negative (A, D, G), weakly positive (B, E, H), or strongly positive (C, F, I).

E, H), or strongly positive (Fig. 1C, F, I). It was determined using TMA cores of those with PTCs ($n = 89$) or benign thyroid diseases ($n = 25$). Pokemon expression intensity of normal thyroid tissue was determined in adjacent normal follicular cells where present, if the TMA core carried an identifiable portion of normal thyroid tissue ($n = 68$).

Detection of *BRAF* mutation

To detect *BRAF* V600E mutation, nucleic acids were isolated from FFPE tissues using a DNeasy Blood and Tissue Kit (Qiagen, Hilden, Germany). Isolated nucleic acids were mixed with a polymerase chain reaction (PCR) master mix using a Seeplex *BRAF* V600E ACE Detection Kit (Seegene, Seoul, Republic of Korea). These mixtures were then immediately transferred to a preheated thermal cycler for 15 minutes. PCR was carried out in a GeneAmp PCR System 9700 (Applied Biosystems, Foster City, CA, USA). The cycling amplification program consisted of 35 cycles of denaturation at 94°C for 30 seconds, annealing

at 63°C for 30 seconds, and extension at 72°C for 1 minute. Amplified PCR products were loaded onto a 2% agarose gel and visualized with a SafeView Nucleic Acid Stain (Applied Biological Materials, Richmond, BC, Canada). The *BRAF* V600E mutation was detected using a Gel Documentation System (Bio-Rad Laboratories, Hercules, CA, USA).

Statistical analysis

Pearson's Chi-square test was performed to compare Pokemon expression intensities in thyroid tissues of PTC, benign thyroid disease, and normal groups. It was also used to analyze associations between Pokemon expression intensity and clinicopathological characteristics. Clinical significance was determined using Kruskal-Wallis test (nonparametric method), linear-by-linear association test, and Pearson's chi-square test. All statistical analyses were performed using SPSS for windows ver. 24.0 (IBM Corp., Armonk, NY, USA). Statistical significance was considered when p -value was less than .05.

Pathologic TNM staging

Pathologic TNM staging was referred to American Joint Committee on Cancer 8th edition of the Cancer Staging Manual for PTC. Pathologic T categories included the following: T1a, tumor ≤ 1 cm in the greatest dimension limited to the thyroid; T1b, tumor > 1 cm but ≤ 2 cm in the greatest dimension, limited to the thyroid; T2, tumor > 2 cm, but ≤ 4 cm in the greatest dimension, limited to thyroid; T3a, tumor > 4 cm limited to the thyroid; T3b, gross extrathyroidal extension invading only strap muscles (sternohyoid, sternothyroid, thyrohyoid, or omohyoid muscles) from a tumor of any size; and T4, gross extrathyroidal extension beyond strap muscles. Pathologic N categories included the following: N0, no evidence of locoregional lymph node metastasis; N0a, one or more cytologically or histologically confirmed benign lymph nodes; N1, metastasis to regional nodes; N1a, metastasis to level VI or VII (pretracheal, paratracheal, or prelaryngeal/Delphian, or upper mediastinal) lymph nodes; and N1b, metastasis to unilateral, bilateral, or contralateral lateral neck lymph nodes (levels I, II, III, IV, or V) or retropharyngeal lymph nodes.

RESULTS

With collected information shown in Table 1, Pokemon expression intensities in thyroid tissues of normal, benign thyroid disease, and PTC groups were determined (Table 2). Statistically significant ($p < .001$) differences in Pokemon expression positivity were observed between normal thyroid tissues (22.0%) and thyroid tissues from patients with benign thyroid disease (44.0%) or PTC (92.1%). Results of Pearson's chi-square test for Pokemon expression intensity in normal, benign, and PTC groups are shown in Supplementary Tables S1–S3. The difference in Pokemon expression intensity between normal and benign thyroid disease groups was statistically significant ($p = .035$). The difference in Pokemon expression intensity between normal and PTC groups was also statistically significant ($p < .001$). Simi-

Table 2. Pokemon expression intensities in thyroid tissues of normal, benign thyroid disease, and PTC groups

Pokemon expression intensity	Normal (n=68)	Benign (n=25)	PTC (n=89)	p-value
Negative	53 (78.0)	14 (56.0)	7 (7.9)	$< .001$
Weakly positive	13 (19.1)	7 (28.0)	30 (33.7)	
Strongly positive	2 (2.9)	4 (16.0)	52 (58.4)	

Values are presented as number (%).

Statistical analysis was performed using linear-by-linear association test.

PTC, papillary thyroid carcinoma.

larly, the difference in Pokemon expression intensity between benign thyroid disease and PTC was significant ($p < .001$).

Pokemon expression intensity in PTC showed significant correlations with tumor size and corresponding pathologic T category groups (Table 3). Reduced mean tumor size was significantly associated with stronger Pokemon expression intensity ($p = .002$). Tumor size and TNM stage were also significantly associated with Pokemon expression intensity. When the tumor size was divided into three groups by a separation point at 0.5 cm and 1 cm, a tumor size less than 0.5 cm was associated with Pokemon expression intensity stronger than 66%. However, increased tumor size was associated with less strong or no Pokemon expression intensity ($p = .028$). Tumor size categorized by conventional TNM staging, excluding T3b and T4 groups for gross extrathyroidal extension to and beyond strap muscles, showed evident negative concordance with Pokemon expression intensity ($p = .010$). T1a group was associated with expression greater than 66%, whereas groups T1b, T2, and T3a were collectively associated with no or weak expression ($p = .006$). Other clinicopathological parameters did not show any significant association with Pokemon expression intensity.

DISCUSSION

Pokemon can act as a genuine proto-oncogene *in vivo* [6]. It can repress the expression of tumor suppressor protein ARF [6]. ARF is a negative regulator of the E3 ubiquitin-protein ligase MDM2 which participates in the degradation of p53 via ubiquitin-dependent degradation by the proteasome. Reduced ARF levels can stimulate cell proliferation by decreasing the stability and activity of p53 via MDM2 [6]. Pokemon expression in malignancy is generally related to poor cancer outcome in various organs. It promotes tumorigenesis, acting as a pro-oncogene by repressing or enhancing the expression of genes involved in apoptosis, cell proliferation, and differentiation [18]. For example, Pokemon expression can promote breast cancer progression by up-regulating survivin expression [11]. In the nasopharynx, high Pokemon protein expression is closely associated with non-keratinizing nasopharyngeal carcinoma [19]. In the liver, suppression of Pokemon can impair the invasion of hepatocellular carcinoma (HCC) cells [20]. However, to the best of our knowledge, contribution of Pokemon to thyroid malignancy has yet to be reported.

Pokemon expression intensity showed a statistically significant ($p = .035$) difference between normal and benign thyroid disease groups in the present study. Although Pokemon expres-

Table 3. Correlations of Pokemon expression intensity with clinicopathological parameters in PTC

Variable	Pokemon expression intensity			p-value
	Negative (n = 7)	Weak expression (n = 30)	Strong expression (n = 52)	
Age (yr)	39.0 ± 9.3	43.4 ± 12.8	43.5 ± 11.7	.678
Sex				.793
Female	4 (57.1)	21 (70.0)	36 (69.2)	
Male	3 (42.9)	9 (30.0)	16 (30.8)	
Mean tumor size (cm)	2.1 ± 1.7	1.0 ± 0.8	0.9 ± 0.4	.018
Tumor size (cm)				.028
≤ 0.5	0	8 (26.7)	11 (21.2)	
> 0.5 and ≤ 1	1 (14.3)	14 (46.7)	27 (51.9)	
> 1	6 (85.7)	8 (26.7)	14 (26.9)	
T category by group				.006
T1a	1 (14.3)	22 (73.3)	38 (73.1)	
T1b, T2, T3a	6 (85.7)	8 (26.7)	14 (26.9)	
T category				.010
T1a	1 (14.3)	22 (73.3)	38 (73.1)	
T1b	4 (57.1)	7 (23.3)	13 (25.0)	
T2	1 (14.3)	0	1 (1.9)	
T3a	1 (14.3)	1 (3.3)	0	
N category				.306
N0	2 (28.6)	10 (33.3)	24 (46.2)	
N1a	4 (57.1)	15 (50.0)	26 (50.0)	
N1b	1 (14.3)	5 (16.7)	2 (3.8)	
Lymphovascular invasion				.134
Negative	7 (100)	28 (93.3)	52 (100)	
Positive	0	2 (6.7)	0	
Extrathyroidal invasion				.234
Negative	1 (14.3)	14 (46.7)	25 (48.1)	
Positive	6 (85.7)	16 (53.3)	27 (51.9)	
Number of tumors				.647
Single	6 (85.7)	24 (80.0)	38 (73.1)	
Multiple	1 (14.3)	6 (20.0)	14 (26.9)	
Background disease				.594
None	6 (85.7)	20 (66.7)	35 (67.3)	
Thyroiditis	1 (14.3)	10 (33.3)	17 (32.7)	
BRAF mutation				.296
Wild type	0	1 (5.6)	7 (19.4)	
Mutant	3 (100)	17 (94.4)	29 (80.6)	

Values are presented as mean ± SD or number (%).

Statistical analysis of patient age and mean tumor size was performed using Kruskal-Wallis test. Statistical analysis of other clinicopathological parameters was performed using Pearson's chi-square test. T category was referred to American Joint Committee on Cancer 8th edition of the Cancer Staging Manual for papillary thyroid carcinoma.

PTC, papillary thyroid carcinoma.

sion was positive in 44% of patients with benign thyroid disease regardless of its expression intensity, it was more significantly ($p < .001$) associated with PTC than with benign thyroid disease (Table 2). Pokemon overexpression has also been observed in several malignancies, such as T and B cell lymphomas in transgenic mice model via direct binding of Pokemon and the tumor suppressor gene ARF [6], prostate carcinoma via increased Pokemon expression stimulated by epidermal growth factor [16], ovarian carcinomas of all four major histological

types (serous, endometrioid, clear cell, and mucinous) via elevated RNA transcription [21], breast carcinoma by upregulating survivin, a member of the inhibitor of apoptosis proteins [11]. However, the mechanism which Pokemon overexpression leads to tumorigenesis of PTC remains to be investigated.

When Pokemon expression intensity was compared according to mean PTC tumor size, stronger expression levels were observed in smaller tumors (0.9 ± 0.4 cm), whereas larger tumors (2.1 ± 1.7 cm) showed absent or weak expression. These inverse

correlations were evident according to the T category of the tumor when T1a group was compared with the combined group of T1b, T2, and T3a ($p = .006$) (Table 3). These results were contrary to results of several previous studies of tumors involving various organs, where Pokemon expression was positively correlated with tumor size or T category of breast carcinomas [11], HCC [22], or non-small cell lung cancer [23]. These combined results of particularly strong Pokemon expression in small-sized tumors suggest that Pokemon might play an important role in malignant transformation of thyroid cells and in the early stage of PTC tumor formation, while it might have a diminished role as the tumor grows in size.

Such inverse correlation between Pokemon expression and tumor size has also been observed in oropharyngeal squamous cell carcinoma (OSCC) which shows a higher relative expression in smaller tumors (< 2 cm) and lower to no expression in larger tumors (≥ 4 cm) [18]. Although the distribution of Pokemon expression is lower in OSCC than in normal oral mucosa, Sartini et al. [18] have suggested that the downregulation of Pokemon might be related to tumor progression. Presumably, our results suggest such downregulation.

Aerobic glycolysis (the Warburg effect) is a hallmark of human cancer. It plays a crucial role in tumor growth [24]. Receptor tyrosine kinase/PI3K/AKT signaling and MYC act as pro-growth signaling factors that can upregulate aerobic glycolysis. However, Liu et al. [25] have reported that Pokemon, a proto-oncogene, unexpectedly can act as a tumor suppressor by directly binding to the promoter and repressing the transcription of genes responsible for glycolysis metabolism, such as *GLUT3*, *PFKP*, and *PKM*. As a result, a significant decrease in Pokemon copy number variation was observed in several types of human carcinoma in the late stage (N1, N2, N3, M1, stage IV) than in early stage (N0, M0, stage I), including esophageal carcinoma, bladder urothelial carcinoma, colorectal adenocarcinoma, lung squamous cell carcinoma, cutaneous melanoma, and low-grade glioma [25]. We believe that the mechanism underlying the inverse correlation between Pokemon expression and tumor size of PTC might be related to the unexpected negative regulation of aerobic glycolysis by Pokemon.

Regardless of its contrasting behavior in PTC, Pokemon itself is associated with malignant transformation of tumors in various organs. High levels of Pokemon expression in patients with early stages of PTC may potentially be used for screening and identifying malignancies involving other organs.

Our study was performed at a single institution with PTC cases retrieved from a two-year period, which invariably resulted

in limitations involving the follow-up period of patients with PTC and their survival rates. A multi-institutional study with ethnic and racial diversity is needed to further investigate the effect of Pokemon on PTC. Larger patient groups might be needed to elucidate the effect of Pokemon on parameters showing statistical insignificance in the present study. A long-term survival study may provide further insight into the effect of Pokemon on long-term outcomes of PTC, one of the most common malignancies worldwide.

In summary, Pokemon overexpression (when compared to normal thyroid tissues) is associated with formation of PTC and benign thyroid diseases. A smaller PTC tumor shows stronger Pokemon overexpression, which supports the hypothesis that Pokemon overexpression can lead to tumorigenesis of PTC. However, a larger PTC tumor may be associated with Pokemon downregulation, which may be related to tumor progression. Targeting Pokemon in early stages could be effective in suppressing PTC formation and potentially facilitate treatment.

Supplementary Information

The Data Supplement is available with this article at <https://doi.org/10.4132/jptm.2021.06.28>.

Ethics Statement

All procedures performed in this study were approved by the Institutional Review Board at Kangbuk Samsung Hospital (IRB No. 2016-08-006-001) in accordance with the Helsinki Declaration as revised in 2013. The requirement of informed consent was waived due to its retrospective nature.

Availability of Data and Material

The datasets generated or analyzed during the study are available from the corresponding author on reasonable request.

Code Availability

Not applicable.

ORCID

Kyungseek Chang	https://orcid.org/0000-0002-3628-1110
Sung-Im Do	https://orcid.org/0000-0001-8442-5054
Kyungeun Kim	https://orcid.org/0000-0001-7938-4673
Seoung Wan Chae	https://orcid.org/0000-0003-0406-4469
In-gu Do	https://orcid.org/0000-0001-7832-7116
Hyun Joo Lee	https://orcid.org/0000-0002-7656-0093
Dong Hoon Kim	https://orcid.org/0000-0001-5722-6703
Jin Hee Sohn	https://orcid.org/0000-0002-4735-3853

Author Contributions

Conceptualization: SID, SWC. Data curation: KC, SID, SWC. Formal analysis: KC, SID, SWC. Investigation: KC, SID, SWC. Methodology: SID, SWC. Project administration: SID, KK, SWC. Resources: SID, SWC. Supervision: SID, KK, SWC, IGD, HJL, DHK, JHS. Validation: SID, SWC. Visualization: KC, SID, KK. Writing—original draft: KC, SID, KK. Writing—review & editing: KC, SID, KK. Approval of final manuscript: all authors.

Conflicts of Interest

The authors declare that they have no potential conflicts of interest.

Funding Statement

No funding to declare.

References

- Al-Brahim N, Asa SL. Papillary thyroid carcinoma: an overview. *Arch Pathol Lab Med* 2006; 130: 1057-62.
- Ito Y, Miyauchi A, Kihara M, Fukushima M, Higashiyama T, Miya A. Overall survival of papillary thyroid carcinoma patients: a single-institution long-term follow-up of 5897 patients. *World J Surg* 2018; 42: 615-22.
- Soares P, Celestino R, Melo M, Fonseca E, Sobrinho-Simoes M. Prognostic biomarkers in thyroid cancer. *Virchows Arch* 2014; 464: 333-46.
- Mercante G, Frasoldati A, Pedroni C, et al. Prognostic factors affecting neck lymph node recurrence and distant metastasis in papillary microcarcinoma of the thyroid: results of a study in 445 patients. *Thyroid* 2009; 19: 707-16.
- D'Cruz AK, Vaish R, Vaidya A, et al. Molecular markers in well-differentiated thyroid cancer. *Eur Arch Otorhinolaryngol* 2018; 275: 1375-84.
- Maeda T, Hobbs RM, Merghoub T, et al. Role of the proto-oncogene Pokemon in cellular transformation and ARF repression. *Nature* 2005; 433: 278-85.
- Mao A, Chen M, Qin Q, et al. ZBTB7A promotes migration, invasion and metastasis of human breast cancer cells through NF-kappaB-induced epithelial-mesenchymal transition in vitro and in vivo. *J Biochem* 2019; 166: 485-93.
- Jeon BN, Yoo JY, Choi WI, Lee CE, Yoon HG, Hur MW. Proto-oncogene FBI-1 (Pokemon/ZBTB7A) represses transcription of the tumor suppressor Rb gene via binding competition with Sp1 and recruitment of co-repressors. *J Biol Chem* 2008; 283: 33199-210.
- Choi WI, Jeon BN, Yun CO, et al. Proto-oncogene FBI-1 represses transcription of p21CIP1 by inhibition of transcription activation by p53 and Sp1. *J Biol Chem* 2009; 284: 12633-44.
- Zhang NN, Sun QS, Chen Z, Liu F, Jiang YY. Homeostatic regulatory role of Pokemon in NF-kappaB signaling: stimulating both p65 and Ikbalpha expression in human hepatocellular carcinoma cells. *Mol Cell Biochem* 2013; 372: 57-64.
- Zu X, Ma J, Liu H, et al. Pro-oncogene Pokemon promotes breast cancer progression by upregulating survivin expression. *Breast Cancer Res* 2011; 13: R26.
- Yang X, Zu X, Tang J, et al. Zbtb7 suppresses the expression of CDK2 and E2F4 in liver cancer cells: implications for the role of Zbtb7 in cell cycle regulation. *Mol Med Rep* 2012; 5: 1475-80.
- Lee DK, Suh D, Edenberg HJ, Hur MW. POZ domain transcription factor, FBI-1, represses transcription of ADH5/FDH by interacting with the zinc finger and interfering with DNA binding activity of Sp1. *J Biol Chem* 2002; 277: 26761-8.
- Choi WI, Jeon BN, Park H, et al. Proto-oncogene FBI-1 (Pokemon) and SREBP-1 synergistically activate transcription of fatty-acid synthase gene (FASN). *J Biol Chem* 2008; 283: 29341-54.
- Aggarwal A, Hunter WJ 3rd, Aggarwal H, et al. Expression of leukemia/lymphoma-related factor (LRF/POKEMON) in human breast carcinoma and other cancers. *Exp Mol Pathol* 2010; 89: 140-8.
- Aggarwal H, Aggarwal A, Agrawal DK. Epidermal growth factor increases LRF/Pokemon expression in human prostate cancer cells. *Exp Mol Pathol* 2011; 91: 496-501.
- Hong X, Hong XY, Li T, He CY. Pokemon and MEF2D co-operationally promote invasion of hepatocellular carcinoma. *Tumour Biol* 2015; 36: 9885-93.
- Sartini D, Lo Muzio L, Morganti S, et al. Pokemon proto-oncogene in oral cancer: potential role in the early phase of tumorigenesis. *Oral Dis* 2015; 21: 462-9.
- Jiao W, Liu F, Tang FZ, et al. Expression of the Pokemon proto-oncogene in nasopharyngeal carcinoma cell lines and tissues. *Asian Pac J Cancer Prev* 2013; 14: 6315-9.
- Kong J, Liu X, Li X, et al. Pokemon promotes the invasiveness of hepatocellular carcinoma by enhancing MEF2D transcription. *Hepatology Int* 2016; 10: 493-500.
- Jiang L, Siu MK, Wong OG, et al. Overexpression of proto-oncogene FBI-1 activates membrane type 1-matrix metalloproteinase in association with adverse outcome in ovarian cancers. *Mol Cancer* 2010; 9: 318.
- Zhang QL, Tian DA, Xu XJ. Depletion of Pokemon gene inhibits hepatocellular carcinoma cell growth through inhibition of H-ras. *Onkologie* 2011; 34: 526-31.
- Apostolopoulou K, Pateras IS, Evangelou K, et al. Gene amplification is a relatively frequent event leading to ZBTB7A (Pokemon) overexpression in non-small cell lung cancer. *J Pathol* 2007; 213: 294-302.
- Vander Heiden MG, Cantley LC, Thompson CB. Understanding the Warburg effect: the metabolic requirements of cell proliferation. *Science* 2009; 324: 1029-33.
- Liu XS, Haines JE, Mehanna EK, et al. ZBTB7A acts as a tumor suppressor through the transcriptional repression of glycolysis. *Genes Dev* 2014; 28: 1917-28.

Robust home brew fragment sizing assay for detection of *MET* exon 14 skipping mutation in non–small cell lung cancer patients in resource constrained community hospitals

Anurag Mehta¹, Shrinidhi Nathany², Aanchal Chopra², Sakshi Mattoo², Dushyant Kumar², Manoj Kumar Panigrahi²

¹Department of Laboratory Services, Molecular Diagnostics and Transfusion Medicine, Rajiv Gandhi Cancer Institute and Research Centre, New Delhi;

²Section of Molecular Diagnostics, Rajiv Gandhi Cancer Institute and Research Centre, New Delhi, India

Background: A mutation/deletion involving donor or acceptor sites for exon 14 results in splicing out of exon 14 of the mesenchymal epithelial transition (*MET*) gene and is known as “*MET* exon 14 skipping” (Δ *MET*14). The two recent approvals with substantial objective responses and improved progression-free survival to *MET* inhibitors namely capmatinib and tepotinib necessitate the identification of this alteration upfront. We herein describe our experience of Δ *MET*14 detection by an mRNA-based assay using polymerase chain reaction followed by fragment sizing. **Methods:** This is a home brew assay which was developed with the concept that the transcripts from true Δ *MET*14 will be shorter by ~140 bases than their wild type counterparts. The cases which were called *MET* exon 14 skipping positive on next-generation sequencing (NGS) were subjected to this assay, along with 13 healthy controls in order to establish the validity for true negatives. **Results:** Thirteen cases of Δ *MET*14 mutation were detected on NGS using RNA-based sequencing. Considering NGS as a gold standard, the sizing assay using both gel and capillary electrophoresis that showed 100% specificity for both with concordance rates of 84.6% and 88.2% with NGS, respectively, were obtained. **Conclusions:** Owing to the cost-effective nature and easy to use procedures, this assay will prove beneficial for small- and medium-sized laboratories where skilled technical personnel and NGS platforms are unavailable.

Key Words: *MET* exon 14 skipping; Lung neoplasms; Fragment sizing assay; Home brew; Electrophoresis

Received: May 11, 2021 **Revised:** June 8, 2021 **Accepted:** July 15, 2021

Corresponding Author: Shrinidhi Nathany, MD, Molecular Diagnostics, Rajiv Gandhi Cancer Institute and Research Centre, New Delhi 110085, India
 Tel: +91-11-47022030, Fax: +91-11-27051037, E-mail: drshrinidhinathany@gmail.com

A mutation/deletion involving donor or acceptor sites for exon 14 results in splicing out of the exon 14 of the mesenchymal epithelial transition (*MET*) gene and is known as “*MET* exon 14 skipping” (Δ *MET*14) [1–3]. This change in turn abolishes the site for ubiquitination and aborts the physiologically timed decay of *MET* protein [4]. Persistent *MET* activation turns it oncogenic. This genetic alteration has emerged as a Tier 1 biomarker [5] in non–small cell lung carcinoma (NSCLC) with a reported incidence of ~4% in lung adenocarcinoma [6,7] and 2% in squamous cell carcinoma [6]. This frequency supersedes that of other Tier1 driver alterations in NSCLC like *ROS1* and *BRAF* p.V600E which occur at 1%–2% and 2%–3%, respectively [8]. The two recent approvals with substantial objective responses and improved progression-free survival to *MET* inhibitors, namely capmatinib [9] and tepotinib [10], necessitate the

identification of this alteration upfront.

Next-generation sequencing (NGS), especially RNA sequencing, has emerged as the most relied platform to detect this variation as it detects the structural variation and nullifies the need to detect the 120 different mutations which may lead to this alteration [5]. DNA-based assay suffers from limitations in detecting large deletions (>20 bp) that are common at the 5' donor site [11]. Moreover, many popular NGS panels do not cover the 5' region of the exon 14 and the upstream region of the intron 13 adequately [10]. Far easier is the mRNA-based approach that simply demonstrates the fusion of exon 13 with exon 15 limiting the size and numbers of interrogated regions. However, the RNA-based NGS is not widely available. Besides, the lack of accessibility to NGS and design flaws in DNA panels that do not adequately cover all the mutational sites, necessitates a more

practical alternative that can be used by basic molecular laboratories intending to provide $\Delta MET14$ testing.

Single-gene assays by Sanger sequencing can be designed using DNA as a substrate. However, low analytical sensitivity and the lack of awareness of all genetic changes that leads to $\Delta MET14$ limits the diagnostic utility of Sanger sequencing particularly in the context of limited availability of testing material.

We herein describe our experience of $\Delta MET14$ detection by an mRNA-based assay using polymerase chain reaction followed by fragment sizing, with a final product size being 140 bp smaller in $\Delta MET14$ compared to the wild type *MET* exon 14. The assay has been validated against an RNASeq NGS assay (OncoPrint Focus Assay, Thermo Fisher Scientific, Waltham, MA, USA).

MATERIALS AND METHODS

Specimen collection

All cases of NSCLC that tested negative on single-gene testing for epidermal growth factor receptor (*EGFR*)/anaplastic lymphoma kinase (*ALK*)/ROS proto-oncogene 1 (*ROS1*) alterations and underwent NGS-based genomic profiling upfront at our center from 2018 to 2020 were included. The clinical and pathological features were retrieved and collated from the medical record archives of the hospital.

Next-generation sequencing

The NGS panel used was the OncoPrint Focus Assay comprising 52 genes implicated across various solid organ malignancies, interrogating single nucleotide variations and fusions as well as copy number alterations. The details of this assay methodology can be found elsewhere [12].

Fragment sizing assay

This is a home brew assay which was developed with the concept that the transcripts from true $\Delta MET14$ will be shorter by ~140 bases than their wild type counterparts. The cases which were called *MET* exon 14 skipping positive on NGS were subjected to this assay, along with 13 healthy controls in order to establish the validity for true negatives (Fig. 1).

Primer design

This is an RNA-based polymerase chain reaction (PCR) assay and the primers have been designed using hg19 human reference genome sequence of the *MET* gene (NM_001127500.2). The primers were designed using NCBI (National Center for

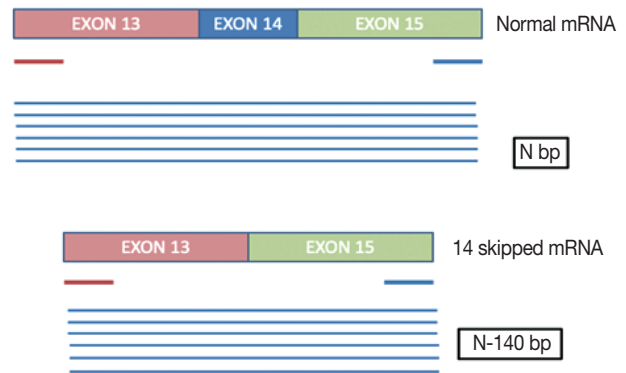


Fig. 1. Image illustrates the difference in size of the fragments between wild type and mutant $\Delta MET14$ mRNA.

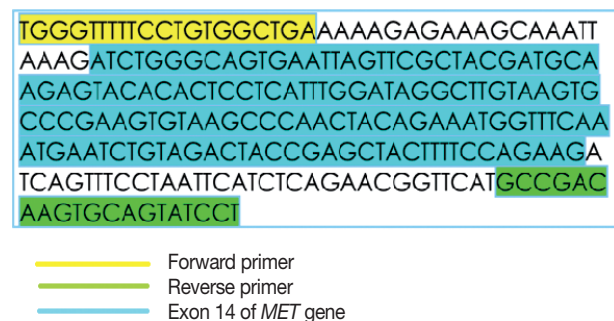


Fig. 2. Primer design for fragment sizing assay for $\Delta MET14$. The bases highlighted in yellow comprise the forward primer while those in green make the reverse primer. Nucleotides in blue belong to exon 14 (National Center for Biotechnology Information).

Biotechnology Information) primer blast using cDNA molecule. The product size is 235 bp for *MET* exon 14 skipping wild type, whereas the *MET* exon 14 skipping mutant was 141 bp shorter. The primer design is depicted in Fig. 2 and the primer sequences are as follows: forward primer, 5'-TGGGTTTTCTGTGGCTGA-3'; reverse primer, 5'-AGGATACTGCACTTGTCGGC-3'.

To assess the presence of RNA, housekeeping gene β -actin is used as assay process and extraction control. The product size is ~92 bp which is concordant with the 94-bp product size of the mutant *MET* exon 14 skipping. The primer sequences used for β -actin are as follows: forward primer, 5'-CCACACTGTGCCATCTACG-3'; reverse primer, 5'-AGGATCTTCATGAGGTAGTCAGTCAG-3'.

RNA extraction and cDNA synthesis

Total RNA was extracted from formalin-fixed paraffin-embedded (FFPE) tumor blocks using the Promega ReliaPrep FFPE Total RNA Mini-prep System (Z1002, Madison, WI, USA). Nucleic acid was quantified using Qubit 3.0 Fluorometer (Invi-

trogen, Life Technologies, Carlsbad, CA, USA). cDNA was synthesized from 10 ng of RNA using the SuperScript VILO cDNA synthesis kit (11754050, Thermo Fisher Scientific). The protocol followed was according to the vendor's insert and the cycling conditions were as follows: reverse transcription step at 42°C for 30 minutes and enzyme denaturation at 85°C for 5 minutes.

Polymerase chain reaction for *MET* exon 14 skipping mutation

The PCR reaction mixture was prepared in proportions as per manufacturer recommendations. The Thermo Fisher Scientific Applied Biosystems Veriti 96-Well Thermal Cycler was used for amplifying this reaction mix with the following cycling conditions: 45 cycles of denaturation at 95°C for 30 seconds, followed by annealing at 56°C for 20 seconds, then elongation at 72°C for 30 seconds, and final extension step at 72°C for 7 minutes. The prepared PCR products were electrophoresed using 3% agarose gel. The expected PCR products using the primers described above are (1) *MET* exon 14 wild type, ~235 bp and (2) Δ *MET14*, ~94 bp. The presence of a single small band of ~94 bp was also considered positive for *MET* exon 14 skipping. For each reaction, a 100 bp ladder, a known positive control, and a known negative control along with no-template controls were run (Fig. 3).

Fragment length analysis using TapeStation

Following the analysis using agarose gel-based electrophoresis, the products were also analyzed using capillary electrophoresis/fragment length analysis on the Agilent 4200 TapeStation system (Agilent, Santa Clara, CA, USA). Tape station examination was done using high sensitivity D1000 DNA screen tapes for analyzing the size, quantity, and integrity of the samples. For each sample, 2 μ L of high sensitivity D1000 sample buffer was added to 2 μ L of the sample in the provided tube strip which was sealed using the cap strip. After this, the product was vortex mixed using IKA vortex at 2,000 rpm for 1 minute and spun at 1,000 rpm for 1 minute. The sample was then loaded in the TapeStation and analyzed using the Agilent TapeStation Analysis Software. The presence of a single peak at 235 bp length was considered *MET* exon 14 wildtype and the presence of single peak at 90–110 bp was considered mutant. The presence of two peaks, each at 235 bp and 90–110 bp, was also considered *MET* exon 14 mutant (Fig. 3).

RESULTS

Baseline characteristics

Of the four hundred and three cases of NSCLC, single-gene testing for *EGFR* mutations, *ALK* rearrangements, and *ROS1* rearrangements were positive in 161 cases (40%) (*EGFR* alterations, 117 [29.1%] cases; *ALK* rearrangements, 32 cases [8%]; and *ROS1* rearrangements, 12 cases [2.7%]). The 242 cases which were wild type for these three underwent NGS testing upfront, of which 13 cases of Δ *MET14* (3.2%) were detected. The median age of the cohort was 61 years (range, 37 to 82 years). There were six males (46.2%) and seven females (53.8%). There were three smokers (23.1%) and 10 non-smokers (76.9%). All cases (100%) depicted adenocarcinoma histology with acinar pattern (Table 1).

Comparison of NGS and agarose gel electrophoresis

Thirteen cases of Δ *MET14* mutation were detected on NGS using RNA-based sequencing. However, no corresponding DNA alteration in terms of indels or missense mutations was found in any of these cases. All these cases were subjected to agarose gel electrophoresis as described above, and nine cases were found to be positive on gel electrophoresis. Four of these cases were negative on gel electrophoresis. All 13 healthy controls also yielded a negative result. Considering the NGS as a gold standard, the overall concordance rate was 84.6%, with sensitivity of 69.2% and specificity of 100% ($p < .01$). The lack of any bands in the negative cases was not the consequence of poor quality of the extracted RNA, as the beta-actin housekeeper amplified and yielded an optimal product.

Comparison of NGS and automated electrophoresis using TapeStation

All 13 cases that were subjected to agarose gel electrophoresis also underwent automated capillary electrophoresis using TapeStation. 10 cases showed peaks at 95–100 bp (positive for Δ *MET14*) and three cases were negative. The overall concordance rate was 88.4% with a calculated sensitivity of 76.9% and specificity of 100% ($p < .001$). An overview of patient recruitment and results is depicted in Fig. 4.

DISCUSSION

Δ *MET14* has gained importance owing to the recent development and approvals of selective *MET* inhibitors like capmatinib and tepotinib [9,10]. These are usually reported at a frequency of 3%–5% in NSCLC [13], and in this study, the frequency

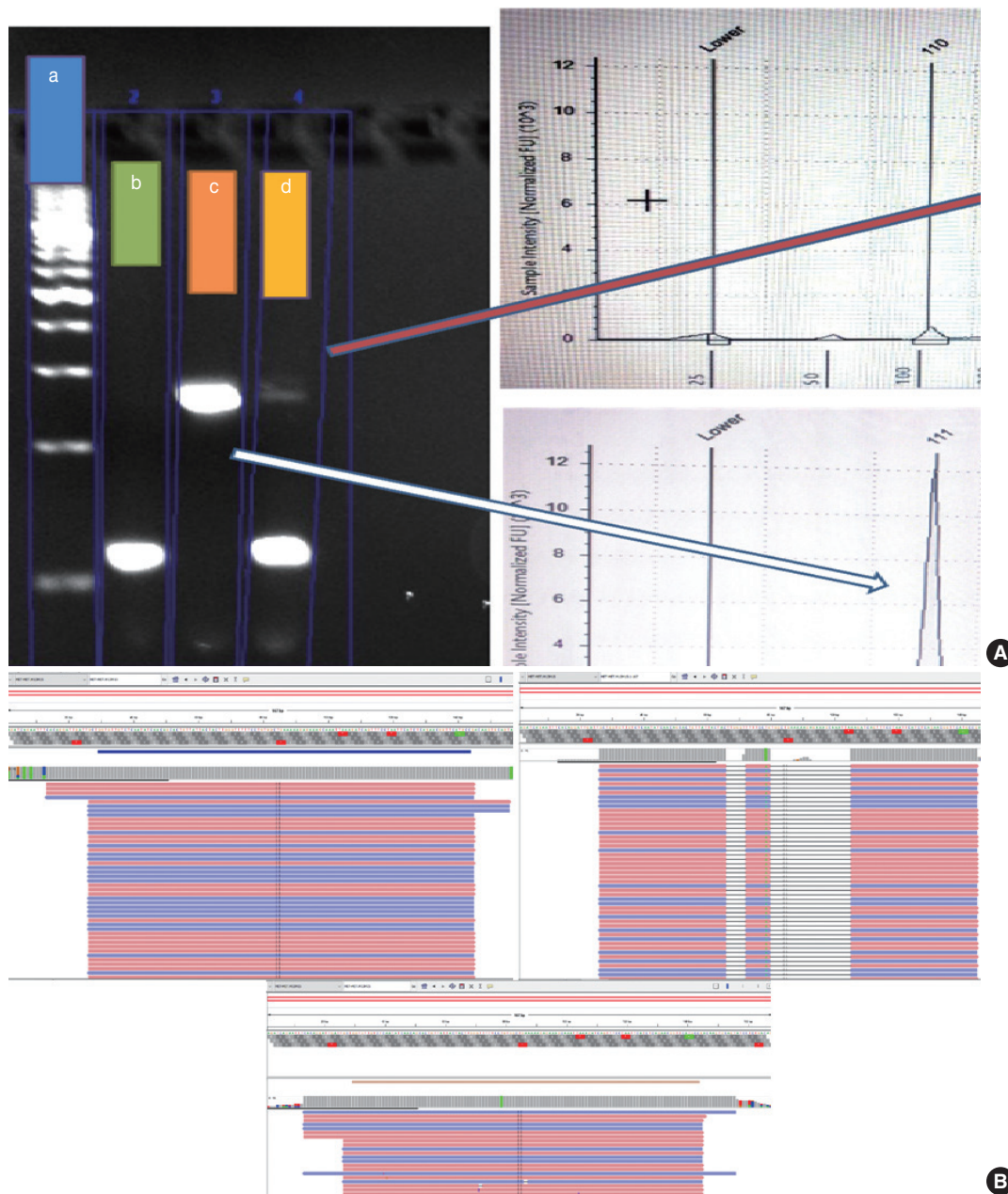


Fig. 3. (A) Analysis of two representative cases on polymerase chain reaction (PCR)-based gel electrophoresis and automated electrophoresis using Tape Station. a, DNA ladder; b, positive control for Δ *MET14*; c, sample positive for Δ *MET14*; d, sample negative for Δ *MET14*. (B) Mapped reads for Δ *MET14* using next-generation sequencing-based assay. Good mapped reads for Δ *MET14* (upper left panel). False call due to reads showing big deletions and polymorphism resulting in poor mapping quality (upper right panel). Integrative Genomics Viewer showing fewer mapped reads (low mutant allele frequency which may lead to a negative result of PCR-based assays (lower panel).

was 5.3% among cases that were tested by NGS, whereas the frequency was 3.2% among the entire NSCLC cohort.

We described an mRNA-based fragment sizing assay using both gel and capillary electrophoresis and we demonstrated 100% specificity for both, with concordance rates of 84.6% and 88.2% with NGS, respectively. Currently, there are no single-

gene assay kits available for the detection of this alteration. Several home brew assays have been described in literature using different modalities like real-time PCR and Sanger sequencing. Kim et al. [14] described the concordance of mRNA-based real-time reverse transcriptase PCR (qRT-PCR) and DNA-based Sanger sequencing against NGS as a gold standard, and dem-

onstrated 100% sensitivity and 97.4% specificity for qRT-PCR. The same for Sanger-based assay was 61.5% and 100%, respectively. The specificity of our assay was also 100%; however, the sensitivity was lower than qRT-PCR, and higher than Sanger sequencing. This may be attributed to the inability to detect large deletions on DNA-based alterations, as well as lower sensitivity of Sanger sequencing. A similar assay has been described by O'Brien et al. [15] using a one-step RNA-based PCR assay to detect $\Delta MET14$, and they reported that this assay could potentially detect *MET* exon 14 skipped RNA with a lower limit of detection of approximately 10%.

Cases that tested negative on fragment sizing assay and positive on NGS-based assay had low mutant allele frequency as observed on Integrative Genomics Viewer (IGV) (Fig. 3B). The

Table 1. Baseline clinical characteristics of the study cohort

Clinical feature	No. (%)
Age (yr), median (range)	61 (37–82)
Sex	
Male	6 (46.2)
Female	7 (53.8)
Smoking status	
Never smoker	10 (76.9)
Smoker	3 (23.1)
Histology	
Adenocarcinoma	13 (100)
Acinar pattern	13 (100)

NGS-based tests have a higher analytical sensitivity (limit of detection) of 1%, which is not likely to be matched by PCR-based assays as described here.

DNA-based alteration was not detected in any of the cases included in this study. This is attributed to the design of the OncoPrint Focus Assay Panel. The 5' end of the exon 14 of the *MET* gene is not covered by the primers and amplicons are not generated for sequencing as depicted in Fig. 5. This region is the major

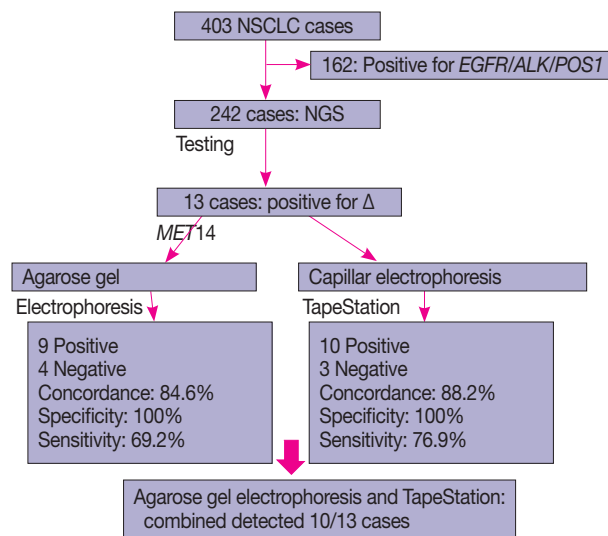


Fig. 4. Consort diagram showing an overview of cases included in the study along with the test results.

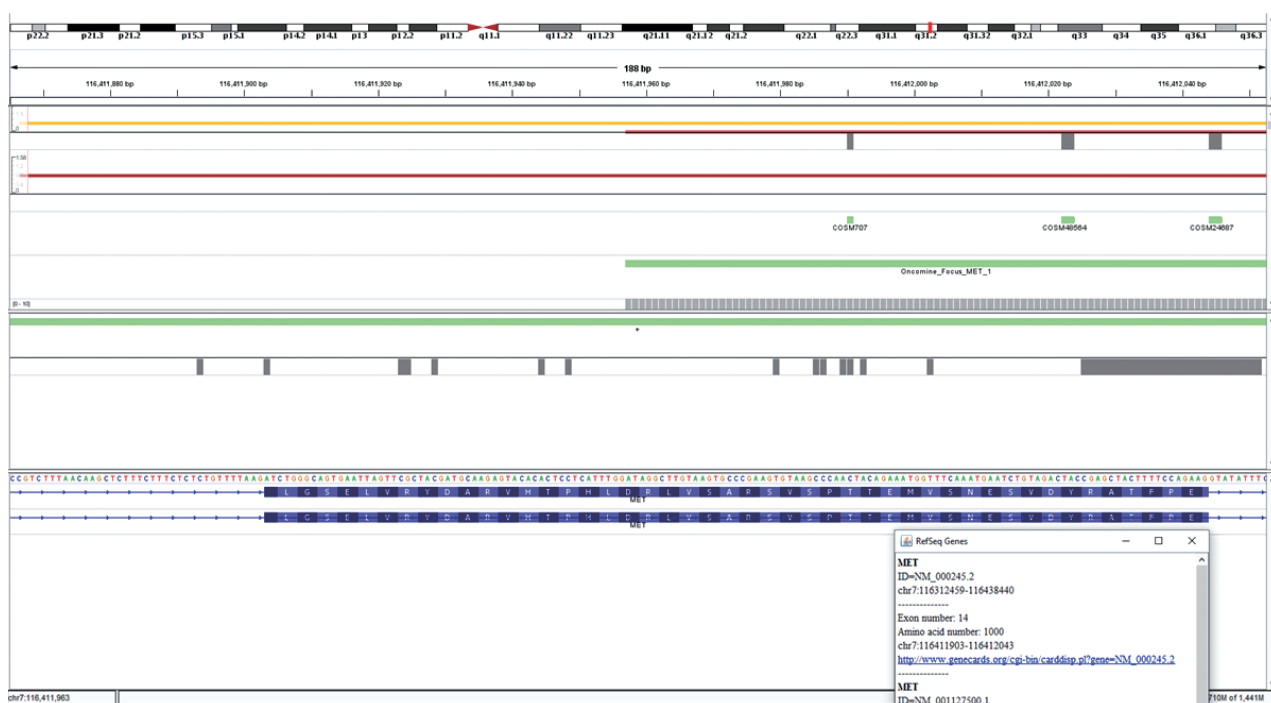


Fig. 5. Integrative Genomics Viewer image showing the coverage of *MET* exon 14 in the OncoPrint Focus Assay.

site for missense variants and indels resulting in ΔMET^{14} . These are therefore likely to be on DNA-based analysis.

There were four discordant cases on agarose gel electrophoresis and three on automated capillary electrophoresis. These are attributed to lower sensitivities of these two assays when compared to the NGS gold standard. However, combining both improved the sensitivity to 76.9%.

Although validated in-house, this assay suffers from a few limitations. The extraction process control used is beta-actin and not another conserved area of the *MET* gene, as most of the exons in the *MET* gene depict high rates of occurrence of single nucleotide polymorphisms. The assay has not been validated on an external control/cell line, and the samples used for validation are from known patients, hence the accuracy of the assay may not be representative. However, this assay will prove beneficial for small- and medium-sized labs where skilled technical personnel and NGS platforms are unavailable. Additionally, squamous carcinomas with ΔMET^{14} are also considered actionable and usually do not undergo broad panel-based testing, hence single-gene assays which are cost-effective will prove beneficial in such settings.

Ethics Statement

This material is author's original work which has not been published elsewhere. This study has been done in accordance with the Declaration of Helsinki and has received approval from Institutional Ethics Committee and Review Board (RGCIRC/IRB-BHR/46/2021). Since no extra samples were taken, written consent of the patients was not required.

Availability of Data and Material

The datasets generated or analyzed during the study are available from the corresponding author on reasonable request.

Code Availability

Not applicable.

ORCID

Anurag Mehta	https://orcid.org/0000-0001-6517-3664
Shrinidhi Nathany	https://orcid.org/0000-0001-6006-6309
Aanchal Chopra	https://orcid.org/0000-0001-6875-9222
Sakshi Mattoo	https://orcid.org/0000-0001-7396-3711
Dushyant Kumar	https://orcid.org/0000-0003-2749-789X
Manoj Kumar Panigrahi	https://orcid.org/0000-0003-0005-1230

Author Contributions

Conceptualization: AM. Data curation: SN. Formal analysis: SN. Investigation: AC. Methodology: SM, AC. Project administration: DK. Resources: MKP. Software: SN. Supervision: AM. Validation: AC, MKP, DK. Visualization: SN. Writing—original draft: SN, AC. Writing—review & editing: AM.

Conflicts of Interest

The authors declare that they have no potential conflicts of interest.

Funding Statement

No funding to declare.

References

1. Organ SL, Tsao MS. An overview of the c-MET signaling pathway. *Ther Adv Med Oncol* 2011; 3(1 Suppl): S7-19.
2. Saffroy R, Fallet V, Girard N, et al. *MET* exon 14 mutations as targets in routine molecular analysis of primary sarcomatoid carcinoma of the lung. *Oncotarget* 2017; 8: 42428-37.
3. Tong JH, Yeung SF, Chan AW, et al. *MET* amplification and exon 14 splice site mutation define unique molecular subgroups of non-small cell lung carcinoma with poor prognosis. *Clin Cancer Res* 2016; 22: 3048-56.
4. Socinski MA, Pennell NA, Davies KD. *MET* exon 14 skipping mutations in non-small-cell lung cancer: an overview of biology, clinical outcomes, and testing considerations. *JCO Precis Oncol* 2021; 5: PO.20.00516.
5. Chakravarty D, Gao J, Phillips SM, et al. OncoKB: a precision oncology knowledge base. *JCO Precis Oncol* 2017; 2017: PO.17.00011.
6. Heist RS, Shim HS, Gingipally S, et al. *MET* exon 14 skipping in non-small cell lung cancer. *Oncologist* 2016; 21: 481-6.
7. Schrock AB, Frampton GM, Suh J, et al. Characterization of 298 patients with lung cancer harboring *MET* exon 14 skipping alterations. *J Thorac Oncol* 2016; 11: 1493-502.
8. Cancer Genome Atlas Research Network. Comprehensive molecular profiling of lung adenocarcinoma. *Nature* 2014; 511: 543-50.
9. Wolf J, Han J, Nishio M, et al. GEOMETRY Mono-1: phase II, multicenter study of MET inhibitor capmatinib (INC280) in EGFR wt, MET-dysregulated advanced NSCLC. *J Thorac Oncol* 2017; 12(11 Suppl 1): S1578-9.
10. Reungwetwattana T, Liang Y, Zhu V, Ou SI. The race to target MET exon 14 skipping alterations in non-small cell lung cancer: the why, the how, the who, the unknown, and the inevitable. *Lung Cancer* 2017; 103: 27-37.
11. Buermans HP, den Dunnen JT. Next generation sequencing technology: advances and applications. *Biochim Biophys Acta* 2014; 1842: 1932-41.
12. Mehta A, Nathany S, Tripathi R, Sharma SK, Saifi M, Batra U. Non-amplification genetic alterations of *HER2* gene in non-small cell lung carcinoma. *J Clin Pathol* 2021; 74: 106-10.
13. Pilotto S, Gkoutakos A, Carbognin L, Scarpa A, Tortora G, Bria E. *MET* exon 14 juxtamembrane splicing mutations: clinical and therapeutic perspectives for cancer therapy. *Ann Transl Med* 2017; 5: 2.
14. Kim EK, Kim KA, Lee CY, et al. Molecular diagnostic assays and clinicopathologic implications of *MET* exon 14 skipping mutation in non-small-cell lung cancer. *Clin Lung Cancer* 2019; 20: e123-32.
15. O'Brien O, Wright MC, O'Brien C, et al. Cost-efficient and easy to perform PCR-based assay to identify *Met* exon 14 skipping in formalin-fixed paraffin-embedded (FFPE) non-small cell lung cancer (NSCLC) samples. *Diagnostics (Basel)* 2019; 9: 13.

Upward trend in follicular lymphoma among the Korean population: 10-year experience at a large tertiary institution

Meejeong Kim¹, Hee Sang Hwang¹, Hyungwoo Cho², Dok Hyun Yoon²,
 Cheolwon Suh², Chan Sik Park¹, Heounjeong Go¹, Jooryung Huh¹

Departments of ¹Pathology and ²Oncology, Asan Medical Center, University of Ulsan College of Medicine, Seoul, Korea

Background: Follicular lymphoma (FL) is the second most common non-Hodgkin lymphoma (NHL) in Western countries. However, it is relatively rare in Asia. This study examined epidemiologic characteristics of FL in South Korea, with an emphasis on recent trends of increase in cases. **Methods:** We retrospectively examined 239 cases of newly diagnosed FL at a large tertiary institution in Korea (Asan Medical Center, Seoul, Republic of Korea) between 2008 and 2017. Age-adjusted incidence rates and clinicopathological variables were analyzed, and joinpoint regression analysis was used to identify the changes. **Results:** The age-adjusted incidence of FL significantly increased during the study period ($p = .034$), and the ratio of (relative incidence) patients with FL to patients with NHL increased from 4.28% to 9.35% in the same period. Over the 10-year study assessment duration, the proportion of patients with stage III/IV FL ($p = .035$) and expression of BCL2 ($p = .022$) or BCL6 ($p = .039$) significantly increased. From 2013–2017, the proportion of patients with high-risk Follicular Lymphoma International Prognostic Index (FLIPI) score increased (21.5% to 28.7%), whereas that of low-risk FLIPI decreased (55.4% to 38.6%), although those results were not statistically significant ($p = .066$). **Conclusions:** We found an increasing incidence of FL, with a disproportionate increase in the incidence of high-stage disease and recent changes in the clinicopathologic features of the Korean patient population.

Key Words: Follicular lymphoma; Korea; Follicular Lymphoma International Prognostic Index (FLIPI); BCL2; BCL6

Received: April 13, 2021 **Revised:** June 26, 2021 **Accepted:** July 25, 2021

Corresponding Author: Jooryung Huh, MD, PhD, Department of Pathology, Asan Medical Center, University of Ulsan College of Medicine, 88 Olympic-ro 43-gil, Songpa-gu, Seoul 05505, Korea

Tel: +82-2-3010-4553, Fax: +82-2-472-7898, E-mail: jrhu@amc.seoul.kr

Corresponding Author: Heounjeong Go, MD, PhD, Department of Pathology, Asan Medical Center, University of Ulsan College of Medicine, 88 Olympic-ro 43-gil, Songpa-gu, Seoul 05505, Korea

Tel: +82-2-3010-5888, Fax: +82-2-472-7898, E-mail: damul37@amc.seoul.kr

Follicular lymphoma (FL) is the second most common non-Hodgkin lymphoma (NHL) in Western countries and accounts for 20% to 35% of all lymphomas [1,2]. In Asia, until recently, the incidence has been characteristically low, at approximately 5% to 10% of all lymphomas in most studies [3,4]. However, the relative proportion of FL in many Asian populations has increased rapidly in recent years, and FL is now the second most common low-grade B-cell lymphoma after mucosa-associated lymphoid tissue lymphoma in Asia [3,5-7]. The proportion of FL to NHL increased from 8.1% to 23.5% in China and 5% to 20% in Japan [3,4,7,8]; additionally, an increase in the proportion in Korea, from 3.4% to 4.8% between 1999 and 2012, has been reported [9,10].

FL is characterized by indolent clinical behavior, and most

cases involve a low histologic grade and low-risk Follicular Lymphoma International Prognostic Index (FLIPI), which is determined based on the sum of points assigned for each of the following risk factors: age > 60 years, elevated lactate dehydrogenase (LDH) level, hemoglobin (Hb) level < 12 g/dL, Ann Arbor stage III/IV, and involvement of more than four nodal sites. Grade 3B FL or transformation to high-grade B-cell lymphoma significantly reduces survival [11,12]. However, due to the availability and broad use of rituximab, the incidence of transformation has been reduced, and the distribution of clinicopathologic features including histologic grade and FLIPI subgroup has changed, although the differences have not been reported consistently [12-14]. Most of the information in the literature is based on studies involving Caucasian patients, and characteristics of FL in East Asians have

not been delineated well. In light of the recent increase in the incidence of FL in the Korean population, we investigated the trends in incidence of FL from 2008 to 2017, using data from a large tertiary institution in South Korea, and examined the clinicopathologic features of FL in the Korean population.

MATERIALS AND METHODS

Age-adjusted incidence rate of FL and frequency of FL and NHL

The age-adjusted incidence rate, which is a weighted average of the age-specific crude rate, was calculated using data from Korean Statistical Information Service (<http://kosis.kr/index/index.do>). The age-adjusted incidence rates per 100,000 were calculated by dividing the annual number of FL cases observed in a specific age group of patients treated at Asan Medical Center between 2008 and 2017, by the number of corresponding person-years of observation; the obtained result was multiplied by 100,000.

Additionally, we retrieved the total numbers of inpatients and of patients with NHL or FL treated at Asan Medical Center, Seoul, between 2008 and 2017, using the Asan Biomedical research Environment, i.e., ABLE, research information retrieval system. The annual frequency of patients with NHL or FL was calculated using the date of initial diagnosis.

Patient selection

A total of 239 patients diagnosed with FL between 2008 and 2017, at Asan Medical Center was included in this retrospective study. The study included patients from whom excisional ($n = 215$) and needle ($n = 24$) biopsy specimens were collected before treatment. The following demographic and clinical data were collected by reviewing the patients' medical records: age, sex, presence or absence of B symptoms (fever, night sweats, and weight loss), transformation to diffuse large B-cell lymphoma (DLBCL) (during follow-up), complete blood count, serum LDH level, bone marrow involvement, Ann Arbor stage, FLIPI risk group, and treatment modalities.

Pathological review and immunohistochemistry data

All cases were reviewed, and based on the revised 4th edition of the World Health Organization classification criteria, patients with testicular FL, duodenal-type FL, and pediatric-type FL were excluded [2]. The following pathological parameters were recorded: histologic grade (grades 1–2, grade 3A, and grade 3B), histologic pattern (follicular, follicular and diffuse, and diffuse), and immunophenotype (expression of BCL2, BCL6, CD10, or

Ki-67). Immunohistochemical (IHC) staining was performed on whole slides using a fully automated IHC assay on a Ventana BenchMark XT Autostainer (Ventana Medical Systems, Woonsocket, RI, USA). Antibodies specific for the following markers were used: CD3 (clone PS1, mouse mAb, Novocastra, Newcastle-upon-Tyne, UK), CD5 (clone 4C7, mouse mAb, Novocastra), CD20 (clone L26, mouse mAb, Novocastra), Ki-67 (mouse mAb, Dako, Glostrup, Denmark), CD10 (clone 56C6, mouse mAb, Novocastra), CD21 (clone 2G9, mouse mAb, Novocastra), BCL2 (clone E17, rabbit mAb, Cell Marque, Rocklin, CA, USA), and BCL6 (clone GI191E/A8, mouse mAb, Cell Marque). Immunostained slides from 239 FL cases were reviewed, and immunopositivity was defined as protein expression by $\geq 30\%$ of the tumor cells [15–18]. Ki-67 proliferation index (PI) was assessed manually in neoplastic follicles, and a Ki-67 PI $\geq 30\%$ was deemed as high expression [19–23].

Statistical analyses

Joinpoint regression analysis was performed to identify the changes in the incidence rates of FL at Asan Medical Center, using the Joinpoint Trend Analysis Software (ver. 4.8.0.1, Statistical Methodology and Application Branch, Surveillance Research Program, Division of Cancer Control and Population Sciences, National Cancer Institute). Joinpoint regression analysis usually is applied to study varying trends over time to identify the time point(s) at which the trends show significant changes [24–26]. Based on the trend analysis, we estimated the annual percentage change (APC) in the rates between trend-change points and the average annual percentage change (AAPC) for the entire study period. When there was no joinpoint (no significant change in trend), the APC was equal to AAPC.

Simple linear regression analysis was conducted to investigate changes in the proportion of clinicopathologic features of FL over the study period. Chi-square and Fisher exact tests were performed to evaluate the changes in clinicopathologic characteristics from 2008 to 2012, and from 2013 to 2017. In addition, overall survival (OS) was analyzed using the Kaplan-Meier method from the date of diagnosis to the date of death or the last follow-up visit, and data were compared using the log-rank test. All statistical analyses were conducted using SPSS software package ver. 18.0.0 (SPSS Statistics software, SPSS Inc., Chicago, IL, USA) and R ver. 3.6.3 (R Foundation for Statistical Computing, Vienna, Austria). Statistical significance was defined by p -value $< .05$.

RESULTS

Incidence of FL between 2008 and 2017

In total, 8,406 patients (0.17% of total inpatients) with NHL were treated at Asan Medical Center between 2008 and 2017, and 498 patients (0.01% of total inpatients and 5.92% of NHL) had FL. The proportion of FL patients (patients with FL/total inpatients) increased from 0.01% in 2008 to 0.02% in 2017, and the ratio of patients with FL to patients with NHL increased from 4.28% (26/607 cases) in 2008 to 9.35% (103/1102 cases) in 2017 (Supplementary Fig. S1).

Fig. 1 presents the increasing trend in the age-adjusted incidence rates of FL at Asan Medical Center between 2008 and 2017, and one joinpoint that was identified in 2010; the fastest increasing trend was observed in 2008–2010 (APC, 48.3; 95% confidence interval [CI], 9.0 to 101.7) and a moderately increasing trend was observed in 2010–2017 (APC, 10.1; 95% CI, 5.7 to 14.8) (p = .034) (Fig. 1).

Clinicopathologic characteristics during defined periods

The patients with FL (n = 239) included in this study had a median age of 52.1 years (range, 17 to 82 years) with a male:female ratio of 1.13:1. The overall clinicopathologic characteristics and initial treatment modalities used for the 239 patients and changes in the baseline characteristics from 2008 to 2012 and 2013 to 2017 are summarized in Table 1. The proportion of patients aged > 60 years significantly increased from 13.2% in 2008–2012 to 34.5% in 2013–2017 (p = .001) (Table 1). In 2013–2017, the proportion of patients with high-risk FLIPI (21.5% to 28.7%)

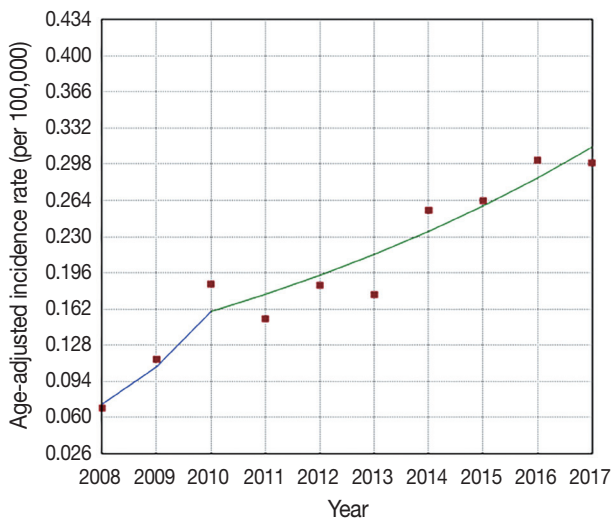


Fig. 1. Age-adjusted incidence rates of follicular lymphoma between 2008 and 2017.

and grade 3B FL (5.9% to 14.0%) increased but not at a statistically significant level (p = .270 and p = .077, respectively) (Table 1).

Fig. 2 outlines the changes in the proportion of patients >60 years of age, with Hb level < 12 g/dL, elevated LDH level, and involvement of more than four nodal sites, which were the factors included in FLIPI score. The proportion of patients aged > 60

Table 1. Baseline patient characteristics

Characteristic	Total (n=239)	Year		p-value
		2008–2012 (n=68)	2013–2017 (n=171)	
Age > 60 yr	68 (28.6)	9 (13.2)	59 (34.5)	.001
Sex				.267
Male	127 (53.1)	40 (58.8)	87 (50.9)	
Female	112 (46.9)	28 (41.2)	84 (49.1)	
B symptom				.751
Absent	212 (90.2)	62 (91.2)	150 (89.8)	
Present	23 (9.8)	6 (8.8)	17 (10.2)	
Hb < 12 g/dL	41 (17.2)	12 (17.9)	29 (17.0)	.861
Elevated LDH	46 (19.8)	15 (23.8)	31 (18.3)	.353
Ann Arbor stage				.111
Stage I/II	90 (37.7)	31 (45.6)	59 (34.5)	
Stage III/IV	149 (62.3)	37 (54.4)	112 (65.5)	
Bone marrow involvement	87 (37.8)	24 (35.8)	63 (38.7)	.688
FLIPI				.270
Low to intermediate	173 (73.3)	51 (78.5)	122 (71.3)	
High	63 (26.7)	14 (21.5)	49 (28.7)	
Histologic grade				.077
1–2/3A	211 (88.3)	64 (94.1)	147 (86.0)	
3B	28 (11.7)	4 (5.9)	24 (14.0)	
Histologic pattern				.018
Follicular	207 (87.7)	56 (82.4)	151 (89.9)	
Follicular and diffuse	20 (8.5)	11 (16.2)	9 (5.4)	
Diffuse	9 (3.8)	1 (1.5)	8 (4.8)	
BCL2 expression				.086
Negative	25 (11.3)	11 (16.9)	14 (8.9)	
Positive	197 (88.7)	54 (83.1)	143 (91.1)	
BCL6 expression				.002
Negative	10 (4.3)	7 (11.1)	3 (1.8)	
Positive	222 (95.7)	56 (88.9)	166 (98.2)	
CD10 expression				.461
Negative	44 (18.8)	14 (21.9)	30 (17.6)	
Positive	190 (81.2)	50 (78.1)	140 (82.4)	
Ki-67 PI ≥ 30%	86 (37.9)	15 (25.0)	71 (42.5)	.016
Treatment				.049
Watch-and-wait	44 (18.4)	6 (8.8)	38 (22.2)	
Rituximab-based	130 (54.4)	40 (58.8)	90 (52.6)	
Radiation monotherapy	30 (12.9)	11 (16.4)	19 (11.5)	
Transformation to DLBCL	19 (8.0)	5 (7.4)	14 (8.2)	.821
Deaths	15 (6.6)	6 (9.0)	9 (5.7)	.387

Values are presented as number (%).

Hb, hemoglobin; LDH, lactate dehydrogenase; FLIPI, Follicular Lymphoma International Prognostic Index; Ki-67 PI, Ki-67 proliferation index; DLBCL, diffuse large B-cell lymphoma.

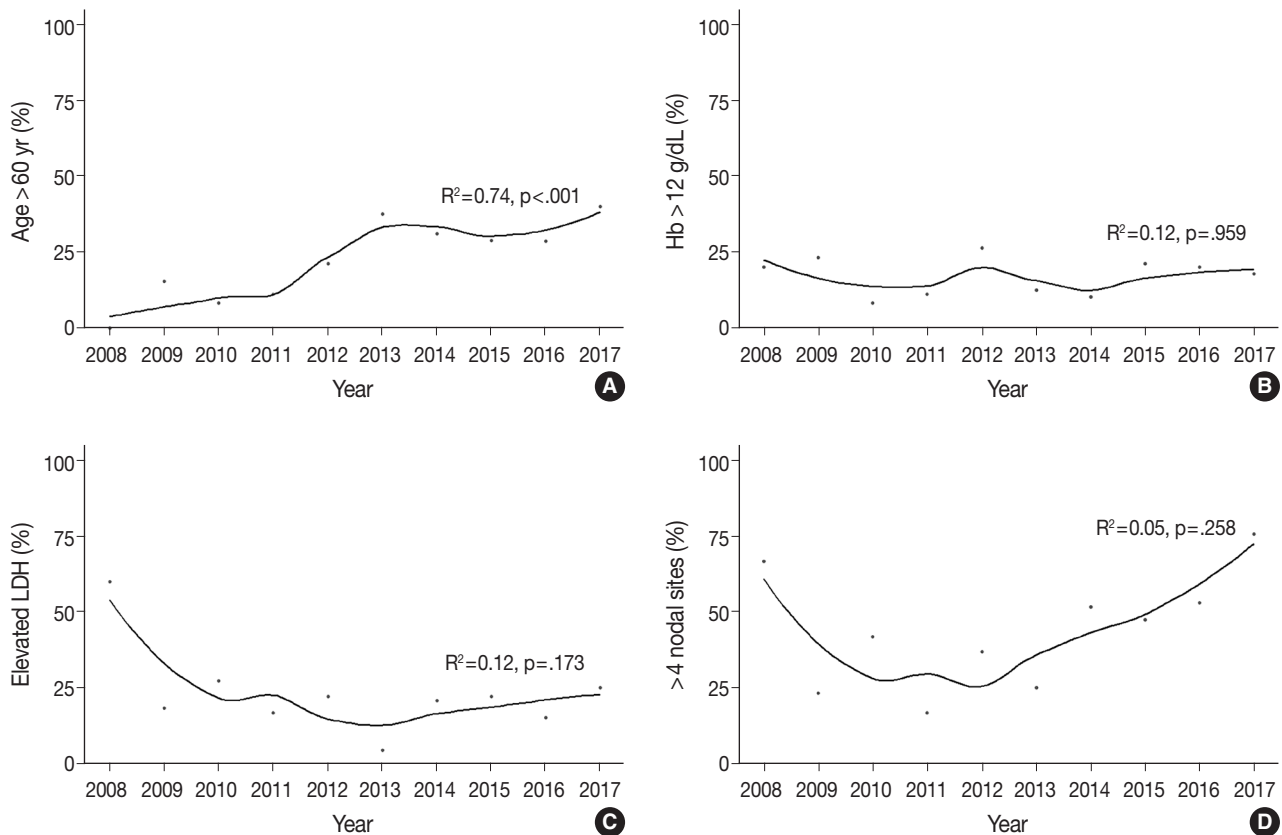


Fig. 2. Scatter plots with trend lines of the annual proportion of patients aged >60 years (A), with hemoglobin (Hb) level < 12 g/dL (B), elevated lactate dehydrogenase (LDH) level (C), and involvement of more than four nodal sites (D).

years significantly increased between 2008 and 2017 ($R^2 = 0.74$, $p < .001$) (Fig. 2A). In contrast, the rates of patients with Hb level < 12 g/dL remained stable ($R^2 = -0.12$, $p = .959$) (Fig. 2B). The proportion of patients with elevated LDH level sharply decreased between 2008 and 2013 (60.0% to 4.3%) and gradually increased to 25.0% in 2017; however, these changes were not statistically significant ($R^2 = 0.12$, $p = .173$) (Fig. 2C). The proportion of patients with involvement of greater than four nodal sites rapidly decreased during 2008–2010 (66.7% to 41.7%), but increased to 75.6% in 2017 ($R^2 = 0.05$, $p = .258$) (Fig. 2D).

Over 10 years, the proportion of patients with stage III/IV disease significantly increased ($R^2 = 0.36$, $p = .039$) (Fig. 3A), as was observed on the joinpoint regression analysis (AAPC, 5.0; 95% CI, 0.4 to 9.7; $p = .035$) (Table 2). We found a decreasing trend in the number of cases of low-risk FLIPI ($R^2 = 0.23$, $p = .094$) and a slightly increasing trend in the number of cases of grade 3B FL ($R^2 = -0.20$, $p = .111$), although the result was not statistically significant (Fig. 3B, C). Regarding histological pattern, the proportions of follicular pattern ($R^2 = 0.24$, $p = .086$) and diffuse pattern ($R^2 = 0.15$, $p = .145$) showed increasing trends,

whereas follicular and diffuse patterns decreased ($R^2 = 0.34$, $p = .045$) (Fig. 3D), and these variations were significant during 2008–2012 and 2013–2017 ($p = .018$) (Table 1).

For the IHC staining results, the rates of FL cases with BCL2 or BCL6 expression and those with Ki-67 PI $\geq 30\%$ increased from 2008 to 2012 and from 2013 to 2017 ($p = .086$, $p = .002$, and $p = .016$, respectively) (Table 1). In the joinpoint regression analysis, the expression levels of BCL2 (AAPC, 2.6; 95% CI, 0.7 to 4.6, $p = .022$) and BCL6 (AAPC, 3.0; 95% CI, 0.4 to 5.7; $p = .028$) significantly increased over the 10 years (Table 2).

Since the 2000s, rituximab has been used widely, and a majority of the patients (54.4%) in this study underwent rituximab-based chemotherapy; however, the proportion of patients on a watch-and-wait strategy significantly increased by 8.8% in 2008–2012 and by 22.2% in 2013–2017, while there was a slight decrease in the number of patients on rituximab-based therapy ($p = .049$) (Table 1). There was no significant variation in other clinicopathologic features, e.g., sex, bone marrow involvement, transformation to DLBCL, and mortality, over the study period.

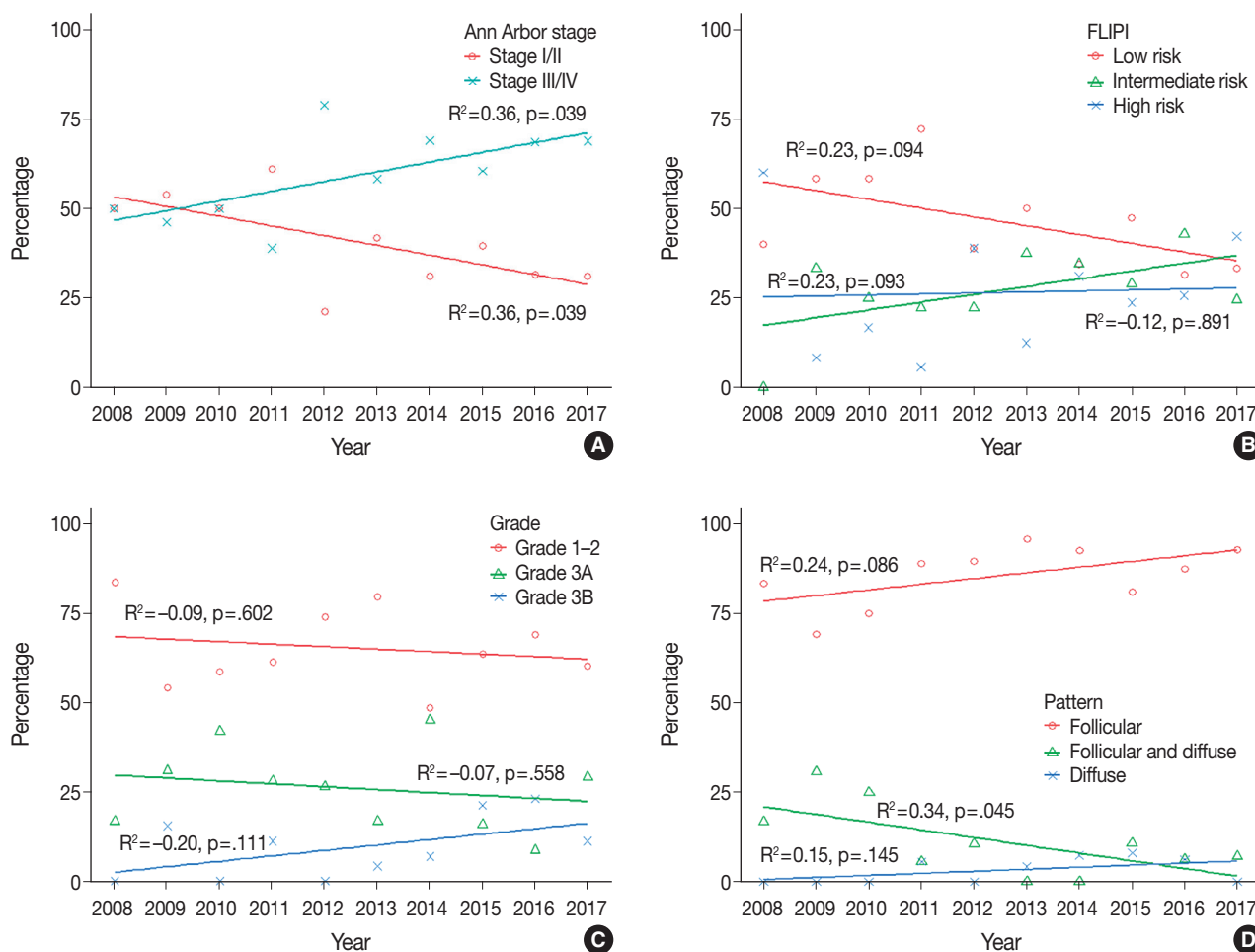


Fig. 3. Scatter plots with trend lines of the annual proportion of patients with follicular lymphoma: (A) Ann Arbor stage, (B) Follicular Lymphoma International Prognostic Index (FLIPI), (C) histologic grade, and (D) histologic pattern.

In survival analysis, during a median follow-up of 47 months (range, 0 to 222 months), 15 patients died, and the mean OS was 199 months. There was no significant OS difference between 2008–2012 and 2013–2017 (Supplementary Fig. S2).

DISCUSSION

The incidence rate of FL, which has been low in Korea, has increased in recent years. Lee et al. [9] studied 65,948 lymphoid diseases in the South Korean population and found increasing incidence of lymphoid malignancies (6.85% to 13.18%) and FL (0.22% to 0.39%) between 1999 and 2012. Kim et al. [27] studied epidemiologic changes in B-cell NHL in South Korea using the National Health Information Database and found that the incidence of FL has increased since 2006: the ratio of FL to NHL increased from 5.6% to 7.8% during 2006–2015, and the age-adjusted incidence of FL increased by 25% between

2011 and 2015. Similarly, in the current study, the incidence of FL significantly increased between 2008 and 2017, with an increasing ratio of FL:NHL. Although previous studies ascribed the low incidence of FL in Asian populations to ethnic differences, the recent trend of increased incidence rates might reflect the increasing adoption of a Westernized lifestyle by Asian populations [6,28].

Currently, the etiology of FL is not understood fully; however, age, sex, ethnicity, genetic, clinical and environmental factors including lifestyle can affect the development of FL. Multiple large cohort studies have investigated the influence of smoking, alcohol intake, obese or overweight status and their relationship to FL development; however, the results have been conflicting [29]. A population-based study by Le et al. [30] in Canada during 1992–2010, demonstrated that the incidence rate of FL increased, especially in concentrated industrial zones, suggesting that industrial exposures play an important role in the develop-

Table 2. Trends in clinicopathologic characteristics of FL: average annual percentage change

Characteristic	AAPC (95% CI)	p-value
Age > 60 yr	na ^a	
Hb < 12 g/dL	1.0 (-0.91 to 12.2)	.833
Elevated LDH	-6.5 (-20.9 to 10.5)	.378
>4 nodal areas involved	6.6 (-5.5 to 20.2)	.254
Ann Arbor stage		
Stage I/II	-6.2 (-12.6 to 0.7)	.070
Stage III/IV	5.0 (0.4 to 9.7)	.035
Bone marrow involvement	3.5 (-5.9 to 13.8)	.455
FLIPI		
Low	-5.3 (-10.8 to 0.6)	.071
Intermediate	na ^a	
High	6.6 (-12.4 to 29.7)	.486
Histologic grade		
1-2	-0.9 (-5.3 to 3.7)	.661
3A	-4.7 (-16.3 to 8.6)	.424
3B	na ^a	
Histologic pattern		
Follicular	2.0 (-0.3 to 4.3)	.120
Follicular and diffuse	na ^a	
Diffuse	na ^a	
BCL2-positive	2.6 (0.7 to 4.6)	.022
BCL6-positive	3.0 (0.4 to 5.7)	.028
CD10-positive	1.0 (-3.0 to 5.2)	.666
Ki-67 PI ≥30%	5.4 (-5.4 to 17.3)	.309
Treatment		
Watch-and-wait	na ^a	
Rituximab-based	2.1 (-4.7 to 9.4)	.550
Radiation monotherapy	na ^a	
Transformation to DLBCL	na ^a	

FL, follicular lymphoma; AAPC, average annual percent change; CI, confidence interval; Hb, hemoglobin; LDH, lactate dehydrogenase; FLIPI, Follicular Lymphoma International Prognostic Index; Ki-67 PI, Ki-67 proliferation index; DLBCL, diffuse large B-cell lymphoma.

^aNot applicable due to zero case counts for some years.

ment of FL. Further, it has been reported that exposure to herbicides is associated with FL by causing a t(14;18)-translocation [30].

In the current study, we found an increasing trend of stage III/IV disease over 10 years, and that the proportions of high-risk FLIPI and grade 3B FL also increased between 2008–2012 and 2013–2017, although the results were not statistically significant. In a study by Conconi et al. [14] that included 281 FL cases from 1979 to 2007, the trend in the proportion of patients aged ≥60 years with stage III/IV disease and high-risk FLIPI scores increased over the study period, although the result was not statistically significant. Mozas et al. [13] studied 727 grade 1–3A FL cases reported between 1980 and 2017, and found that grade 1–2 disease showed a decreasing trend over time, while high-risk FLIPI showed an increasing trend in recent years. These findings can be attributed to the increasing life expectancy

and increase in the number of patients that present with advanced FL status at initial diagnosis, as a majority of the patients are asymptomatic.

We also note that most patients with FL have stage III/IV disease, a low-risk FLIPI score, and grade 1–2 FL, and the findings are comparable to those in the United States, showing predominance of stage III/IV, low-risk FLIPI score, and grade 1–2, with similar results to our data [29,31]. Cho et al. [5] retrospectively analyzed clinical characteristics and pathologic features of BCL2 expression in 343 FL patients in Korea during 1993–2013, and demonstrated that predominance of stage III/IV, low-risk FLIPI score, and grade 1–2 FL, suggesting that there was no significant difference between Korean and Western populations.

In this study, BCL2 or BCL6 immunopositivity significantly increased over the study period. We investigated whether the expression of BCL2 or BCL6 was associated with histologic grade; however, those unexpected findings were not associated with changes in the proportion of histologic grade (Supplementary Table S1). Although several studies have shown that the expression of BCL2 was less common in high-grade FL, the relationship between expression of BCL2 or BCL6 and histologic grade was not definitive in most prior studies [32–35].

The proportion of FL cases with Ki-67 PI ≥30% and diffuse pattern significantly increased between 2008–2012 and 2013–2017, and was significantly correlated with histologic grade (Supplementary Table S1). Most prior studies have shown that higher Ki-PI or diffuse pattern in FL generally correlates with higher grade or poor prognosis, although several FL cases with low grade and high Ki-PI have been described [2,22,23,36]. In this study, Ki-PI was estimated manually and might have produced intra- and interobserver variability. However, recent studies using software-automated quantification of Ki-67 PI in FL have shown that high Ki-67 PI was associated with grade 3 FL or poor prognosis [19,21].

There were some limitations to this study. The low incidence of FL in our institutional series might have led to overestimation of the proportion of clinicopathologic features and inadequate statistical significance in the changes over the study period. FL has an indolent prognosis with a favorable outcome, and the number of events (e.g., death) per group was insufficient in the current study, in which large numbers of individuals were censored in the survival analysis. Thus, multicenter studies should be performed to precisely address the trends of FL in Korea. Our study was not a population-based study and lacks representativeness. However, we found an increase in the age-adjusted incidence rate of FL using data from a large tertiary institution,

which is an accepted approach that can be adopted to allow better comparison [37,38]. In addition, the increasing incidence of FL and the ratio of FL to NHL observed in our data were similar to the trends observed in the National Health Information Database [27].

In conclusion, our study demonstrated an increase in the incidence rates of FL at a large tertiary institution in South Korea over the last 10 years, and we found recent changes in the clinicopathologic features of FL, an aspect that rarely has been studied.

Supplementary Information

The Data Supplement is available with this article at <https://doi.org/10.4132/jptm.2021.07.25>.

Ethics Statement

All procedures performed in the current study were approved by the Institutional Review Board (IRB) of Asan Medical Center with a waiver of informed consent (IRB No. 2019-0509) and performed in accordance with the principles of the Declaration of Helsinki.

Availability of Data and Material

The datasets generated or analyzed during the study are available from the corresponding author on reasonable request.

Code Availability

Not applicable.

ORCID

Meejeong Kim <https://orcid.org/0000-0002-1232-8439>
 Hee Sang Hwang <https://orcid.org/0000-0001-9486-9214>
 Hyungwoo Cho <https://orcid.org/0000-0003-4307-2795>
 Dok Hyun Yoon <https://orcid.org/0000-0002-8289-3548>
 Cheolwon Suh <https://orcid.org/0000-0002-9178-4431>
 Chan Sik Park <https://orcid.org/0000-0001-9783-4498>
 Heounjeong Go <https://orcid.org/0000-0003-0412-8709>
 Jooryung Huh <https://orcid.org/0000-0002-2148-5778>

Author Contributions

Conceptualization: MK, JH. Data curation: MK, HSH. Formal analysis: MK, HSH. Investigation: MK, HC, DHY, CS, HG. Methodology: MK, HSH, HC, HG. Project administration: HG, JH. Resources: MK, DHY, CS. Supervision: HG, CSP, JH. Validation: HSH, HG, CSP, JH. Visualization: MK, HSH. Writing—original draft: MK, HG, JH. Writing—review & editing: MK, HSH, HG, CSP, JH. Approval of final manuscript: all authors.

Conflicts of Interest

H.G., a contributing editor of the *Journal of Pathology and Translational Medicine*, was not involved in the editorial evaluation or decision to publish this article. All remaining authors have declared no conflicts of interest.

Funding Statement

No funding to declare.

References

1. Freedman A. Follicular lymphoma: 2018 update on diagnosis and

- management. *Am J Hematol* 2018; 93: 296-305.
2. Swerdlow SH, Campo E, Harris NL, et al. WHO classification of tumours of haematopoietic and lymphoid tissues. Lyon: International Agency for Research on Cancer, 2017.
3. Guidelines for the diagnosis and treatment of follicular lymphoma in China. *Cancer Biol Med* 2013; 10: 36-42.
4. Yoshino T, Takata K, Tanaka T, Sato Y, Tari A, Okada H. Recent progress in follicular lymphoma in Japan and characteristics of the duodenal type. *Pathol Int* 2018; 68: 665-76.
5. Cho SH, Suh C, Do YR, et al. Clinical features and survival of patients with follicular lymphoma in Korea. *Clin Lymphoma Myeloma Leuk* 2016; 16: 197-202.
6. Intragumtornchai T, Bunworasate U, Wudhikarn K, et al. Non-Hodgkin lymphoma in South East Asia: an analysis of the histopathology, clinical features, and survival from Thailand. *Hematol Oncol* 2018; 36: 28-36.
7. Takata K, Miyata-Takata T, Sato Y, Yoshino T. Pathology of follicular lymphoma. *J Clin Exp Hematop* 2014; 54: 3-9.
8. Bai B, Huang HQ. Individualized management of follicular lymphoma. *Chin Clin Oncol* 2015; 4: 7.
9. Lee H, Park HJ, Park EH, et al. Nationwide statistical analysis of lymphoid malignancies in Korea. *Cancer Res Treat* 2018; 50: 222-38.
10. Yoo KH, Lee H, Suh C; CISL. Lymphoma epidemiology in Korea and the real clinical field including the Consortium for Improving Survival of Lymphoma (CISL) trial. *Int J Hematol* 2018; 107: 395-404.
11. Mustafa Ali M, Rybicki L, Nomani L, et al. Grade 3 follicular lymphoma: outcomes in the rituximab era. *Clin Lymphoma Myeloma Leuk* 2017; 17: 797-803.
12. Federico M, Caballero Barrigon MD, Marcheselli L, et al. Rituximab and the risk of transformation of follicular lymphoma: a retrospective pooled analysis. *Lancet Haematol* 2018; 5: e359-67.
13. Mozas P, Nadeu F, Rivas-Delgado A, et al. Patterns of change in treatment, response, and outcome in patients with follicular lymphoma over the last four decades: a single-center experience. *Blood Cancer J* 2020; 10: 31.
14. Conconi A, Motta M, Bertoni F, et al. Patterns of survival of follicular lymphomas at a single institution through three decades. *Leuk Lymphoma* 2010; 51: 1028-34.
15. Karube K, Guo Y, Suzumiya J, et al. CD10-MUM1+ follicular lymphoma lacks BCL2 gene translocation and shows characteristic biologic and clinical features. *Blood* 2007; 109: 3076-9.
16. Hans CP, Weisenburger DD, Greiner TC, et al. Confirmation of the molecular classification of diffuse large B-cell lymphoma by immunohistochemistry using a tissue microarray. *Blood* 2004; 103: 275-82.
17. Shustik J, Han G, Farinha P, et al. Correlations between BCL6 rearrangement and outcome in patients with diffuse large B-cell lymphoma treated with CHOP or R-CHOP. *Haematologica* 2010; 95: 96-101.
18. Miyaoka M, Kikuti YY, Carreras J, et al. Clinicopathological and genomic analysis of double-hit follicular lymphoma: comparison with high-grade B-cell lymphoma with MYC and BCL2 and/or BCL6 rearrangements. *Mod Pathol* 2018; 31: 313-26.
19. Kawaguchi Y, Shiozawa E, Shimada S, et al. Ki-67 expression of immunohistochemistry using computerized image analysis is a useful prognostic marker in follicular lymphomas. *Int J Clin Exp Pathol* 2018; 11: 3366-74.
20. Szczuraszek K, Mazur G, Jelen M, Dziegiel P, Surowiak P, Zabel M.

- Prognostic significance of Ki-67 antigen expression in non-Hodgkin's lymphomas. *Anticancer Res* 2008; 28: 1113-8.
21. Samols MA, Smith NE, Gerber JM, et al. Software-automated counting of Ki-67 proliferation index correlates with pathologic grade and disease progression of follicular lymphomas. *Am J Clin Pathol* 2013; 140: 579-87.
 22. Koster A, Tromp HA, Raemaekers JM, et al. The prognostic significance of the intra-follicular tumor cell proliferative rate in follicular lymphoma. *Haematologica* 2007; 92: 184-90.
 23. Martin AR, Weisenburger DD, Chan WC, et al. Prognostic value of cellular proliferation and histologic grade in follicular lymphoma. *Blood* 1995; 85: 3671-8.
 24. Kim HJ, Fay MP, Feuer EJ, Midthune DN. Permutation tests for joint-point regression with applications to cancer rates. *Stat Med* 2000; 19: 335-51.
 25. Picci P, Mercuri M, Ferrari S, et al. Survival in high-grade osteosarcoma: improvement over 21 years at a single institution. *Ann Oncol* 2010; 21: 1366-73.
 26. Shewale JB, Correa AM, Brown EL, et al. Time trends of perioperative outcomes in early stage non-small cell lung cancer resection patients. *Ann Thorac Surg* 2020; 109: 404-11.
 27. Kim JS, Liu Y, Ha KH, Qiu H, Rothwell LA, Kim HC. Increasing incidence of B-cell non-Hodgkin lymphoma and occurrence of second primary malignancies in South Korea: 10-year follow-up using the Korean National Health Information database. *Cancer Res Treat* 2020; 52: 1262-72.
 28. Biagi JJ, Seymour JF. Insights into the molecular pathogenesis of follicular lymphoma arising from analysis of geographic variation. *Blood* 2002; 99: 4265-75.
 29. Ma S. Risk factors of follicular lymphoma. *Expert Opin Med Diagn* 2012; 6: 323-33.
 30. Le M, Ghazawi FM, Alakel A, et al. Incidence and mortality trends and geographic patterns of follicular lymphoma in Canada. *Curr Oncol* 2019; 26: e473-81.
 31. Friedberg JW, Taylor MD, Cerhan JR, et al. Follicular lymphoma in the United States: first report of the national LymphoCare study. *J Clin Oncol* 2009; 27: 1202-8.
 32. Bilalovic N, Blystad AK, Golouh R, et al. Expression of bcl-6 and CD10 protein is associated with longer overall survival and time to treatment failure in follicular lymphoma. *Am J Clin Pathol* 2004; 121: 34-42.
 33. Guo Y, Karube K, Kawano R, et al. Low-grade follicular lymphoma with t(14;18) presents a homogeneous disease entity otherwise the rest comprises minor groups of heterogeneous disease entities with *Bcl2* amplification, *Bcl6* translocation or other gene aberrances. *Leukemia* 2005; 19: 1058-63.
 34. Schraders M, de Jong D, Kluin P, Groenen P, van Krieken H. Lack of Bcl-2 expression in follicular lymphoma may be caused by mutations in the *BCL2* gene or by absence of the t(14;18) translocation. *J Pathol* 2005; 205: 329-35.
 35. Choi SM, Betz BL, Perry AM. Follicular lymphoma diagnostic caveats and updates. *Arch Pathol Lab Med* 2018; 142: 1330-40.
 36. Wang SA, Wang L, Hochberg EP, Muzikansky A, Harris NL, Hasserjian RP. Low histologic grade follicular lymphoma with high proliferation index: morphologic and clinical features. *Am J Surg Pathol* 2005; 29: 1490-6.
 37. Yoon SO, Suh C, Lee DH, et al. Distribution of lymphoid neoplasms in the Republic of Korea: analysis of 5318 cases according to the World Health Organization classification. *Am J Hematol* 2010; 85: 760-4.
 38. Sandvik OM, Soreide K, Kvaloy JT, Gudlaugsson E, Soreide JA. Epidemiology of gastrointestinal stromal tumours: single-institution experience and clinical presentation over three decades. *Cancer Epidemiol* 2011; 35: 515-20.

Prognostic significance of viable tumor size measurement in hepatocellular carcinomas after preoperative locoregional treatment

Yoon Jung Hwang¹, Youngeun Lee², Hyunjin Park³, Yangkyu Lee³, Kyoungbun Lee¹, Haeryoung Kim¹

¹Department of Pathology, Seoul National University Hospital, Seoul National University College of Medicine, Seoul;

²Department of Pathology, Seoul Medical Center, Seoul;

³Department of Pathology, Gangnam Severance Hospital, Yonsei University College of Medicine, Seoul, Korea

Background: Preoperative locoregional treatment (LRT) for hepatocellular carcinoma (HCC) often induces intratumoral necrosis without affecting the overall tumor size, and residual viable tumor size (VTS) on imaging is an important clinical parameter for assessing post-treatment response. However, for surgical specimens, it is unclear whether the VTS would be more relevant to prognosis compared to total tumor size (TTS). **Methods:** A total of 142 surgically resected solitary HCC cases were retrospectively reviewed. The TTS and VTS were assessed by applying the modified Response Evaluation Criteria in Solid Tumors method to the resected specimens, and correlated with the clinicopathological features and survival. **Results:** As applying VTS, 13/142 cases (9.2%) were down-staged to ypT1a. Although the survival analysis results for overall survival according to TTS or VTS were similar, VTS was superior to predict disease-free survival (DFS; $p = .023$) compared to TTS ($p = .08$). In addition, multivariate analysis demonstrated VTS > 2 cm to be an independent predictive factor for decreased DFS ($p = .001$). In the subpopulation of patients with LRT ($n = 54$), DFS in HCCs with TTS or VTS > 2 cm were significantly shorter than those with TTS or VTS ≤ 2 cm ($p = .047$ and $p = .001$, respectively). Interestingly, HCCs with TTS > 2 cm but down-staged to VTS ≤ 2 cm after preoperative LRT had similar survival to those with TTS ≤ 2 cm. **Conclusions:** Although the prognostic impact of tumor size was similar regardless of whether TTS or VTS was applied, reporting VTS may help to increase the number of candidates for surgery in HCC patients with preoperative LRT.

Key Words: Hepatocellular carcinoma; Necrosis; Tumor size; Neoadjuvant therapy; Prognosis

Received: June 5, 2021 Revised: July 21, 2021 Accepted: July 26, 2021

Corresponding Author: Haeryoung Kim, MD, PhD, Department of Pathology, Seoul National University College of Medicine, 103 Daehak-ro, Jongno-gu, Seoul 03080, Korea
 Tel: +82-2-740-8322, Fax: +82-2-765-5600, E-mail: haeryoung.kim@snu.ac.kr

Hepatocellular carcinoma (HCC) is the sixth most common cancer and the fourth leading cause of cancer-related death worldwide [1]. Several different staging systems exist for HCC, including the tumor-node-metastasis (TNM) staging system of the American Joint Committee on Cancer (AJCC)/Union for International Cancer Control (UICC) [2,3], the Barcelona Clinic Liver Cancer (BCLC) staging system [4], Japan Integrated Staging scoring system, the Okuda score, the Hong Kong Liver Cancer staging system [5], and the Chinese University Prognostic Index (CUPI) [6]. Notably, tumor size is a common parameter for all of these staging systems, and indeed, tumor size is a well-known prognostic factor for HCC, along with histological differentiation, vascular invasion status, multiplicity, and expression of cytokeratin 19 (CK19) [6-10].

Surgical resection is the treatment of choice for patients with

solitary HCCs and well-preserved liver function [4]. For patients with very early or early stage HCCs (BCLC stage 0-A) who are not suitable candidates for surgery, and for those with intermediate stage HCCs (BCLC stage B), locoregional treatment (LRT), such as radiofrequency ablation (RFA), percutaneous ethanol injection, or trans-arterial chemoembolization (TACE), is recommended [4,11,12]. These LRT modalities often induce direct tumor necrosis, and the tumor size often remains unchanged [11,12]. This is different from some other tumors of the solid organs, such as pancreatic ductal adenocarcinoma, in which preoperative neoadjuvant treatment induces shrinkage of tumor size in responsive cases, in addition to changes in tumor cellularity [13]. Therefore, in the case of HCCs, the tumor size after preoperative LRT would not reflect the degree of tumor response to treatment and the amount of tumor necrosis is reported in pathology

reports, often expressed as percentages.

Tumor size assessment is an important part of macroscopic and microscopic pathological examination for most solid organ tumors, including HCC. However, in the case of treated HCCs that are surgically resected or explanted, there is no definite guideline as to whether the tumor size including necrosis should be measured and used for assigning post-treatment pathologic T (ypT) categories for staging, or whether the size of the residual viable tumor is more relevant for staging purposes. Thus, the aim of this study was to assess whether reporting the viable tumor size (VTS) instead of the total tumor size (TTS) would be more useful for prognostication of HCCs.

MATERIALS AND METHODS

Patient selection and clinicopathological analysis

All HCC cases that were surgically resected HCCs between 2007 and 2011 were retrieved from the pathology database of the Department of Pathology, Seoul National University Hospital, and retrospectively reviewed. To examine the prognostic

significance of tumor size in this study, we excluded multiple HCCs, including those with satellite nodules or intrahepatic metastasis at the time of surgical resection. Liver explantation cases were also excluded from this study (Fig. 1). Only cases for which at least one entire cross-section of the tumor could be reconstructed with the slides (i.e., histological mapping) were included in this study. Clinical data including age, sex, underlying etiology, preoperative LRT details, and serum α -fetoprotein (AFP) and prothrombin induced by vitamin K absence-II (PIVKA-II) levels were retrieved from the electronic medical records. Pathological data were analyzed by reviewing pathology reports, gross images and glass slides, and included tumor size, gross type, histologic differentiation (Edmondson-Steiner grade), presence and extent (%) of necrosis, presence of microvascular invasion, major vessel invasion, or underlying cirrhosis, and the pathological T categories according to AJCC TNM staging system (8th edition). Gross types—according to the General Rules for the Study of Primary Liver Cancer by the Korean Liver Cancer Association [14]—were grouped as types 1 and 2, as previously described: type 1 HCCs consisted of expanding nodular and vaguely nodular

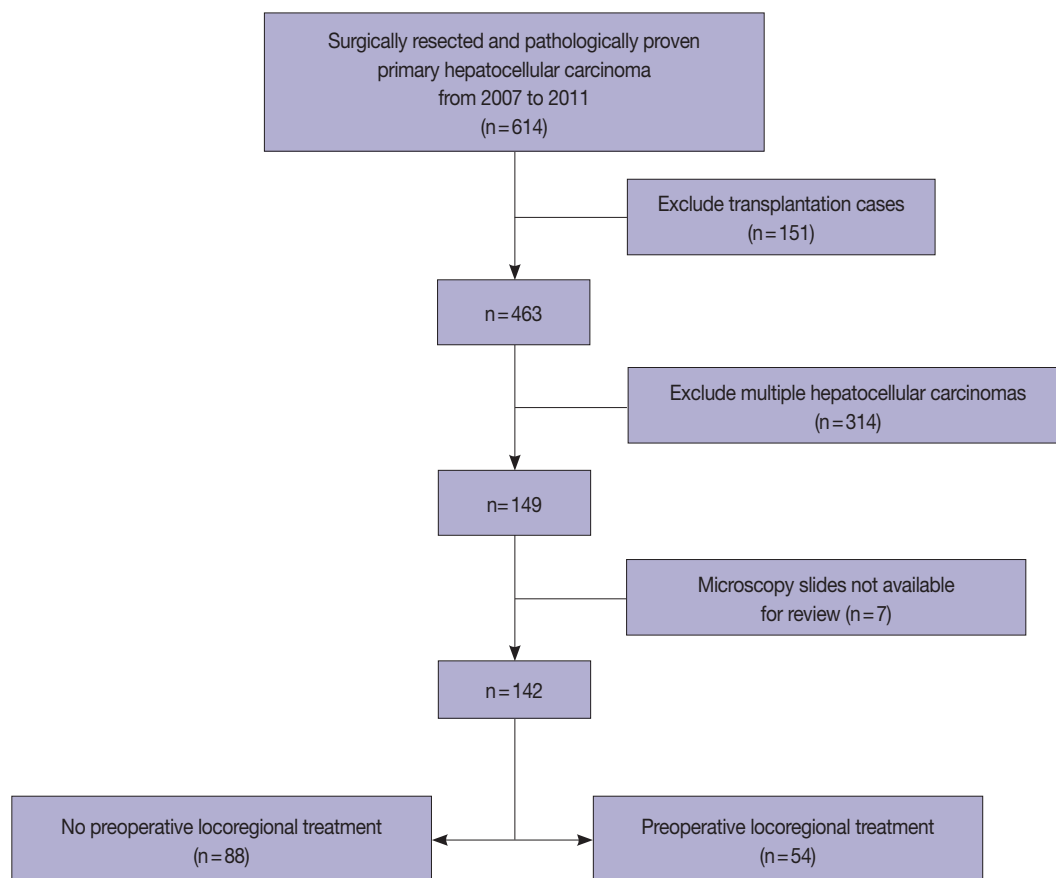


Fig. 1. Patient selection algorithm for this study.

types, and type 2 HCCs consisted of multinodular confluent, nodular with perinodular extension and infiltrative types [15]. The extent of necrosis was expressed as a percentage of the area of tumor necrosis over the total tumor area in a representative whole section. Major vessel invasion was defined as gross or microscopic invasion of main or first-order branches of the portal vein or hepatic vein, and microvascular invasion was defined as tumor invasion of microscopic vessels excluding the aforementioned major vessels. CK19 expression status was also assessed on representative whole tissue sections, when available. Follow-up data was obtained from the electronic medical records, including the status at last follow-up and the occurrence of extrahepatic metastasis or local recurrence.

Tumor size assessment

The tumor size was assessed by reviewing the primarily the gross images of the representative section of the tumor, and the size measurement in the pathology reports. However, especially in HCCs with necrosis, it was often not possible to discriminate between viable and necrotic foci purely on gross morphology, and therefore the matching glass slides were reviewed for all cases to confirm the presence or absence of viable tumor. As previously mentioned, only cases where a full histological mapping of an

entire cross-section was performed were included in this study. First, the greatest dimension of tumor was measured irrespective of the presence or absence of tumor necrosis, and this was designated as the TTS. Then, we applied the modified Response Evaluation Criteria in Solid Tumors (mRECIST) criteria for VTS evaluation, by measuring the greatest dimension of the viable tumor (Fig. 2) [16]. When there were multifocal viable areas within a single tumor, the greatest dimension of the largest viable focus was assessed.

Statistical analysis

All statistical analyses were performed using SPSS ver. 25.0 (IBM Corp., Armonk, NY, USA). Continuous data were presented as median with range and were analyzed by Mann-Whitney test, one-way analysis of variance (ANOVA) and Pearson's correlation analysis. Categorical data were evaluated by chi-square test, Fisher exact test, and linear-by-linear association. Survival analyses for overall survival (OS) and disease-free survival (DFS) were carried out by the Kaplan-Meier method and log-rank test. OS was defined as the interval between the date of operation and the date of last hospital visit or death. DFS was defined as the interval between the date of operation and the date of the relapse (first post-operative recurrence or extrahepatic metastasis). To

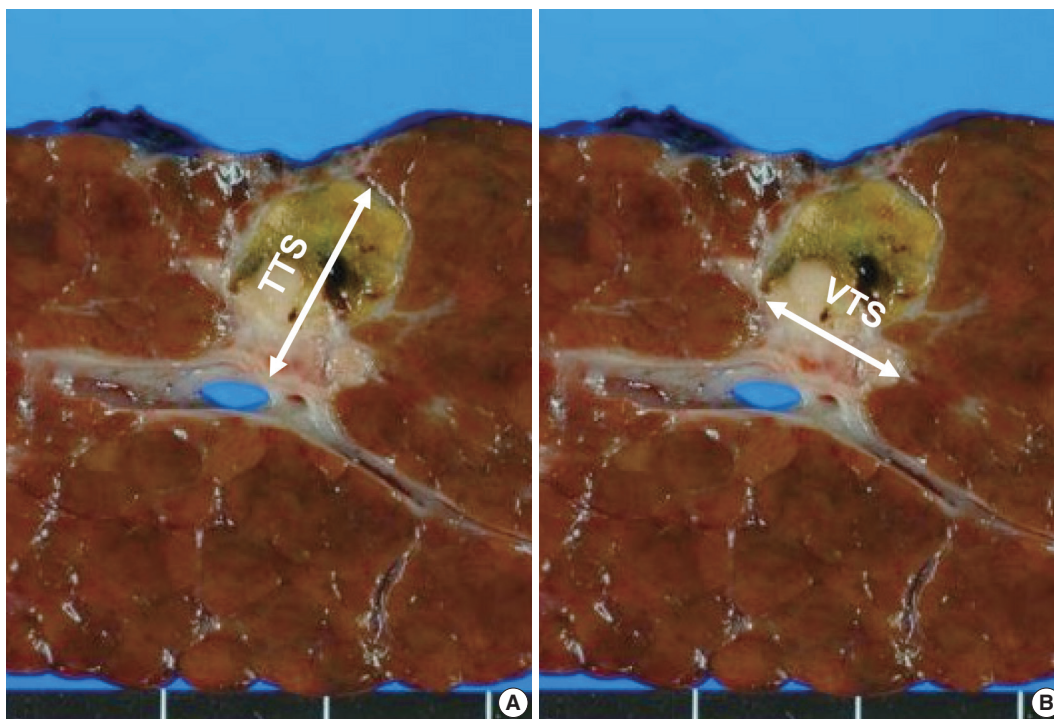


Fig. 2. Method of total tumor size (TTS) and viable tumor size (VTS) assessment. (A) For TTS assessment, the longest dimension of the tumor, including the necrosis, was measured. (B) For VTS assessment, the longest dimension of the viable tumor was measured.

identify factors associated with TTS or VTS, univariate and multivariate logistic regression analyses were performed. Variables with p -values $< .05$ in univariate analysis were included in the multivariate analysis. p -value $< .05$ was considered to be statistically significant.

RESULTS

Patient characteristics

A total of 142 cases of surgically resected solitary HCC were included in the study. The clinicopathological features of the study population are presented in Table 1. The median age was 60 years (range, 28 to 82 years), and 77.5% (110/142) of the patients were male. The majority of the cases (78.9%, 112/142) were associated with chronic hepatitis B virus (HBV) infection, and 38% (54/142) of the patients received preoperative LRT. The median tumor size was 5.1 cm (range, 0.4 to 16.7 cm), and 34.5% (49/142) of the cases showed intratumoral necrosis of any degree. CK19 expression was seen in 8.8% (10/142) of the HCCs. Pathologic T stages were pT1a in 12.7% (18/142), pT1b in 43.7% (62/142), pT2 in 29.6% (42/142), and pT4 in 14.1% (20/142) of cases. As only solitary HCCs were included in this study, there were no pT3 cases. Surgical resection margins were negative in 94.4% cases (134/142), positive in 4.9% cases (7/142), and not evaluable in one case.

Relationship between the TTS and the clinicopathological characteristics

The TTS of the HCCs were ≤ 2 cm in 19 cases (13.4%) and > 2 cm in 123 cases (86.6%) (2–5 cm in 51 cases [35.9%], 5–10 cm in 52 cases [36.6%], and > 10 cm in 20 cases [14.1%]) (Table 2, Supplementary Table S1). HCCs with TTS > 2 cm were more frequently associated with high preoperative serum PIVKA-II level ($p = .001$) and microvascular invasion ($p = .009$). On further stratification with 2 cm, 5 cm and 10 cm cutoffs, larger HCCs were less frequently associated with an HBV etiology ($p = .028$), and were more frequently associated with high preoperative serum AFP and PIVKA-II levels ($p = .013$ and $p < .001$, respectively) (Supplementary Table S1). LRT was performed less frequently in the larger tumors ($p = .038$). On microscopy, larger tumors more frequently demonstrated microvascular invasion ($p = .038$), and major vascular invasion, although marginally significant ($p = .071$). Larger HCCs were less frequently associated with cirrhosis in the background liver ($p = .005$). TTS was not correlated with other clinicopathological factors, including age, sex, gross type, the presence of necrosis, Edmond-

Table 1. Clinicopathologic characteristics

	Total (n= 142)
Clinical findings	
Age ≥ 60 yr	73 (51.4)
Sex (male/female)	110 (77.5)/32 (22.5)
Etiology	
HBV	110 (77.5)
HCV	5 (3.5)
Alcohol	1 (0.7)
HBV + HCV	1 (0.7)
HBV + alcohol	1 (0.7)
Budd-Chiari syndrome	1 (0.7)
Unknown	23 (16.2)
Preoperative locoregional treatment	
TACE	35 (24.6)
RFA	3 (2.1)
PEI	3 (2.1)
TACE + RFA	2 (1.4)
TACE + PEI	10 (7.0)
TACE + RFA + PEI	1 (0.7)
None	88 (62.0)
Serum AFP level $\geq 1,000$ ng/mL	36 (25.4)
Serum PIVKA-II level ≥ 200 mAU/mL (n= 120)	60 (50.0)
Pathological findings	
Total tumor size (cm)	5.1 (0.4–16.7)
Viable tumor size (cm)	4.3 (0.02–16.7)
Gross type	
Type 1 (vaguely nodular, expanding nodular)	68 (47.9)
Type 2 (multinodular confluent, infiltrative, cirrhomimetic)	74 (52.1)
Necrosis (present)	49 (34.5)
Extent of necrosis (%) (n= 49)	60.0 (1–99)
Edmondson-Steiner grade	
I, II	42 (29.6)
III, IV	100 (70.4)
Microvascular invasion (present)	53 (37.3)
Major vessel invasion (present)	20 (14.1)
Resection margin status (negative)	134 (94.4)
Underlying cirrhosis (present)	97 (68.3)
pT category	
pT1a	18 (12.7)
pT1b	62 (43.7)
pT2	42 (29.6)
pT4	20 (14.1)
CK19 positivity (n= 112)	10 (8.8)

Values are presented as number (%) or median (range).

HBV, hepatitis B virus; HCV, hepatitis C virus; TACE, trans-arterial chemo-embolization; RFA, radiofrequency ablation; PEI, percutaneous ethanol injection; AFP, α -fetoprotein; PIVKA-II, prothrombin induced by vitamin K absence-II; CK19, cytokeratin 19.

son-Steiner grade, and CK19 positivity.

Relationship between VTS and the clinicopathological characteristics after down-staging

When the VTS was applied for all cases, 13/142 cases (9.2%)

Table 2. Clinicopathological characteristics according to total tumor size (TTS) and viable tumor size (VTS)

	TTS ≤ 2 cm (n = 19, 13.4%)	TTS > 2 cm (n = 123, 86.6%)	p-value	VTS ≤ 2 cm (n = 34, 23.9%)	VTS > 2 cm (n = 108, 76.1%)	p-value
Clinical findings						
Age ≥ 60 yr	10 (52.6)	63 (51.2)	.909	21 (61.8)	52 (48.1)	.166
Sex (male/female)	16 (84.2)/3 (15.8)	94 (76.4)/29 (23.6)	.565	28 (82.4)/6 (17.6)	82 (75.9)/26 (24.1)	.434
B-viral etiology	17 (89.5)	95 (77.2)	.365	30 (88.2)	82 (75.9)	.125
Preoperative locoregional treatment	9 (47.4)	45 (36.6)	.368	23 (67.6)	31 (28.7)	.001
Serum AFP level ≥ 1,000 ng/mL	2 (10.5)	34 (27.6)	.157	4 (11.8)	32 (29.6)	.037
Serum PIVKA-II level ≥ 200 mAU/mL (n = 120)	2/16 (12.5)	58/104 (55.8)	.001	5/29 (17.2)	55/91 (60.4)	<.001
Pathological findings						
Gross type 2	9 (47.4)	65 (52.8)	.656	19 (55.9)	55 (50.9)	.614
Necrosis (present)	3 (15.8)	46 (37.4)	.065	18 (52.9)	31 (28.7)	.010
Extent of necrosis (%) (n = 49)	30.0 (10.0–60.0)	65.0 (1.0–99.0)	.200	72.5 (10.0–99.0)	50.0 (1.0–90.0)	.023
Edmondson-Steiner grade III or IV	10 (52.6)	90 (73.2)	.068	19 (55.9)	81 (75.0)	.033
Microvascular invasion (present)	2 (10.5)	51 (41.5)	.009	7 (20.6)	46 (42.6)	.021
Major vessel invasion (present)	1 (5.3)	19 (15.4)	.475	3 (8.8)	17 (15.7)	.405
Underlying cirrhosis (present)	15 (78.9)	82 (66.7)	.284	29 (85.3)	68 (63.0)	.015
pT category			<.001			<.001
pT1a	18 (94.7)	0		31 (91.2)	0	
pT1b	0	62 (50.4)		0	52 (48.1)	
pT2	0	42 (34.1)		0	39 (36.1)	
pT4	1 (5.3)	19 (15.4)		3 (8.8)	17 (15.7)	
CK19 positivity (n = 112)	2/13 (15.4)	8/99 (8.1)	.327	3/19 (15.8)	7/93 (7.5)	.369

Values are presented as number (%) or median (range).

AFP, α-fetoprotein; PIVKA-II, prothrombin induced by vitamin K absence-II; CK19, cytokeratin 19.

were down-staged according to the AJCC staging system. In detail, 10 cases that were initially pT1b and three cases that were initially pT2 by TTS were down-staged to ypT1a. Of the 13 cases, 12 patients (92.3%) had undergone LRT for HCC, while the remaining one patient did not receive LRT for HCC, but received chemotherapy for a concurrent rectal cancer. The median extent of tumor necrosis for the down-staged 13 cases was 90.0% with a range of 15%–99%. The median VTS for the total 142 cases was 4.3 cm with a range of 0.02–16.7 cm, and that for the 13 down-staged cases was 1.4 cm with a range of 0.02–2.0 cm.

After applying the VTS, 34 patients (23.9%) had tumors of 2 cm or less and 108 (76.1%) had tumors of >2 cm (2–5 cm in 44 cases [31.0%], 5–10 cm in 50 cases [35.2%], and >10 cm in 14 cases [9.9%]) (Table 2, Supplementary Table S2). In addition to high preoperative serum PIVKA-II level ($p < .001$) and microvascular invasion ($p = .021$), high preoperative serum AFP level ($p = .037$) and poor histologic grade ($p = .033$) were more frequent in tumors with VTS > 2 cm. LRT was less frequently performed in tumors with VTS > 2 cm ($p = .001$). The presence and extent of necrosis were also more frequent and higher in tumors with VTS > 2 cm ($p = .010$ and $p = .023$, respectively). On

further stratification with 2 cm, 5 cm, and 10 cm cutoffs, larger tumors were less frequently associated underlying HBV infection ($p = .020$), were more frequently associated with high preoperative serum AFP and PIVKA-II levels ($p = .016$ and $p < .001$, respectively), and were less frequently treated preoperatively ($p < .001$) (Supplementary Table S2). Histopathologically, microvascular invasion was more frequently observed in larger tumors ($p = .013$), and larger HCCs were less frequently associated with cirrhosis in the background liver ($p < .001$). Tumor necrosis was less frequently seen in the larger tumors ($p = .014$). There was no significant difference in age, sex, gross type, and CK19 positivity according to VTS.

Survival analysis results

For the entire cohort of 142 patients, the median OS was 80.5 months (range, 1 to 153 months), and the 5-year and 10-year survival rates were 67.6% and 53.8%, respectively. The median time to relapse was 14 months (range, 0 to 134 months) and DFS rates at 3 and 5 years were 75.3% and 59.6%, respectively.

Univariate analysis showed that AFP level ≥ 1,000 ng/mL ($p = .017$), gross type 2 ($p = .013$), the presence of necrosis ($p = .004$), Edmondson-Steiner grade III or IV ($p = .007$), microvascular

invasion ($p = .014$), major vessel invasion ($p = .019$), and CK19 expression ($p = .005$) were significantly associated with decreased OS (Table 3). Although there was a tendency for lower OS for HCCs with TTS > 2 cm and VTS > 2 cm, the results were not statistically significant (Fig. 3). For DFS, preoperative LRT ($p = .029$), PIVKA-II level ≥ 200 mAU/mL ($p = .044$), VTS > 2 cm ($p = .028$), the presence of necrosis ($p = .004$), Edmonson-Steiner grade III or IV ($p = .025$), microvascular invasion ($p = .006$), and major vessel invasion ($p < .001$) were significantly associated with decreased DFS (Table 3, Fig. 3). Kaplan-Meier analysis demonstrated decreased DFS in HCCs with TTS > 2 cm, although marginally significant ($p = .051$).

On multivariate analysis, AFP level $\geq 1,000$ ng/mL (hazard ratio [HR], 1.946; 95% confidence interval [CI], 1.023 to 3.701; $p = .042$) and necrosis (HR, 3.044; 95% CI, 1.662 to 5.574; $p < .001$) were identified as independent predictive factors for poor OS, and preoperative LRT (HR, 2.315; 95% CI, 1.456 to 3.682; $p < .001$), microvascular invasion (HR, 1.583; 95% CI, 1.012 to 2.476; $p = .044$), major vessel invasion (HR, 1.893; 95% CI, 1.054 to 3.400; $p = .033$), and, notably, VTS > 2 cm (HR, 2.672; 95% CI, 1.502 to 4.755; $p = .001$) were independent predictive factors for decreased DFS.

Subgroup analysis: preoperative LRT cohort

The subgroup of HCC patients who received LRT ($n = 54$) was analyzed separately, and the clinicopathological features are presented in Supplementary Table S3. The median period between the date of the most recent LRT and the operation date was 2 months (range, 0 to 96 months). The median tumor size was 3.8 cm (range, 0.4 to 11.9 cm), and 75.9% (41/54) of the cases showed intratumoral necrosis (extent of necrosis, 1%–99%). CK19 expression was seen in 11.5% (3/26), and there was no statistically significant difference in CK19 expression status in the HCCs according to preoperative treatment status ($p = .594$). According to TTS, nine patients (16.7%) had tumors with ≤ 2 cm, 23 patients (42.6%) had tumors 2–5 cm, 18 patients (33.3%) had tumors with size 5–10 cm, and four patients (7.4%) had tumors > 10 cm. After applying the VTS, the number of HCCs ≤ 2 cm increased to 23 cases (42.6%); 17 and 14 cases (31.5 and 25.9%) had tumor sizes of 2–5 cm and 5–10 cm, respectively, and none of the cases were larger than 10 cm. There was no significant correlation between VTS and the time elapsed from the most recent LRT.

Similarly to the total population, larger tumors in the LRT cohort demonstrated worse OS and DFS. OS in HCCs with TTS or VTS > 2 cm were shorter than those with TTS or VTS ≤ 2

Table 3. Univariate and multivariate analyses of clinical and histopathological features for overall and disease-free survival (total cohort $n=142$)

Variable	Overall survival				Disease-free survival			
	Univariate analysis		Multivariate analysis ($n=112$)		Univariate analysis		Multivariate analysis ($n=120$)	
	HR (95% CI)	p-value	HR (95% CI)	p-value	HR (95% CI)	p-value	HR (95% CI)	p-value
Clinical features								
Male sex	1.499 (0.844–2.664)	.168	-	-	1.460 (0.950–2.245)	.084	-	-
Age > 60 yr	1.221 (0.731–2.039)	.445	-	-	1.043 (0.719–1.514)	.825	-	-
B-viral etiology	1.065 (0.565–2.008)	.845	-	-	1.001 (0.641–1.565)	.995	-	-
Preoperative locoregional treatment	1.454 (0.866–2.443)	.162	-	-	1.530 (1.044–2.242)	.029	2.315 (1.456–3.682)	<.001
AFP $\geq 1,000$ ng/mL	1.946 (1.125–3.368)	.017	1.946 (1.023–3.701)	.042	1.362 (0.889–2.086)	.155	-	-
PIVKA-II level ≥ 200 mAU/mL ($n = 120$)	1.200 (0.688–2.094)	.521	-	-	1.529 (1.012–2.309)	.044	-	-
Pathological features								
Gross type 2	1.972 (1.157–3.362)	.013	-	-	1.407 (0.968–2.045)	.074	-	-
TTS > 2 cm	1.758 (0.703–4.397)	.227	-	-	1.818 (0.974–3.391)	.060	-	-
VTS > 2 cm	1.498 (0.778–2.887)	.227	-	-	1.689 (1.058–2.696)	.028	2.672 (1.502–4.755)	.001
Necrosis	2.157 (1.287–3.615)	.004	3.044 (1.662–5.574)	<.001	1.777 (1.205–2.620)	.004	-	-
E-S grade III or IV	2.468 (1.279–4.763)	.007	2.363 (0.977–5.716)	.056	1.625 (1.064–2.484)	.025	-	-
Microvascular invasion	1.900 (1.139–3.170)	.014	-	-	1.692 (1.159–2.470)	.006	1.583 (1.012–2.476)	.044
Major vessel invasion	2.144 (1.135–4.048)	.019	-	-	2.528 (1.527–4.185)	<.001	1.893 (1.054–3.400)	.033
Underlying cirrhosis	1.257 (0.715–2.209)	.427	-	-	0.965 (0.648–1.437)	.861	-	-
CK19 positivity ($n = 112$)	3.242 (1.433–7.332)	.005	2.156 (0.941–4.940)	.069	1.691 (0.814–3.515)	.159	-	-

HR, hazard ratio; CI, confidence interval; AFP, α -fetoprotein; PIVKA-II, prothrombin induced by vitamin K absence-II; TTS, total tumor size; VTS, viable tumor size; E-S grade, Edmondson-Steiner grade; CK19, cytokeratin 19.

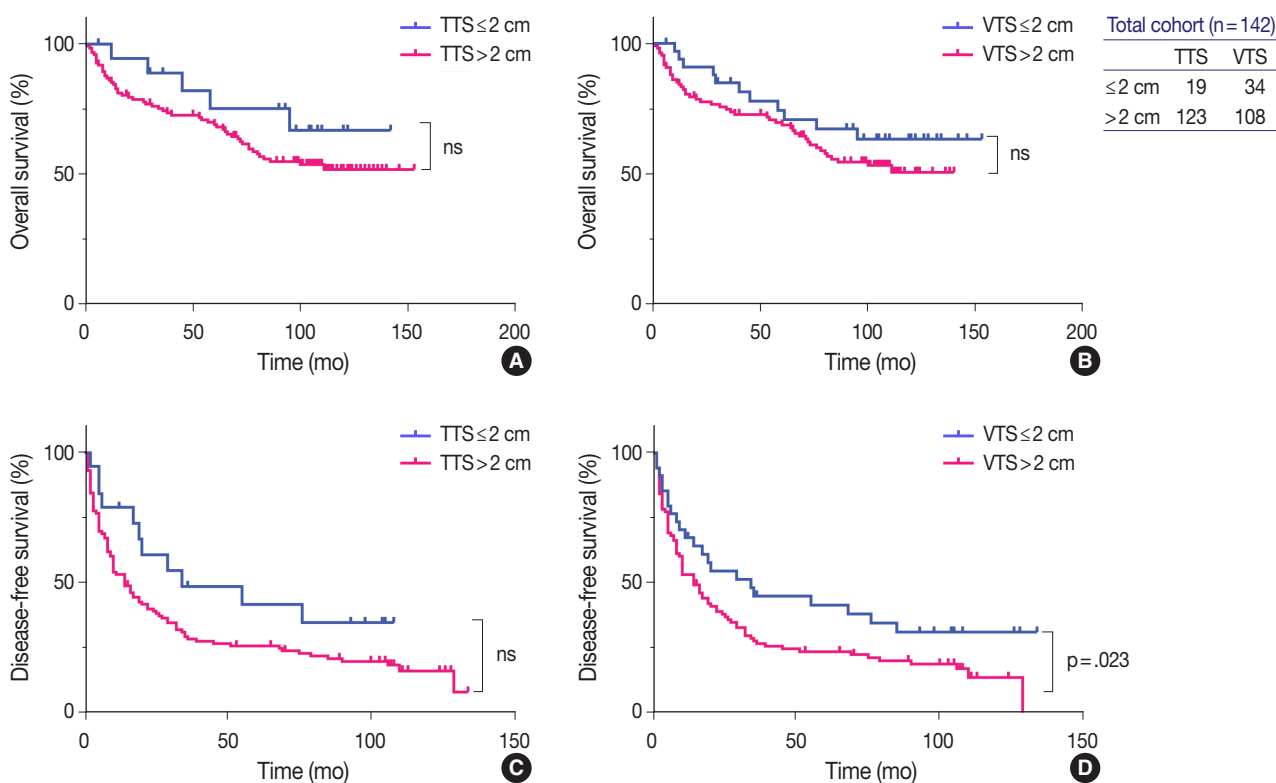


Fig. 3. Kaplan-Meier curves demonstrating the differences in overall (A, B) and disease-free survivals (C, D) in the total cohort (n=142) according to tumor size, by applying the total tumor size (TTS) and viable tumor size (VTS). The survival curves look similar regardless of whether TTS (A, C) or VTS (B, D) is applied, although the difference in disease-free survival reached statistically significant levels only by VTS (D). ns, not significant.

cm, although marginally significant (Fig. 4). DFS was significantly lower for HCCs > 2 cm for both TTS and VTS ($p = .047$ and $p = .001$, respectively). Interestingly, when we further stratified the 23 VTS ≤ 2 cm cases into HCCs that were originally VTS ≤ 2 cm (i.e., TTS ≤ 2 cm, $n = 9$) and those that were originally TTS > 2 cm but down-staged to VTS ≤ 2 cm after preoperative treatment ($n = 14$), there was no difference in the DFS between the two groups (Fig. 5).

DISCUSSION

The extent of residual viable tumor after neoadjuvant treatment is a prognostic factor for various malignant neoplasms, including esophageal, gastric, pancreatic, lung, and colorectal cancers [17-21]. For example, for pancreatic ductal adenocarcinoma, the maximal dimension of the residual tumor is used for assigning the ypT stage according to the TNM system, and although there is still no worldwide consensus on what grading system should be used to evaluate response to neoadjuvant therapy, the degree of tumor response is reported in surgical pathology

practice along with the ypT stage [13,22].

As with tumors of most other organs, tumor size is an important prognostic factor for HCC. It is one of the main parameters for HCC staging, and is included in various different staging systems for HCC [6-9]. For example, in the AJCC TNM staging system, single tumors are staged as pT1a or pT1b using a size cut-off of 2 cm, and multiple tumors are assigned as pT2 or pT3 using a cutoff value of 5 cm [3,23]. In the BCLC staging system, solitary HCCs < 2 cm are categorized as very early stage HCCs (stage 0) [4,24]. However, it is still unclear how the tumor size should be measured in the setting of HCCs after LRT, especially if there is extensive intratumoral necrosis as a result of the LRT: unlike many other tumors that show shrinkage in tumor size after neoadjuvant treatment, the TTS of HCC often remains unaltered after LRT, and therefore may not exactly reflect the actual tumor burden [11,12].

The concept of VTS assessment in HCC after LRT by imaging was initially proposed by a panel of HCC experts convened by the European Association for the Study of the Liver (EASL) in 2000 [25]. This panel considered the reduction of VTS—mea-

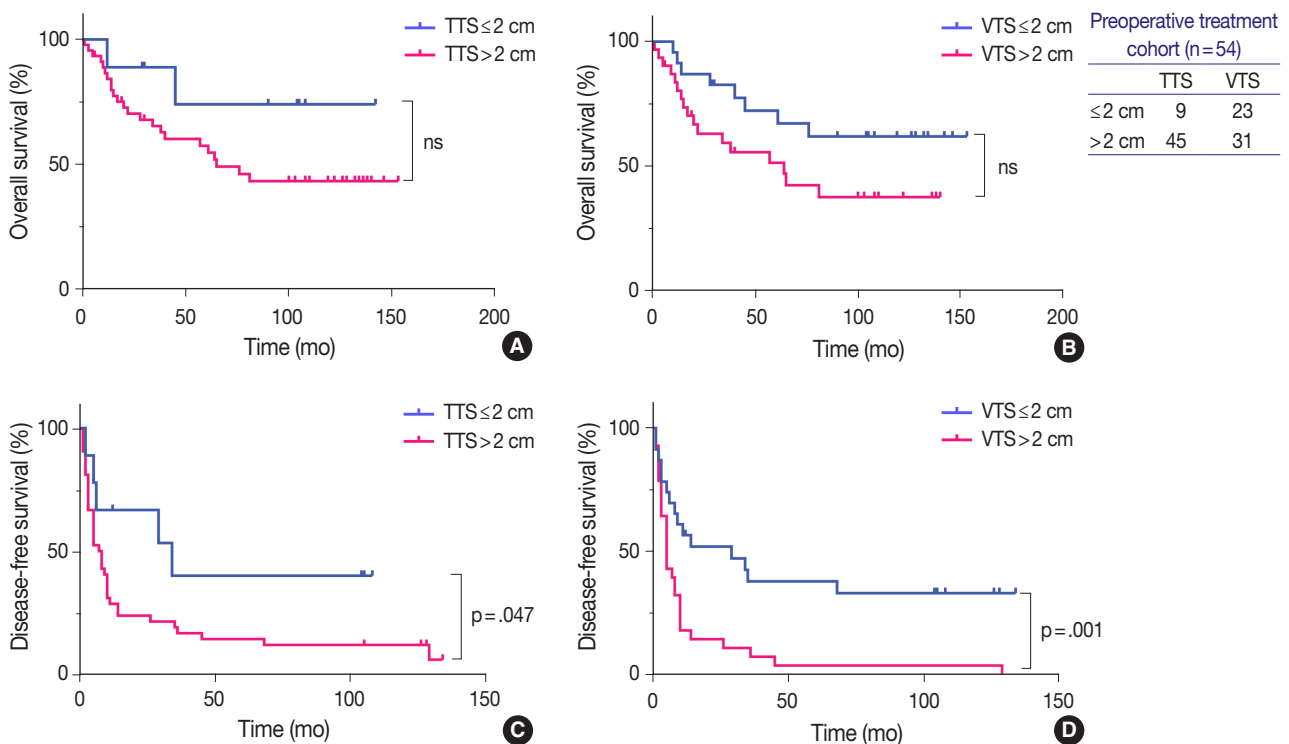


Fig. 4. Survival curves according to total tumor size (TTS) and viable tumor size (VTS) based on 2 cm criteria in the subpopulation with preoperative locoregional treatment (n=54). There is no difference in the overall (A, B) or disease-free survival (C, D) curves according to the type of measurement used. ns, not significant.

sured by the size of the enhancing tumor on contrast-enhanced dynamic computed tomography or magnetic resonance imaging—to be the optimal method for assessing response to treatment. This concept was further endorsed by the American Association for the Study of Liver Diseases (AASLD) in 2005, and subsequently, the AASLD and Journal of the National Cancer Institute (AASLD-JNCI) guidelines formally modified the RECIST (sum of diameters of target lesions) criteria so that VTS (enhancing tumor size by imaging), rather than TTS, is used to assess treatment response in HCCs [26]. Objective tumor response to treatment as measured by the mRECIST criteria was found to be a good predictor of survival in HCC patients treated by LRT or systemic targeted therapy [11,27-29]. In addition, the mRECIST assessment has been shown to have prognostic value even after liver transplantation; one recent study demonstrated that incorporating the mRECIST assessment into the Metroticket 2.0 model for post-liver transplantation HCC-related death prediction could improve its predictive ability [30]. However, there is no study to date on the significance of VTS evaluation by pathology on HCCs. Therefore, we postulated that a measurement of the residual (viable) tumor size (VTS) may be more relevant for prognostication purposes, and questioned whether applying the VTS had

any effect on the clinicopathological features and/or prognosis of HCC patients.

We found that the VTS was not superior to TTS in predicting survival of HCC patients; there was no significant prognostic difference between TTS and VTS in both total population and the LRT subgroup. However, we found that VTS exceeding 2 cm was significantly predictive of a poor DFS on both univariate and multivariate analyses, and that among the group of patients who received preoperative LRT, HCCs with VTS ≤ 2 cm demonstrated significantly longer DFS compared to HCCs with VTS > 2 cm. Moreover, HCCs that were originally larger than 2 cm (TTS > 2 cm) but down-staged to VTS ≤ 2 cm after LRT showed significantly longer DFS compared to HCCs with VTS > 2 cm, and the DFS of the down-staged tumors were similar to that of HCCs that were originally (TTS) ≤ 2 cm. This suggests that VTS ≤ 2 cm could be considered ypT1a regardless of the original TTS before LRT. This may have important clinical implications, as patients with HCCs that are down-staged to ypT1a based on the VTS could become potential candidates for surgical resection or transplantation, providing a chance for curative therapy for patients who were originally deemed as being ineligible for surgery.

From the practical point of view, measuring tumor size may

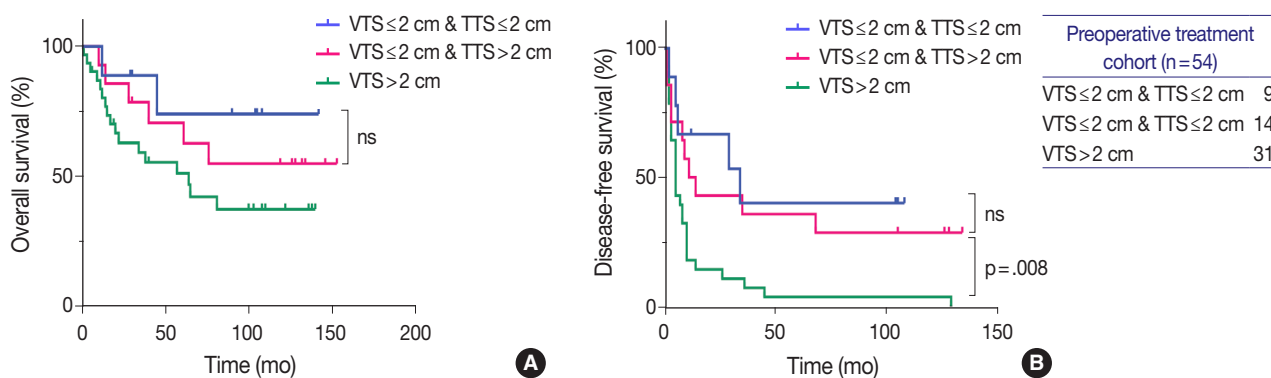


Fig. 5. Survival curves demonstrating the difference in overall (A) and disease-free survival (B) between three groups of treated hepatocellular carcinomas (HCCs, $n=54$): HCCs that were originally ≤ 2 cm before treatment, HCCs that were originally > 2 cm but down-staged to viable tumor size (VTS) ≤ 2 cm after treatment, and HCCs with VTS > 2 cm. Down-staged HCCs demonstrate similar disease-free survival as HCCs with total tumor size (TTS) ≤ 2 cm. ns, no significant differences.

be difficult when there are multifocally scattered residual tumors in treated HCCs. In this study, we adapted the mRECIST method (maximum diameter of enhancing tumor by imaging) to the surgical specimens (maximum diameter of the viable tumor by macroscopic and microscopic evaluation) [16]; therefore, the size of the largest viable tumor was measured in the case of multifocally scattered viable tumors. However, we did experience difficulties with accurately measuring the VTS in some of our cases, especially when there was an irregular geographic distribution of intratumoral necrosis. For example, in one case, the VTS (1.2 cm) was considerably lower than the TTS (8.5 cm), although the percentage of tumor necrosis was only 30%. On the other hand, in another case with 95% necrosis, there was only a small decrease in tumor size, from 3.5 cm (TTS) to 1.9 cm (VTS). Nevertheless, measurement of the VTS was feasible for the majority of cases, and actually easier to assess compared to estimating the extent of intratumoral necrosis, especially for tumors with near total necrosis. Another problem with the TTS is that the TTS may not accurately measure the actual tumor size, as the peritumoral hepatic parenchyme is often infarcted as a result of TACE or RFA, and the infarcted non-neoplastic parenchyme may be misinterpreted as being part of the HCC, potentially resulting in an overestimation of the tumor size.

The VTS measurement used in this study could by no means be an accurate surrogate of the actual viable tumor volume. Measuring the tumor volume and the change in tumor volume after LRT could theoretically reflect the tumor response and prognosis better than this simple one-dimensional VTS measurement. In this aspect, digital pathology may potentially play a role in accurate tumor size or volume assessment in the near future.

This study has its limitations. It is a retrospective cohort study

of archival cases, and therefore the gross photographs taken at the time of accession (and their corresponding slides) were reviewed for TTS and VTS measurement. Therefore, it is possible that the representative cross sections in the photographs did not reflect the exact tumor size. However, we selected only those cases in which histological mapping was performed for at least one whole cross section to ensure an accurate size measurement in the available cross section. This resulted in the smaller number of HCC cases enrolled, which is another limitation of this study.

In conclusion, although the impact on patient survival according to VTS or TTS measurement was not significantly different, HCCs that were down-staged to VTS ≤ 2 cm after preoperative LRT had similar outcomes to HCCs that were originally smaller than 2 cm, suggesting that such tumors may be assigned as ypT1a by the AJCC TNM system and that reporting the VTS may help to increase the number of HCC patients that are eligible for surgery after LRT.

Supplementary Information

The Data Supplement is available with this article at <https://doi.org/10.4132/jptm.2021.07.26>.

Ethics Statement

This study was approved by the Institutional Review Board of Seoul National University Hospital and informed consent was waived due to the retrospective nature of this study (IRB number H-2003-035-1107).

Availability of Data and Material

The datasets generated or analyzed during the study are available from the corresponding author on reasonable request.

Code Availability

Not applicable.

ORCID

Yoon Jung Hwang <https://orcid.org/0000-0002-8519-7521>
 Youngeun Lee <https://orcid.org/0000-0002-0000-1615>
 Hyunjin Park <https://orcid.org/0000-0001-7193-9849>
 Yangkyu Lee <https://orcid.org/0000-0002-6008-7713>
 Kyoungbun Lee <https://orcid.org/0000-0001-8427-3003>
 Haeryoung Kim <https://orcid.org/0000-0002-4205-9081>

Author Contributions

Conceptualization: YJH, HK. Data curation: YJH, YL, HP, YL, HK. Investigation: YJH, HK. Methodology: YJH, HK. Supervision: HK. Writing—original draft: YJH, HK. Writing—review & editing: YJH, YL, HP, YL, KL. Approval of final manuscript: YJH, YL, HP, YL, KL.

Conflicts of Interest

H.K., a contributing editor of the *Journal of Pathology and Translational Medicine*, was not involved in the editorial evaluation or decision to publish this article. All remaining authors have declared no conflicts of interest.

Funding Statement

This work was supported by the National Research Foundation of Korea (NRF) grant funded by the Korea government (NRF-2019R1A2C2010056, NRF-2016R1D1A1A09919042).

References

- Bray F, Ferlay J, Soerjomataram I, Siegel RL, Torre LA, Jemal A. Global cancer statistics 2018: GLOBOCAN estimates of incidence and mortality worldwide for 36 cancers in 185 countries. *CA Cancer J Clin* 2018; 68: 394-424.
- Kamarajah SK, Frankel TL, Sonnenday C, Cho CS, Nathan H. Critical evaluation of the American Joint Commission on Cancer (AJCC) 8th edition staging system for patients with Hepatocellular Carcinoma (HCC): a Surveillance, Epidemiology, End Results (SEER) analysis. *J Surg Oncol* 2018; 117: 644-50.
- Chun YS, Pawlik TM, Vauthey JN. 8th edition of the AJCC cancer staging manual: pancreas and hepatobiliary cancers. *Ann Surg Oncol* 2018; 25: 845-7.
- European Association for the Study of the Liver; European Organisation for Research and Treatment of Cancer. EASL-EORTC clinical practice guidelines: management of hepatocellular carcinoma. *J Hepatol* 2012; 56: 908-43.
- Yau T, Tang VY, Yao TJ, Fan ST, Lo CM, Poon RT. Development of Hong Kong Liver Cancer staging system with treatment stratification for patients with hepatocellular carcinoma. *Gastroenterology* 2014; 146: 1691-700.
- Subramaniam S, Kelley RK, Venook AP. A review of hepatocellular carcinoma (HCC) staging systems. *Chin Clin Oncol* 2013; 2: 33.
- Huang WJ, Jeng YM, Lai HS, Sheu FY, Lai PL, Yuan RH. Tumor size is a major determinant of prognosis of resected stage I hepatocellular carcinoma. *Langenbecks Arch Surg* 2015; 400: 725-34.
- Goh BK, Teo JY, Chan CY, et al. Importance of tumor size as a prognostic factor after partial liver resection for solitary hepatocellular carcinoma: Implications on the current AJCC staging system. *J Surg Oncol* 2016; 113: 89-93.
- Wu G, Wu J, Wang B, Zhu X, Shi X, Ding Y. Importance of tumor size at diagnosis as a prognostic factor for hepatocellular carcinoma survival: a population-based study. *Cancer Manag Res* 2018; 10: 4401-10.
- Rhee H, Kim H, Park YN. Clinico-radio-pathological and molecular features of hepatocellular carcinomas with keratin 19 expression. *Liver Cancer* 2020; 9: 663-81.
- Lencioni R, Montal R, Torres F, et al. Objective response by mRECIST as a predictor and potential surrogate end-point of overall survival in advanced HCC. *J Hepatol* 2017; 66: 1166-72.
- Jiang T, Zhu AX, Sahani DV. Established and novel imaging biomarkers for assessing response to therapy in hepatocellular carcinoma. *J Hepatol* 2013; 58: 169-77.
- Chatterjee D, Katz MH, Foo WC, et al. Prognostic significance of new AJCC tumor stage in patients with pancreatic ductal adenocarcinoma treated with neoadjuvant therapy. *Am J Surg Pathol* 2017; 41: 1097-104.
- Jang JY, Lee JS, Kim HJ, et al. The general rules for the study of primary liver cancer. *J Liver Cancer* 2017; 17: 19-44.
- Lee Y, Park H, Lee H, et al. The clinicopathological and prognostic significance of the gross classification of hepatocellular carcinoma. *J Pathol Transl Med* 2018; 52: 85-92.
- Lencioni R, Llovet JM. Modified RECIST (mRECIST) assessment for hepatocellular carcinoma. *Semin Liver Dis* 2010; 30: 52-60.
- Fanelli GN, Loupakis F, Smyth E, et al. Pathological tumor regression grade classifications in gastrointestinal cancers: role on patients' prognosis. *Int J Surg Pathol* 2019; 27: 816-35.
- Becker K, Langer R, Reim D, et al. Significance of histopathological tumor regression after neoadjuvant chemotherapy in gastric adenocarcinomas: a summary of 480 cases. *Ann Surg* 2011; 253: 934-9.
- Rizk NP, Venkatraman E, Bains MS, et al. American Joint Committee on Cancer staging system does not accurately predict survival in patients receiving multimodality therapy for esophageal adenocarcinoma. *J Clin Oncol* 2007; 25: 507-12.
- Schneider PM, Baldus SE, Metzger R, et al. Histomorphologic tumor regression and lymph node metastases determine prognosis following neoadjuvant radiochemotherapy for esophageal cancer: implications for response classification. *Ann Surg* 2005; 242: 684-92.
- Pataer A, Kalhor N, Correa AM, et al. Histopathologic response criteria predict survival of patients with resected lung cancer after neoadjuvant chemotherapy. *J Thorac Oncol* 2012; 7: 825-32.
- Amin MB, Edge S, Greene F, et al. AJCC cancer staging manual. 8th ed. New York: Springer, 2017.
- Shinkawa H, Tanaka S, Takemura S, Ishihara T, Yamamoto K, Kubo S. Tumor size drives the prognosis after hepatic resection of solitary hepatocellular carcinoma without vascular invasion. *J Gastrointest Surg* 2020; 24: 1040-8.
- Marrero JA, Kulik LM, Sirlin CB, et al. Diagnosis, staging, and management of hepatocellular carcinoma: 2018 practice guidance by the American Association for the Study of Liver Diseases. *Hepatology* 2018; 68: 723-50.
- Bruix J, Sherman M, Llovet JM, et al. Clinical management of hepatocellular carcinoma: conclusions of the Barcelona-2000 EASL conference. European Association for the Study of the Liver. *J Hepatol* 2001; 35: 421-30.
- Bruix J, Sherman M; Practice Guidelines Committee; American Association for the Study of Liver Diseases. Management of hepatocellular carcinoma. *Hepatology* 2005; 42: 1208-36.
- Gillmore R, Stuart S, Kirkwood A, et al. EASL and mRECIST responses are independent prognostic factors for survival in hepatocellular cancer patients treated with transarterial embolization. *J Hepatol* 2011; 55: 1309-16.

28. Kim BK, Kim SU, Kim KA, et al. Complete response at first chemoembolization is still the most robust predictor for favorable outcome in hepatocellular carcinoma. *J Hepatol* 2015; 62: 1304-10.
29. Vincenzi B, Di Maio M, Silletta M, et al. Prognostic relevance of objective response according to EASL criteria and mRECIST criteria in hepatocellular carcinoma patients treated with loco-regional therapies: a literature-based meta-analysis. *PLoS One* 2015; 10: e0133488.
30. Cucchetti A, Serenari M, Sposito C, et al. Including mRECIST in the Metroticket 2.0 criteria improves prediction of hepatocellular carcinoma-related death after liver transplant. *J Hepatol* 2020; 73: 342-8.

Appendiceal actinomycosis mimicking appendiceal tumor, appendicitis or inflammatory bowel disease

You-Na Sung, Jihun Kim

Department of Pathology, Asan Medical Center, University of Ulsan College of Medicine, Seoul, Korea

Appendiceal actinomycosis is very rare and its diagnosis is often difficult even in surgically resected specimens. Here we report two cases of appendiceal actinomycosis confirmed by pathologic examination of surgically resected specimens. Characteristic histologic features included transmural chronic inflammation with Crohn-like lymphoid aggregates and polypoid mucosal protrusion into cecal lumen through fibrous expansion of the submucosa. Chronic active inflammation involved the mucosa of the appendix and cecum around the appendiceal orifice. Crohn's disease with predominant cecal involvement and inflammatory pseudotumor were considered as differential diagnoses. Careful examination revealed a few actinomycotic colonies in the mucosa, confirming the diagnosis. A high index of suspicion with awareness of the characteristic histologic features might prompt careful inspection for the actinomycotic colonies, leading to the appropriate diagnosis of this rare disease.

Key Words: Appendix; Actinomycosis; Mycetoma; Pathology

Received: March 31, 2020 **Revised:** May 12, 2020 **Accepted:** May 17, 2020

Corresponding Author: Jihun Kim, MD, PhD, Department of Pathology, Asan Medical Center, University of Ulsan College of Medicine, 88 Olympic-ro 43-gil, Songpa-gu, Seoul 05505, Korea

Tel: +82-2-3010-4556, Fax: +82-2-472-7898, E-mail: jihunkim@amc.seoul.kr

Actinomyces are gram-positive anaerobic bacteria, one of the commensals of human mucous membrane [1]. They can cause chronic inflammation when normal mucous membrane is damaged due to various causes such as abdominal surgery, bowel preparation, or trauma [2]. The most common species in human is *Actinomyces israelii* and it is known to usually involve cervicofacial, thoracic, and abdominal areas [3,4]. The appendix is the most preferred organ in the abdominal area [4,5]. Appendiceal actinomycosis is very rare and presents with nonspecific symptoms, which can mimic several other diseases including appendiceal malignancy, acute appendicitis, or inflammatory bowel disease. Because treatment is different depending on the diagnosis, unnecessary surgery can be avoided if malignancy is excluded. Therefore, there have been several studies attempting to diagnose this condition with specific radiologic or endoscopic features [1,4,6,7]. However, these radiologic, endoscopic, and clinical features are not diagnostic, and the final diagnosis of actinomycosis usually requires pathologic confirmation after exploratory surgery [5]. Until recently, there have been limited reports in the literature describing the pathologic features of appendiceal acti-

nomycosis [1,5,7-13]. If the causative organism is easily identifiable in biopsy material, the diagnosis can be rendered without surgery. However, a pathologic diagnosis is often difficult even on the resected specimen because this disease can mimic Crohn's disease or inflammatory pseudotumor and the causative organisms are sometimes very hard to find. Here, we report two patients with appendiceal actinomycosis to help pathologists recognize and diagnose this rare disease.

CASE REPORT

Case 1

A 61-year-old woman presented with a mass-like lesion on imaging studies during health screening without any specific symptom. She had been diagnosed with breast cancer 9 years ago. Laboratory tests revealed mild leukocytosis ($11.1 \times 10^2/\mu\text{L}$) and increased C-reactive protein (3.41 mg/dL). Abdominal contrast-enhanced computed tomography (CT) revealed appendicolith, periappendiceal fat infiltration with prominent wall thickening, and arterial enhancement in the appendiceal base

(Fig. 1A). No mural thickening or contrast enhancement was found in the small intestine or other parts of the colon. Based on these findings, appendicitis with peri-appendiceal abscess or other inflammatory mass was suspected, but a primary appendiceal neoplasm could not be completely excluded. Colonofiberscopy (CFS) showed cecal contraction with multiple small polyps and scars in the large intestine. Intestinal tuberculosis was added to the list of differential diagnoses. Colonoscopic biopsy showed a focal active colitis pattern only and no actinomycotic colonies were found (data not shown).

Ileocecal resection was performed for histologic confirmation. Upon surgery, a mass-like lesion was observed in the appendiceal orifice and regional ileocolic lymph nodes were enlarged. On gross examination, the base of the appendiceal wall was markedly thickened and fibrotic (Fig. 1B). The appendiceal lumen was filled with fecal materials. On microscopy, the most striking

features under low magnification were transmural chronic inflammation with Crohn-like lymphoid aggregates and marked mural thickening (Fig. 2A). The thickened appendiceal and peri-appendiceal cecal wall showed multiple foci of mixed chronic inflammatory cell infiltration and fibrosis reminiscent of inflammatory pseudotumor (Fig. 2C). The mucosa showed chronic active inflammation, including cryptitis, crypt abscess, crypt distortion, and lymphoplasmacytic infiltration in the lamina propria (Fig. 2D). Fibrous thickening of the subserosa and reactive regional lymph node hyperplasia were observed but there was no neutrophilic infiltration in the proper muscle. A few colonies of filamentous micro-organism of about 150 μm were found within the mucosa as well as in the appendiceal lumen (Fig. 2E), and the filamentous nature of the colonies were better appreciated on periodic acid-Schiff staining (Fig. 2F). The patient was diagnosed with appendiceal actinomycosis and was discharged without any com-

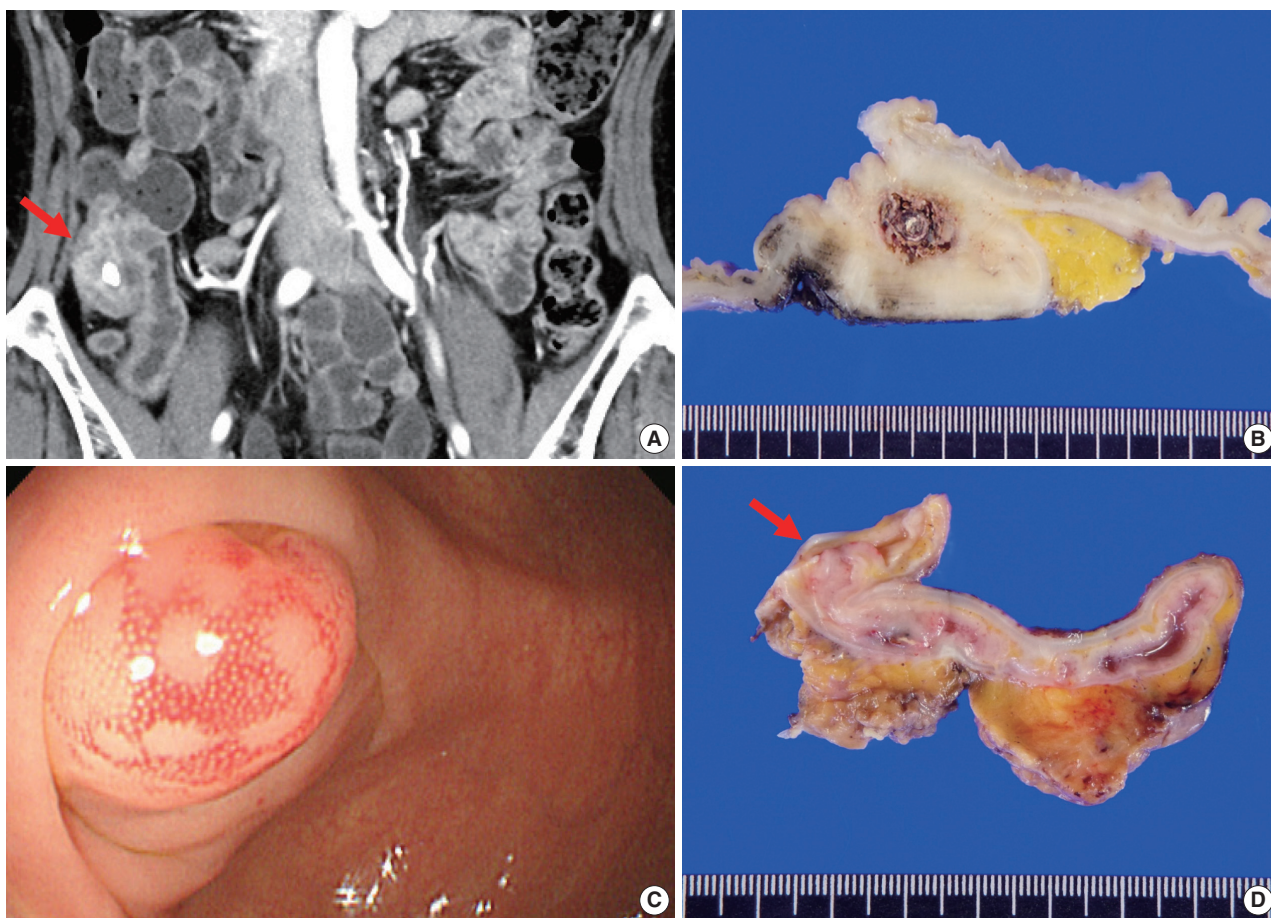


Fig. 1. Radiologic, colonoscopic, and gross features. (A) Contrast-enhanced computed tomography of case No. 1 shows appendicolith, fat infiltration with prominent wall thickening with contrast enhancement in the appendiceal base (arrow). (B) The resected appendix shows marked mural thickening, dilated appendiceal lumen and central fecalith. (C) Colonoscopic image of case No. 2 shows an approximately 10 mm-sized hyperemic mucosal bulging around the appendiceal orifice. (D) Cut surface of the resected specimen shows mucosal bulging (about 1.0cm in great dimension) on the orifice of appendix (arrow).

plications. No additional antibiotics were taken, and until 6 months after surgery, there were no complications or recurrence of actinomycosis.

Case 2

A previously healthy 45-year-old man was incidentally found to have a submucosal mass in the periappendiceal orifice during

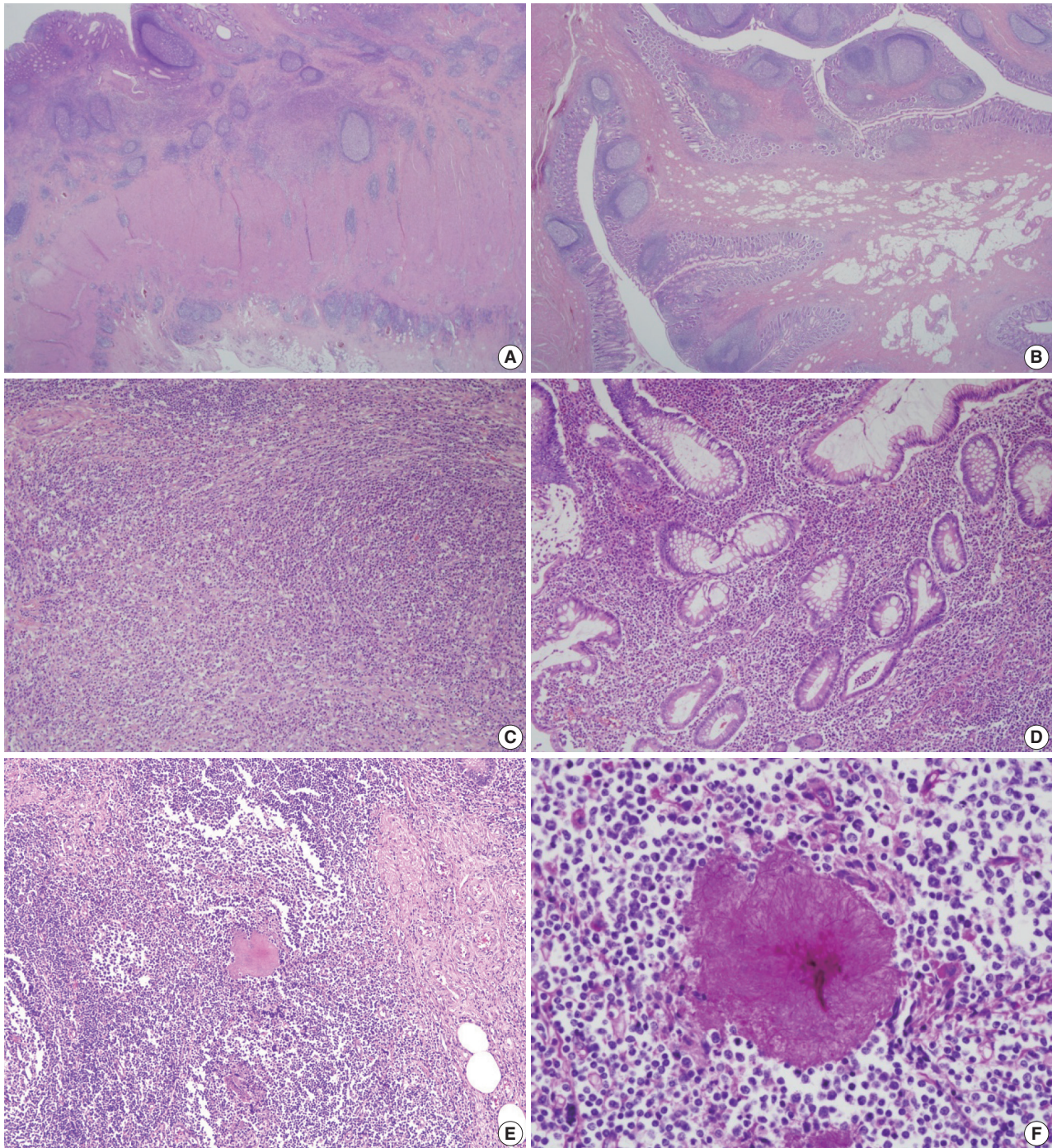


Fig. 2. Representative microscopic pictures. (A) Chronic transmural inflammation with scattered lymphoid follicles or aggregates are observed. (B) The bulging mucosa in colonoscopy is hypertrophic fibroadipose tissue that is covered by inflamed mucosa. (C) One of the fibro-inflammatory foci shows marked lymphoplasmacytic infiltration with fibrosis that is reminiscent of inflammatory pseudotumor. (D) The inflamed mucosa of the appendix shows marked lymphoplasmacytosis, crypt abscess, and crypt distortion. (E) An actinomycotic colony is surrounded by mixed inflammatory cell infiltrates. (F) The filamentous nature is better demonstrated by Periodic acid-Schiff staining.

routine CFS screening. An approximately 1.0 cm-sized hyperemic mucosal bulging was observed around the appendiceal orifice (Fig. 1C). Like case No. 1, the causative organisms were not found in the colonoscopic biopsy specimen. Contrast-enhanced abdominal CT showed intraluminal calcification and enhancing wall thickening in the appendix. Physical examination and laboratory investigation were unremarkable. Based on these findings, both chronic appendicitis and appendiceal malignancy were considered.

The patient underwent ileocecal resection. On gross examination, mucosal bulging (about 1.0 cm in the greatest dimension) was observed in the appendiceal orifice (Fig. 1D). The entire appendiceal wall was fibrotic and the periappendiceal soft tissue was rough and hemorrhagic. A few actinomycotic colonies with surrounding active inflammation were observed in the mucosa. In contrast to case No. 1, additional gross examination and step sectioning were required for identification of the organisms. Prominent transmural reactive lymphoid hyperplasia was also present mainly in the appendix. Mucosal bulging, which looked like a mass lesion on CFS, turned out to be reactive fibroadipose tissue hypertrophy due to chronic inflammation (Fig. 2B). The patient was diagnosed with appendiceal actinomycosis and discharged with oral antibiotics (amoxicillin) for 2 months. Ten months after the surgery, the patient had no other complications or recurrence of actinomycosis.

DISCUSSION

The purpose of this report is to further define the pathologic features of appendiceal actinomycosis so that an accurate pathologic diagnosis can be made. Both cases had localized chronic transmural inflammation with scattered Crohn-like lymphoid aggregates or follicles across the base of the appendix and the cecum around the appendiceal orifice. In addition, there was reactive fibroadipose tissue hypertrophy that appeared as a bulging mass in the appendiceal orifice. Actinomycotic colonies, which are critical for the diagnosis, were relatively hard to find and only a few colonies were observed in the superficial lamina propria and appendiceal lumen. The appendiceal tip had fibrosis similar to chronic appendicitis, and active inflammation was rarely observed. Although a confirmatory diagnosis through colonoscopic biopsy is usually limited, awareness of these pathologic features might lead to an accurate diagnosis of this rare inflammatory mass-like lesion.

To date, there have been a few reports in the literature describing appendiceal actinomycosis, and their clinicopathologic fea-

tures are summarized in Table 1 [1,5,7-13]. Among the 10 cases, six cases were initially diagnosed with appendicitis, while atypical inflammatory condition was suspected in four cases, and one case was suspected to have a malignant tumor on imaging studies. In our series, both patients were asymptomatic, and a wide range of preoperative differential diagnoses including neoplasm, chronic appendicitis, inflammatory mass-like lesion, and tuberculosis were considered. Radiologically, the appendiceal actinomycosis can mimic a malignant neoplasm because it can show contrast enhancement and infiltration into the surrounding tissue. Although these are actually granulation tissue and fibrotic reaction associated with actinomycosis [6], complete exclusion of malignancy is often impossible. Furthermore, goblet cell adenocarcinoma of the appendix may frequently mimic an inflammatory lesion on abdominal CT [14], and tumor cells may not reach the appendiceal orifice in many of them. For these reasons, surgical exploration is frequently required for confirmatory diagnosis.

In pathological perspective, Crohn's disease is histologically quite similar to the actinomycosis in that chronic transmural inflammation is evident. In such cases, it is more suggestive of Crohn's disease when the lesion is not limited to the appendix and histologic features such as patchy lymphoplasmacytic infiltration, non-caseating granulomas, fissure or fistula are observed in bowel segments other than the appendix. Thus, integration of colonoscopic findings and pathologic features is required to exclude Crohn's disease in most cases.

While acute appendicitis should be treated by surgical removal of the appendix [15,16], asymptomatic appendiceal actinomycosis as in our cases might be amenable to medical treatment with antibiotics [5]. Surgery is reserved for patients who fail to respond to antibiotic therapy, or for those with complicated disease as a therapeutic adjunct [4,5,8]. When patients do not show a progressive clinical course, and malignancy is not in the top list of radiologic differential diagnosis, antibiotic therapy might be carefully tried in the presence of microscopic proof of actinomycotic colonies. If patients respond to medical treatment, surveillance endoscopic biopsy along with radiologic test can be used afterwards. If not, pathologic confirmation after surgical resection is required [4,5,7].

To try medical treatment in a patient with suspected appendiceal actinomycosis, detection of the organisms in colonoscopic material is essential. There is a report on an appendiceal actinomycosis case diagnosed by endoscopic biopsy [17]. In the report, the patient had a past history of prior surgical resection for colon adenocarcinoma, and follow up colonoscopic biopsy on a nodular

Table 1. Clinicopathologic features of reported cases of appendiceal actinomycosis

Case	Study	Age (yr)/Sex	Symptom	Radiologic or colonoscopic finding	Initial diagnosis	Pathologic feature	Treatment
1	Atalaia-Martins et al. (2018) [8]	66/F	Abdominal pain	Subepithelial luminal protrusion in the region of the appendiceal orifice with a whitish liquid material discharge	Uncertain	Polymorphic cell infiltrate and erosion with appendiceal fibrosis	Right hemicolectomy
2	Gomez-Torres et al. (2017) [5]	39/M	Abdominal pain, fever, nausea, and vomiting	Non compressible enlarged cecal appendix (58 mm) with peri-appendiceal edema	Appendicitis	Chronic fistulized appendicitis with transmural lymphoid infiltration	Appendectomy
3	Liu et al. (2016) [7]	53/M	Abdominal pain, fever	Distended appendix (9 mm) with surrounding mesenteric stranding	Appendicitis	Lymphoid hyperplasia and chronic inflammatory cells in muscularis propria and serosa	Appendectomy with IV/oral antibiotics (6 months)
4	Liu et al. (2016) [7]	54/F	Abdominal pain, fever	Markedly thickened appendix (18 mm) with periappendiceal fat stranding	Appendicitis	Suppurative granulomatous inflammation	Preoperative antibiotics and drainage with elective appendectomy
5	Ng et al. (2014) [12]	19/F	Abdominal pain, nausea, and vomiting	Markedly swollen appendix (2.3 cm) with a calcified appendicolith	Uncertain	Extensive chronic inflammation and eosinophilic infiltration within the wall of appendix	Ileocecectomy
6	Karakus et al. (2014) [13]	14/M	Abdominal pain and vomiting	Increased (10 mm) thickness of the appendix with nonperistaltic ileocecal region on ultrasonography	Appendicitis	Vermiform appendix with neutrophilic infiltration	Appendectomy
7	Lee et al. (2010) [1]	50/F	Incidental finding (routine screening)	Well defined mass (2 cm) at the origin of appendix	Appendiceal neoplasm of mucosal origin	Localized abscess formation of the appendiceal wall	Appendectomy
8	Nissotakis et al. (2008) [9]	31/M	Abdominal pain	No sign of appendicitis on X-ray and ultrasonography	Appendicitis	Transmural inflammatory cell infiltrate with lymphoid hyperplasia and fibrosis	Appendectomy with oral antibiotics (6 months)
9	Karagulle et al. (2008) [10]	51/F	Abdominal pain, fever and vomiting	3 × 2-cm-sized enhancing mass near cecum	Appendicitis	Chronic active inflammation around sulfur granules	Appendectomy with IV/oral antibiotics (3 months)
10	Koren et al. (2002) [11]	83/F	Abdominal pain	Lobular mass (5 m) attached to the cecum	Uncertain	Dense inflammatory cell infiltration within muscularis and fibropurulent reaction over the serosa	Right hemicolectomy with IV/oral antibiotics (6 months)

lesion in the anastomosis site revealed actinomycotic colonies. However, in general, diagnostic actinomycotic colonies are seldom detected in biopsy material like the present series. Regarding the diagnostic sensitivity for the actinomycotic colonies, there is no consensus upon how many pieces of biopsy are recommended for detection of the causative organisms. In general, a greater number of biopsies would lead to a better diagnostic yield. However, abdominal actinomycosis cannot be easily diagnosed without surgical intervention and colonoscopic approach is often limited in terms of specimen size and accessibility to the lesion especially for that in the appendix. Thus, ultrasound or CT guided aspiration or biopsy, or explorative laparotomy may be a more realistic diagnostic option [5,9-11]. Furthermore, if

there is a past history of previous surgical procedure, bowel preparation, trauma, or prolonged use of intrauterine devices, more aggressive preoperative diagnostic approach might be needed.

In conclusion, integration of clinical, colonoscopic, and radiological features with pathologic findings is necessary to diagnose appendiceal actinomycosis. Awareness of these characteristic clinicopathologic features might lead to suspect and accurately diagnose this uncommon, but clinically important disease. Because the causative organisms are often very hard to find, serial sectioning is advised in colonoscopic biopsy material and extensive sampling is advised in surgically resected specimen.

Ethics Statement

Formal written informed consents were waived by the Institutional Review Board of Asan Medical Center (2019-1213).

Availability of Data and Material

Data sharing not applicable to this article as no datasets were generated or analyzed during the study.

Code Availability

Not applicable.

ORCID

You-Na Sung <https://orcid.org/0000-0003-3340-731X>
 Jihun Kim <https://orcid.org/0000-0002-8694-4365>

Author Contributions

Conceptualization: JK. Data curation: YNS, JK. Investigation: YNS, JK. Writing—original draft: YNS, JK. Approval of final manuscript: all authors.

Conflicts of Interest

The authors declare that they have no potential conflicts of interest.

Funding Statement

No funding to declare.

References

1. Lee SY, Kwon HJ, Cho JH, et al. Actinomycosis of the appendix mimicking appendiceal tumor: a case report. *World J Gastroenterol* 2010; 16: 395-7.
2. Yeguez JF, Martinez SA, Sands LR, Hellinger MD. Pelvic actinomycosis presenting as malignant large bowel obstruction: a case report and a review of the literature. *Am Surg* 2000; 66: 85-90.
3. Cintron JR, Del Pino A, Duarte B, Wood D. Abdominal actinomycosis. *Dis Colon Rectum* 1996; 39: 105-8.
4. Garner JP, Macdonald M, Kumar PK. Abdominal actinomycosis. *Int J Surg* 2007; 5: 441-8.
5. Gomez-Torres GA, Ortega-Garcia OS, Gutierrez-Lopez EG, et al. A rare case of subacute appendicitis, actinomycosis as the final pathology reports: a case report and literature review. *Int J Surg Case Rep* 2017; 36: 46-9.
6. Lee IJ, Ha HK, Park CM, et al. Abdominopelvic actinomycosis involving the gastrointestinal tract: CT features. *Radiology* 2001; 220: 76-80.
7. Liu K, Joseph D, Lai K, Kench J, Ngu MC. Abdominal actinomycosis presenting as appendicitis: two case reports and review. *J Surg Case Rep* 2016; 2016: rjw068.
8. Atalaia-Martins C, Cotrim I, Alves P. Appendiceal tumor or something more? *Gastroenterology* 2018; 154: e14-5.
9. Nissotakis C, Sakorafas GH, Koureta T, Revelos K, Kassaras G, Perros G. Actinomycosis of the appendix: diagnostic and therapeutic considerations. *Int J Infect Dis* 2008; 12: 562-4.
10. Karagulle E, Turan H, Turk E, Kiyici H, Yildirim E, Moray G. Abdominal actinomycosis mimicking acute appendicitis. *Can J Surg* 2008; 51: E109-10.
11. Koren R, Dekel Y, Ramadan E, Veltman V, Dreznik Z. Periappendiceal actinomycosis mimicking malignancy report of a case. *Pathol Res Pract* 2002; 198: 441-3.
12. Ng N, Ng G, Davis BR, Meier DE. Actinomyces appendicitis: diagnostic dilemma--malignancy or infection? *Am Surg* 2014; 80: E33-5.
13. Karakus E, Mambet E, Azili MN, Gulhan B, Tiryaki T, Tezer H. Actinomycosis of the appendix in childhood- an unusual cause of appendicitis. *APSP J Case Rep* 2014; 5: 26.
14. Lee KS, Tang LH, Shia J, et al. Goblet cell carcinoid neoplasm of the appendix: clinical and CT features. *Eur J Radiol* 2013; 82: 85-9.
15. Maternini M, Saucy F, Sandmeier D, Vuilleumier H. Simple appendicitis? *Can J Surg* 2008; 51: E54-5.
16. DeKoning EP. Chapter 84. Acute appendicitis. In: Tintinalli JE, Stapczynski JS, Ma OJ, et al., eds. *Tintinalli's emergency medicine: a comprehensive study guide*. 7th ed. New York: The McGraw-Hill Companies, 2011; 574-8.
17. Piper MH, Schaberg DR, Ross JM, Shartsis JM, Orzechowski RW. Endoscopic detection and therapy of colonic actinomycosis. *Am J Gastroenterol* 1992; 87: 1040-2.

Primary hepatic mixed germ cell tumor in an adult

Hyun-Jung Sung¹, Jihun Kim¹, Kyu-rae Kim¹, Shinkyoo Yoon², Jae Hoon Lee³, Hyo Jeong Kang^{1,4}

Departments of ¹Pathology, ²Oncology, and ³Surgery, ⁴Asan Liver Center, Asan Medical Center, University of Ulsan College of Medicine, Seoul, Korea

Primary hepatic mixed germ cell tumor (GCT) is very rare, and less than 10 cases have been reported. We report a case of mixed GCT composed of a choriocarcinoma and yolk sac tumor, which occurred in the liver of a 40-year-old woman. A large mass was detected by computed tomography solely in the liver. Serum β -human chorionic gonadotropin (hCG) was highly elevated, otherwise, other serum tumor markers were slightly elevated or within normal limits. For hepatic choriocarcinoma, neoadjuvant chemotherapy was administered, followed by right lobectomy. Histologic features of the resected tumor revealed characteristic choriocarcinoma features with diffuse positivity for hCG in the syncytiotrophoblasts and diffuse positivity for α -fetoprotein and Sal-like protein 4 in the yolk sac tumor components. Primary malignant GCT in the liver is associated with a poor prognosis and requires specific treatment. Therefore, GCT should be considered during a differential diagnosis of a rapidly growing mass in the liver.

Key Words: Germ cell tumor; Choriocarcinoma; Yolk sac tumor; Liver; Adult

Received: March 31, 2021 **Revised:** June 15, 2021 **Accepted:** June 16, 2021

Corresponding Author: Hyo Jeong Kang, MD, PhD, Department of Pathology, Asan Medical Center, University of Ulsan College of Medicine, 88 Olympic-ro 43 gil, Songpa-gu, Seoul 05505, Korea
Tel: +82-2-3010-1115, Fax: +82-2-472-7898, E-mail: d100478hjk@gmail.com

Germ cell tumors (GCTs) are currently hypothesized to originate from misplaced primordial germ cells [1]. GCTs usually occur in the gonads. However, GCTs can occur in many extragonadal sites, including the hepatobiliary system, retroperitoneum, and mediastinum from misplaced primordial germ cells during their migration to the gonad [2]. GCTs in the liver are uncommon and constitute less than 1% of all hepatic neoplasms [3]. Most of the reported cases occurred in young children before 3 years of age, and about half of the cases were malignant [4]. Among them, mixed GCTs are extremely rare, and fewer than five cases of mixed GCTs have been reported in the English literature [2-5]. Previously reported mixed GCT primarily had a mature or immature teratoma component [4,5]. In adults, only one yolk sac tumor case with an immature teratoma has been reported [4]. Herein, we report the first case of primary hepatic mixed GCT composed of a choriocarcinoma and yolk sac tumor in a middle-aged Korean woman.

CASE REPORT

A 40-year-old female patient visited an outside hospital and

presented with a 1-month history of uncontrolled abdominal pain. The patient was previously healthy without any notable medical history and her obstetric history was G1P0 with one miscarriage due to spontaneous abortion. She was referred to the Asan Medical Center and computed tomography (CT) indicated that she had a very large liver mass. Her serum β -human chorionic gonadotropin (hCG) was highly elevated (204,200 mIU/mL; normal range, < 3 mIU/mL). Other serum tumor markers of alpha-fetoprotein (AFP, 39.8 ng/mL; normal range, < 7.5 ng/mL) and prothrombin induced by the absence of vitamin K (PIVKA-II, 42 mAU/mL; normal range, < 40 mAU/mL) were slightly elevated, while the levels of serum carbohydrate antigens (CA19-9) and carcinoembryonic antigens (CEA) were within normal limits. Magnetic resonance imaging showed a growing mass that measured 15 × 8.5 cm in the right lobe with multiple intrahepatic metastases in segment IV and the right lobe, which is not a radiological specific finding for hepatocellular carcinoma (Fig. 1A). Positron emission tomography-computed tomography (PET-CT) did not show any extrahepatic lesions. In addition, gynecological ultrasonography did not detect any gestational lesions or malignancy. A target liver biopsy showed nearly all necrotic tis-

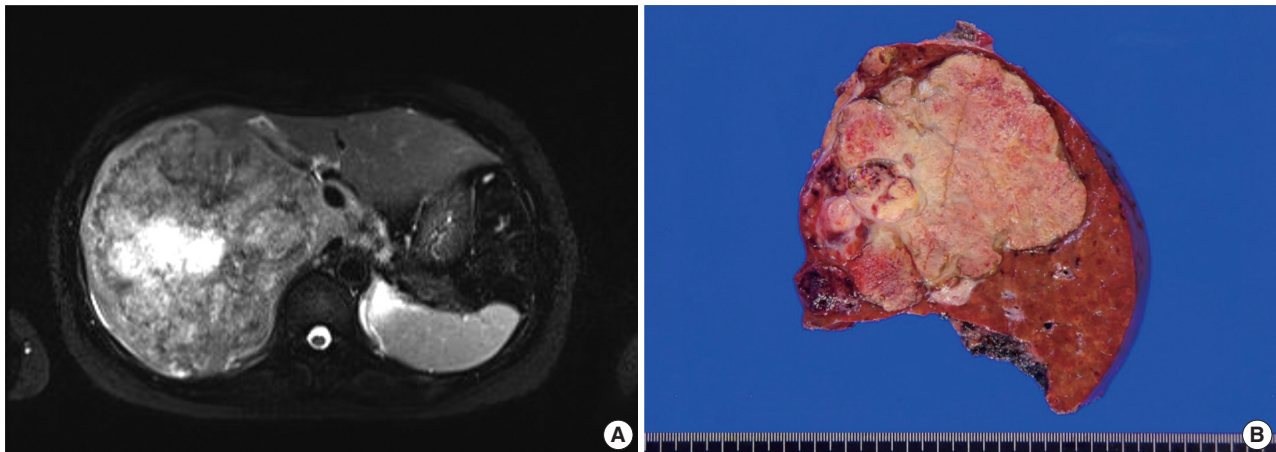


Fig. 1. Radiologic and gross findings. (A) Magnetic resonance image shows hepatomegaly with a large hypervascular mass in the right lobe. (B) The cut surface of a slice from a surgically resected specimen shows a heterogenous pinkish-yellow color, extensive necrosis, and hemorrhage.

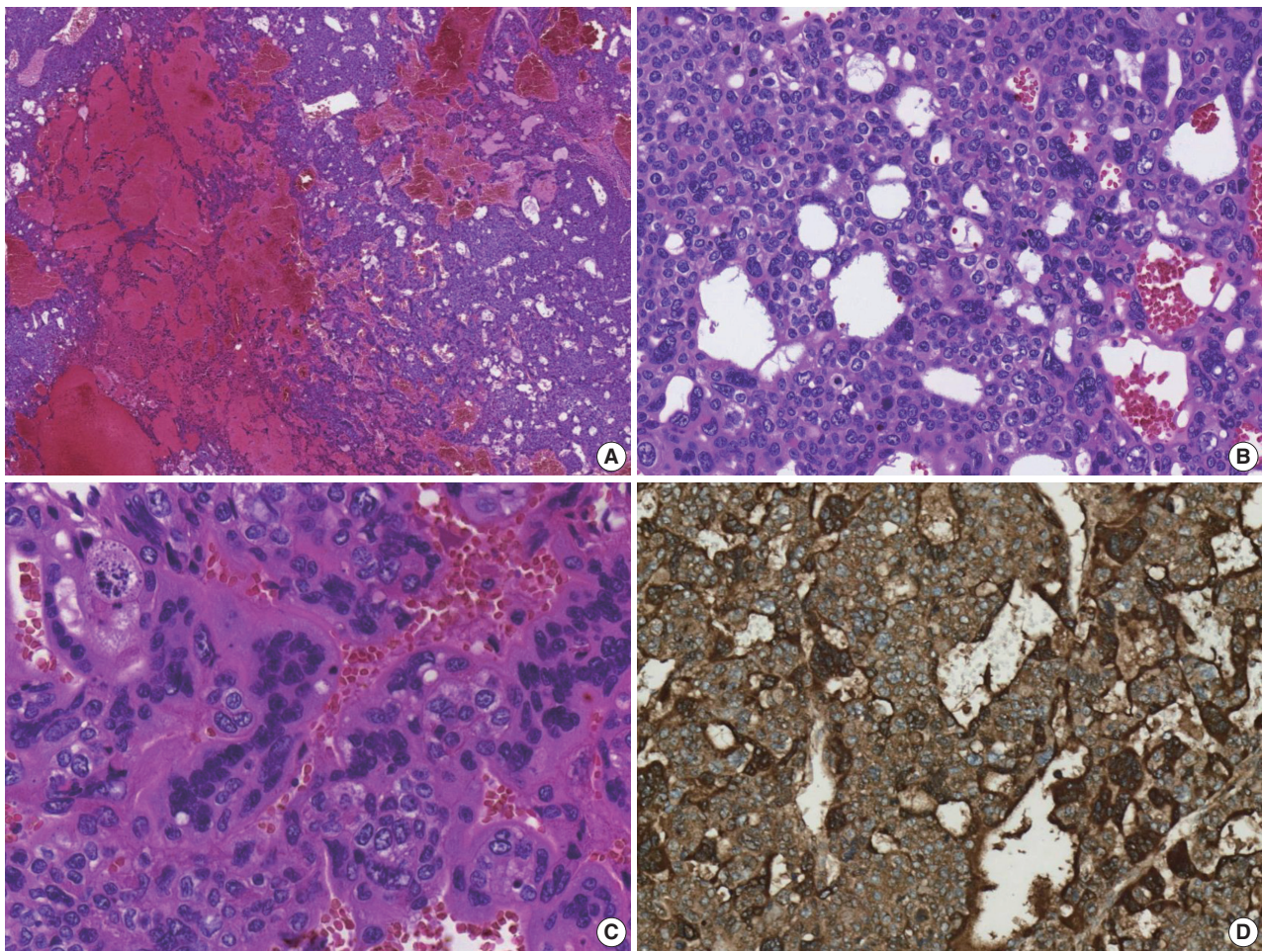


Fig. 2. Microscopic and immunohistochemical (IHC) findings of the choriocarcinoma area. (A) Tumor cells are accompanied by extensive hemorrhage. (B) Tumor cells consist of a mixture of syncytiotrophoblastic and cytotrophoblastic cells. (C) The syncytiotrophoblastic cells are multinucleated with pleomorphic nuclei. (D) β -Human chorionic gonadotropin IHC staining is strongly and diffusely positive.

sue with only a few atypical cells that were diagnosed as insignificant. Based on the clinical information, she was diagnosed with primary hepatic choriocarcinoma, and the patient received neoadjuvant chemotherapy (etoposide, methotrexate, actinomycin D, cyclophosphamide, and vincristine, EMA-CO) before surgical resection. After nine cycles of chemotherapy, the serum β -hCG level was markedly decreased to 47 mIU/mL.

The patient underwent a right hepatectomy and recovered without immediate postoperative complications. Macroscopically, the resected specimen was entirely composed of a well-demarcated and multilobulated 15 × 8.5 cm solid mass. The cut surface revealed a heterogenous pinkish-yellow color, extensive necrosis, and hemorrhage (Fig. 1B). Histologically, the tumor was composed of two GCT components including choriocarcinoma and yolk sac tumors with hepatoid component variants. The choriocarcinoma area showed extensive hemorrhage (Fig. 1A)

and numerous syncytiotrophoblasts surrounded by cytotrophoblasts (Fig. 2B, C). The syncytiotrophoblasts were diffusely positive for hCG in immunohistochemical (IHC) staining (Fig. 2D). The histological features of the yolk sac tumor showed endodermal sinus-like patterns with Schiller-Duval bodies (Fig. 3A). Hepatoid variant components were multifocally identified in the yolk sac tumor area (Fig. 3B). The tumor cells in the yolk sac tumor area were diffusely positive for AFP and Sal-like protein 4 (SALL4) based on IHC staining (Fig. 3C, D). The serum β -hCG level returned to normal (2.3 mIU/mL) after surgery. Despite adjuvant chemotherapy (EMA-CO), multiple intrahepatic and pulmonary metastases were found on a follow-up CT scan on postoperative day 58. She then received gamma knife radiosurgery for 1.2 cm brain metastases in the right parietal lobe on postoperative day 219, and continued adjuvant chemotherapy.

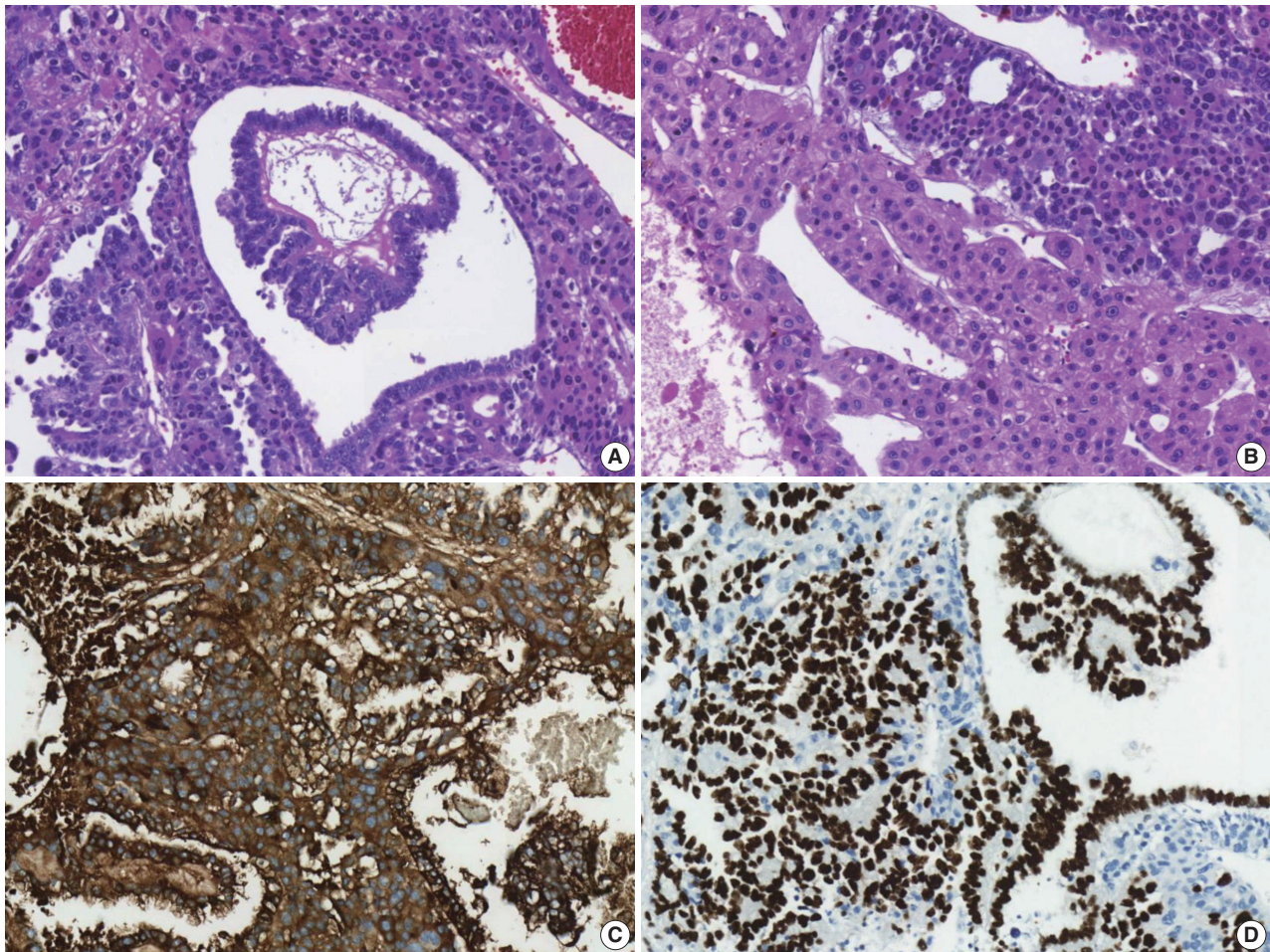


Fig. 3. Microscopic and immunohistochemical (IHC) findings of a yolk sac tumor with a hepatoid variant area. (A) A typical Schiller-Duval body is identified. (B) A hepatoid variant component of the yolk sac tumor is observed. (C) α -Fetoprotein IHC staining is strongly and diffusely positive. (D) Sal-like protein 4 IHC staining is partially positive.

Table 1. Overview of histologically confirmed primary hepatic GCT cases in adults

No.	Author	Age (yr)/Sex	Size (cm)	Treatment	Survival	Diagnosis	Metastasis	IHC (+)
1	Narita et al. [11]	27/F	11	Resection, CTx	> 12 mo	Yolk sac tumor	No	AFP
2	Villaschi and Balistreri [12]	28/F	15	Resection	-	Yolk sac tumor	No	SALL4
3	Wong et al. [18]	28/F	15	Resection	> 12 mo	Yolk sac tumor	No	AFP
4	Arai et al. [20]	65/M	-	None	45 days	Choriocarcinoma	No	hCG
5	Shi et al. [13]	39/M	12	Resection, CTx	6 mo	Choriocarcinoma	No	hCG
6	Shi et al. [13]	45/M	11	CTx	2 mo	Choriocarcinoma	Lung, brain	hCG
7	Shi et al. [13]	48/M	13	CTx	3 mo	Choriocarcinoma	Lung	hCG
8	Shi et al. [13]	36/M	10	CTx	5 mo	Choriocarcinoma	Peritoneum, adrenal gland	hCG
9	Shi et al. [13]	40/M	9	Resection, CTx	8 mo	Choriocarcinoma	No	hCG
10	Bakhshi et al. [21]	40/M	-	Resection	10 days	Choriocarcinoma	No	hCG
11	Sekine et al. [15]	49/M	10	Resection	2 mo	Choriocarcinoma	No	hCG
12	Makhmud et al. [8]	54/F	-	Resection, CTx	-	Choriocarcinoma	Lung	hCG
13	Kohler et al. [14]	64/M	14.5	Resection, CTx	5 mo	Choriocarcinoma	Lung	hCG

GCT, germ cell tumor; IHC, immunohistochemistry; F, female; CTx, chemotherapy; AFP, α -fetoprotein; SALL4, Sal-like protein 4; M, male; hCG, human chorionic gonadotropin.

DISCUSSION

GCTs are germinal neoplasms that arise in the gonads and extragonadal sites. GCTs account for about 3% of neoplasms in childhood and adolescence. The incidence is bimodal, and peaks at around 2 years of age, with another peak after puberty [2]. Extragonadal GCTs commonly arise from midline structures, including the mediastinum and retroperitoneum [6].

Gastrointestinal GCTs, especially primary hepatic GCTs, are very uncommon and constitute less than 1% of hepatic neoplasms. Therefore, collective descriptions of the clinicopathological features and prognosis of these tumors are rare. The etiology, clinical course, and prognosis of hepatic GCTs are not well-understood. The possible mechanisms for the development of primary hepatic GCTs are arrest and survival of germ cell precursors at ectopic sites during embryological migration as well as proliferation of pluripotent cells [7].

When diagnosing primary hepatic GCTs, the main challenge is the differential diagnosis of primary hepatic GCT from metastasis of other organs, especially from the ovaries or testis, because hepatic GCTs are more likely to have metastasized [8]. Therefore, it is important to exclude a metastasis from gonadal origin. The patient in this report showed no notable medical history and no other tumor sites were identified after extensive preoperative imaging studies. Applying either isochromosome 12p or 12p overrepresentation by fluorescence in situ hybridization (FISH) may be helpful for diagnosing germ cell tumors [9,10], but it is difficult to conduct FISH testing in most hospitals. Therefore, the primary hepatic mixed GCT in this case was diagnosed based on the clinicopathologic features and the IHC staining results.

To the best of our knowledge, this is the first report of mixed

GCT composed of choriocarcinoma and yolk sac tumors that originated in the liver of an adult. To date, only 13 cases of primary hepatic GCTs in adult case reports or case series have been reported in the literature, all of which are summarized in Table 1 [4,6,8,11-19]. Primary hepatic GCTs predominantly affect males with a male to female ratio of 2:1. The average age for the occurrence in adults was 43 years (range, 27 to 65 years). Although most patients received surgical resections and some received adjuvant chemotherapy, they had poor prognoses (mean survival, 3.64 ± 2.49 months).

In summary, primary hepatic GCTs should be considered during the differential diagnosis of a rapidly growing solid mass in the liver because they require different treatment approaches, compared with other primary hepatic malignancies, such as hepatocellular carcinomas and cholangiocarcinomas.

Ethics Statement

The study was approved by the Institutional Review Board of Asan Medical Center (IRB 2021-0180). Formal written informed consent was not required, with a waiver from the appropriate Institutional Review Board.

Availability of Data and Material

All data generated or analyzed during the study are included in this published article (and its supplementary information files).

Code Availability

Not applicable.

ORCID

Hyun-Jung Sung <https://orcid.org/0000-0002-8791-5945>
 Jihun Kim <https://orcid.org/0000-0002-8694-4365>
 Kyu-rae Kim <https://orcid.org/0000-0002-5781-7447>
 Shinkyoo Yoon <https://orcid.org/0000-0001-7544-0404>
 Jae Hoon Lee <https://orcid.org/0000-0002-6170-8729>
 Hyo Jeong Kang <https://orcid.org/0000-0002-5285-8282>

Author Contributions

Conceptualization: HJK. Data curation: HJS. Investigation: HJS. Supervision: HJK. Visualization: HJS. Writing—original draft: HJS. Writing—review & editing: HJK, JK, KK, SY, JHL. Approval of final manuscript: all authors.

Conflicts of Interest

The authors declare that they have no potential conflicts of interest to disclose.

Funding Statement

No funding to declare.

References

1. Murat E, Dagdemir A, Bilgici MC, Sullu Y. Primary yolk sac tumor of the retroperitoneal region. *Contemp Oncol (Pozn)* 2013; 17: 530-2.
2. Fanelli MC, Duarte AA, de Souza FK, et al. Primary germ cell tumor of the liver. *J Pediatr Surg Case Rep* 2019; 51: 101324.
3. Theegarten D, Reinacher A, Graeven U, Philippou S. Mixed malignant germ cell tumour of the liver. *Virchows Arch* 1998; 433: 93-6.
4. Xu AM, Gong SJ, Song WH, et al. Primary mixed germ cell tumor of the liver with sarcomatous components. *World J Gastroenterol* 2010; 16: 652-6.
5. Verma M, Agarwal S, Mohta A. Primary mixed germ cell tumour of the liver: a case report. *Indian J Pathol Microbiol* 2003; 46: 658-9.
6. Vanidassane I, Sharma V, Ramteke P, Yadav MK, Batra A. Primary yolk sac tumor of the liver in an adult man. *ACG Case Rep J* 2019; 6: e00050.
7. Bosman FT, Carneiro F, Hruban RH, Theise ND. WHO classification of tumours of the digestive system. Lyon: IARC, 2010.
8. Makhmud M, Shin E, Cho JY, et al. Primary hepatic choriocarcinoma in a female patient. *Korean J Clin Oncol* 2015; 11: 33-6.
9. Kranendonk MEG, Hackeng WM, Offerhaus GJA, et al. The decisive role of molecular pathology in presumed somatic metastases of type II testicular germ cell tumors: report of 2 cases. *Diagn Pathol* 2020; 15: 99.
10. Wehle D, Yonescu R, Long PB, Gala N, Epstein J, Griffin CA. Fluorescence in situ hybridization of 12p in germ cell tumors using a bacterial artificial chromosome clone 12p probe on paraffin-embedded tissue: clinical test validation. *Cancer Genet Cytogenet* 2008; 183: 99-104.
11. Narita T, Moriyama Y, Ito Y. Endodermal sinus (yolk sac) tumour of the liver: a case report and review of the literature. *J Pathol* 1988; 155: 41-7.
12. Villaschi S, Balistreri P. Endodermal sinus tumour of the liver. *Histopathology* 1991; 18: 86-8.
13. Shi H, Cao D, Wei L, Sun L, Guo A. Primary choriocarcinoma of the liver: a clinicopathological study of five cases in males. *Virchows Arch* 2010; 456: 65-70.
14. Kohler A, Welsch T, Sturm AK, et al. Primary choriocarcinoma of the liver: a rare, but important differential diagnosis of liver lesions. *J Surg Case Rep* 2018; 2018: rjy068.
15. Sekine R, Hyodo M, Kojima M, et al. Primary hepatic choriocarcinoma in a 49-year-old man: report of a case. *World J Gastroenterol* 2013; 19: 9485-9.
16. Fernandez Alonso J, Saez C, Perez P, Montano A, Japon MA. Primary pure choriocarcinoma of the liver. *Pathol Res Pract* 1992; 188: 375-7.
17. Natori T, Teshima S, Kikuchi Y, et al. Primary yolk sac tumor of the liver: an autopsy case with ultrastructural and immunopathological studies. *Acta Pathol Jpn* 1983; 33: 555-64.
18. Wong NA, D'Costa H, Barry RE, Alderson D, Moorghen M. Primary yolk sac tumour of the liver in adulthood. *J Clin Pathol* 1998; 51: 939-40.
19. Whelan JS, Stebbings W, Owen RA, Calne R, Clark PI. Successful treatment of a primary endodermal sinus tumor of the liver. *Cancer* 1992; 70: 2260-2.
20. Arai M, Oka K, Nihei T, et al. Primary hepatic choriocarcinoma: a case report. *Hepatogastroenterology* 2001; 48: 424-6.
21. Bakhshi GD, Borisa AD, Bhandarwar AH, Tayade MB, Yadav RB, Jadhav YR. Primary hepatic choriocarcinoma: a rare cause of spontaneous haemoperitoneum in an adult. *Clin Pract* 2012; 2: e73.

Metastatic leiomyosarcoma of the thyroid gland: cytologic findings and differential diagnosis

Jiyeon Lee, Yunjoo Cho, Kyue Hee Choi, Inwoo Hwang, Young Lyun Oh

Department of Pathology and Translational Genomics, Samsung Medical Center, Sungkyunkwan University School of Medicine, Seoul, Korea

Metastatic leiomyosarcoma to the thyroid is an extremely rare occurrence, and only 18 cases have been reported. Here, we report a case of a 37-year-old woman who presented with multiple masses on the scalp. Excisional biopsy was done and the mass revealed fascicles of smooth muscle fibers which showed positive staining for smooth muscle actin, thus confirming the diagnosis of leiomyosarcoma. The patient was also found to have a 0.9 cm mass within the left thyroid. Fine-needle aspiration was done and the cytological smear showed hypercellular spindle cell clusters with hyperchromatic and large nuclei. Normal thyroid follicular cells were found within or around tumor cells. In this report, we present the cytologic findings of metastatic leiomyosarcoma to the thyroid and offer differential diagnoses of the aspirated spindle cells.

Key Words: Leiomyosarcoma, secondary; Cytology; Leiomyosarcoma; Thyroid neoplasms

Received: March 25, 2021 **Revised:** June 14, 2021 **Accepted:** June 22, 2021

Corresponding Author: Young Lyun Oh, MD, PhD, Department of Pathology and Translational Genomics, Samsung Medical Center, 81 Ilwon-ro, Gangnam-gu, Seoul 06351, Korea
Tel: +82-2-3410-2805, Fax: +82-2-3410-2831, E-mail: bjou@skku.edu

Soft tissue sarcoma metastatic to the thyroid is extremely rare, and it poses a challenge for a pathologist to diagnose it on cytology aspiration alone. Here, we report a case of metastatic leiomyosarcoma to the thyroid and describe in detail its cytologic findings.

CASE REPORT

A 37-year-old woman presented with multiple masses on the scalp. She underwent an excisional biopsy of the scalp mass at a local clinic and visited our hospital for further work up. Computed tomography of the neck revealed a poorly enhancing mass lesion in the left lobe of the thyroid measuring about 1 cm with ipsilateral cervical lymph node metastasis (Fig. 1A). An ultrasonographic examination of the thyroid revealed a 0.9 cm hypoechoic mass without increased vascularity (Fig. 1B). Ultrasound-guided fine-needle aspiration (FNA) was done to rule out the possibility of primary thyroid cancer. Unlike a typical thyroid malignancy, the aspirated material was sticky and difficult to aspirate.

The alcohol-fixed smears were stained with hematoxylin and

eosin and Papanicolaou for the cytologic examination. The cytological smears were hypercellular and displayed spindle cell clusters in hemorrhagic background. No necrotic material was observed. The spindle cells were arranged in a fascicular pattern and showed an indistinct cell border. The cells had eosinophilic and fibrillary cytoplasm. Individual cells showed variation in nuclear size and shape. However, the nuclei of most of the cells were hyperchromatic and large, and they demonstrated an elongated shape with blunt ends (Fig. 2A, B). Normal follicular cells were admixed with pleomorphic tumor cells, and were also observed around tumor cell clusters (Fig. 2C, D). These features raised the suspicion for a malignant tumor of mesenchymal origin.

Histological slides from the resection specimen of the scalp mass revealed a small nodular mass measuring 0.8×0.6 cm. The tumor cells were arranged in bundles or fascicles of smooth muscle fibers (Fig. 3A). They were highly pleomorphic and had a centrally located, blunted, cigar-shaped nucleus adjacent to perinuclear cytoplasmic vacuoles. The mitotic rate was high (7 mitosis per 10 high-power field), but there was no area of necrosis. Immunohistochemical staining showed a positive result for smooth muscle actin (SMA) and desmin (Fig. 3).

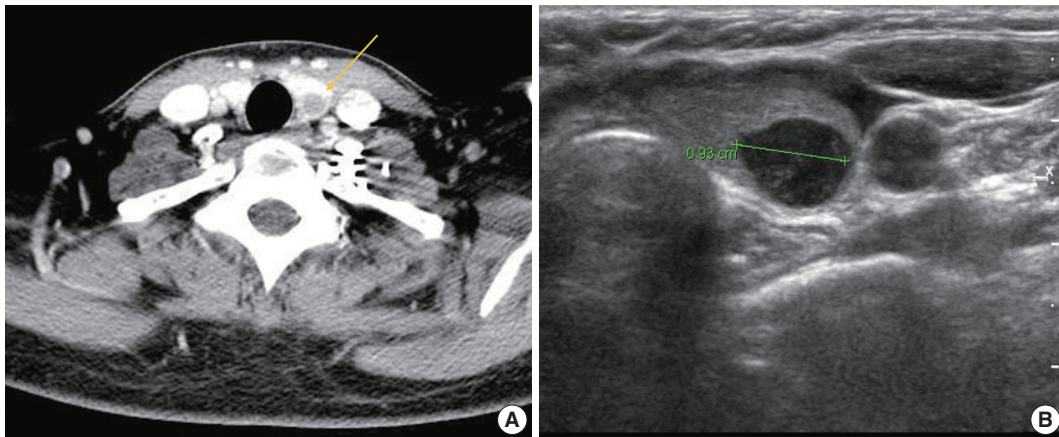


Fig. 1. Radiologic findings of metastatic leiomyosarcoma. (A) Computed tomography scan reveals 1 cm sized poorly enhancing space occupying lesion (arrow) in left thyroid. (B) Ultrasound shows marked hypoechoic nodule in the inferior pole of left thyroid.

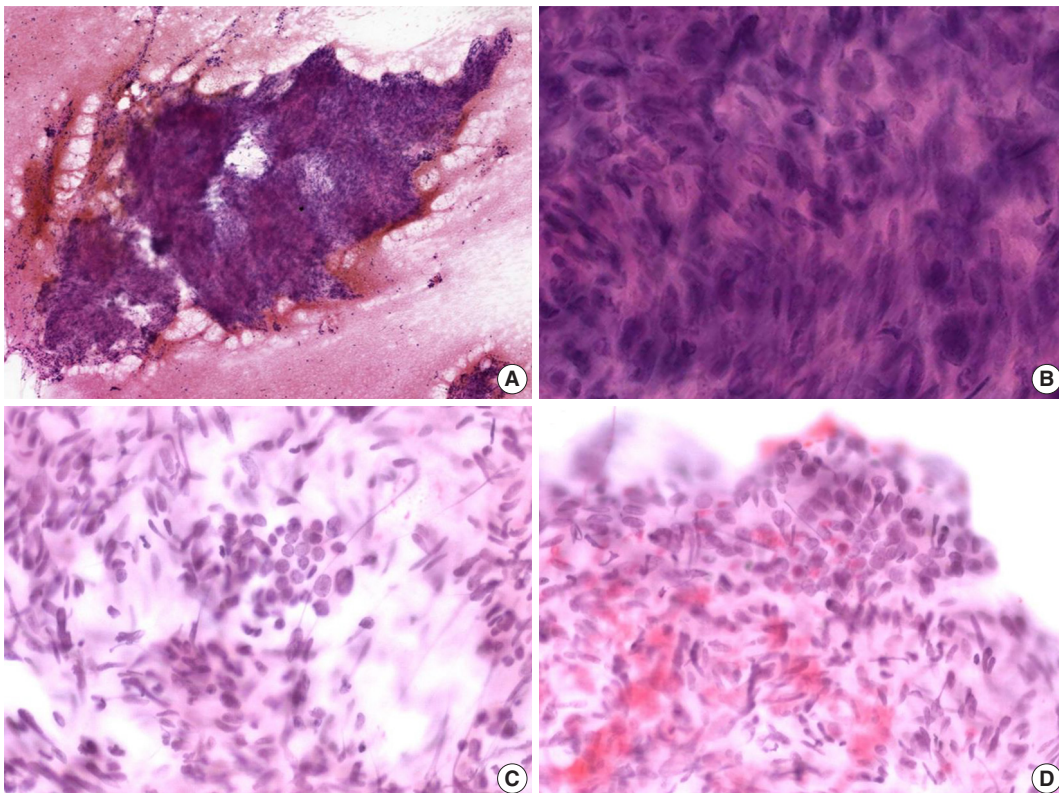


Fig. 2. Cytologic features of metastatic leiomyosarcoma. (A) Hypercellular spindle cell clusters are arranged in a fascicular pattern. (B) The cells show indistinct cell borders, eosinophilic cytoplasm, and hyperchromatic, large, elongated nuclei with blunt ends. (C, D) Normal follicular cells are admixed with pleomorphic tumor cells (C) or discovered around tumor cell clusters (D).

Positron emission tomography–computed tomography revealed several hypermetabolic masses on the right side of the abdomen, the largest of which measured 5.8 cm. One mass was located in the mesentery, which had no association with the uterus. In addition, there were multiple hypermetabolic lesions in the left internal mammary area, both thigh, and the lung. To exclude other

spindle cell tumors which can arise in the abdominal cavity, immunostaining for S100, CD34, MDM2, c-Kit, and anaplastic lymphoma kinase were performed. All of the additional immunohistochemical stainings turned out negative, and the possibility of schwannoma, solitary fibrous tumor, liposarcoma, gastrointestinal stromal tumor and inflammatory myofibroblastic

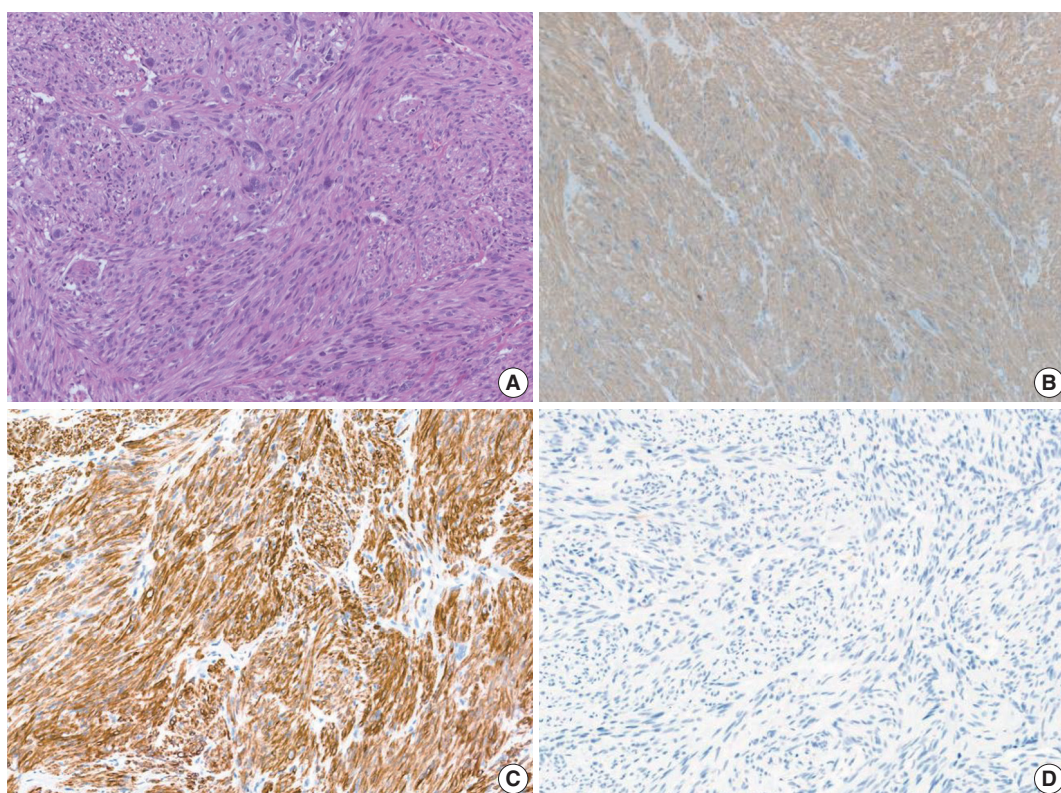


Fig. 3. Histologic features of the scalp mass. (A) Excisional biopsy specimen from the scalp mass shows bundles or fascicles of smooth muscle fibers. The tumor cells are highly pleomorphic and have a centrally located, blunted, cigar-shaped nucleus adjacent to perinuclear cytoplasmic vacuoles. (B, C) Smooth muscle actin (B) and desmin (C) immunostaining shows positivity. (D) c-Kit immunostaining shows negativity.

tumor were ruled out, respectively. Considering all the clinical, morphological and immunohistochemical features, we determined that the final diagnosis of the tumor located in the thyroid gland to be metastatic leiomyosarcoma from the mesentery. Because of the presence of metastatic disease, the patient received doxorubicin-based chemotherapy instead of further surgical intervention. She is still alive 22 months after her first visit.

DISCUSSION

Metastasis of sarcoma to the thyroid is rare with a few cases reported in the literature. To date, 18 cases have been reported as metastatic leiomyosarcoma to the thyroid, most of which are from uterine leiomyosarcoma (Table 1). Furthermore, it is very rare to be diagnosed using FNA cytology [1-3].

FNA cytology of metastatic leiomyosarcoma tends to show hypercellular spindle cell clusters with marked pleomorphism, and there can be conspicuous mitoses. Therefore, the differential diagnosis should include primary thyroid tumors showing spindle cell features; such as medullary carcinoma, anaplastic carcinoma and spindle epithelial tumor with thymus-like differenti-

ation (SETTLE). Likewise, primary or metastatic mesenchymal tumors like malignant peripheral nerve sheath tumor (MPNST) or synovial sarcoma should be considered.

Medullary thyroid carcinoma is one of the first differential diagnosis to consider when spindle cells are observed in thyroid FNA. However, the characteristic cytology of medullary carcinoma is dispersed single cells having “salt-and-pepper” nuclei. In most cases, oval-to-plasmacytoid cells were observed together.

Cytomorphologically, SETTLE has a close resemblance to leiomyosarcoma. They can be shown as variably sized groups of spindle cells with uniform, elongated, and cigar-shaped nuclei similar to those of leiomyosarcoma [4]. In addition, epithelial components of SETTLE can mimic benign follicular cells that appear in metastatic leiomyosarcoma. However, diffuse immunoreactivity for cytokeratin in both components is the most obvious difference from leiomyosarcoma.

Anaplastic carcinomas also have spindle-shaped cells. However, anaplastic carcinomas rarely occur below the age of 50 and usually present as a rapidly growing mass infiltrating surrounding soft tissues. Spindle cells in anaplastic carcinoma show a more bizarre morphology compared to that shown in leiomyosarcoma

Table 1. Clinicopathological and immunohistochemical data on 18 reported cases of metastatic leiomyosarcoma of the thyroid gland

Author	Age (yr)	Sex	Origin	Chief complaint	Location/size	Cytology	Pathology	Vimentin	Desmin	SMA	CD34	S100	Cytokeratin	Thyroglobulin
Gross and Horton (1975) [5]	46	M	Great saphenous vein	Painless swelling in neck	N/M	-	-	-	-	-	-	-	-	-
Cruickshank (1988) (as cited in Vankalakunti et al. [6])	30	F	Uterus	Diffuse thyroid swelling	N/M	-	-	-	-	-	-	-	-	-
Gattuso et al. (1989) [2]	N/M	N/M	Retroperitoneal	N/M	Left thyroid/3 cm	-	-	-	-	-	-	-	-	-
Bode-Lesniewska et al. (1994) [7]	69	F	Duodenum	N/M	5 cm	-	-	-	-	-	-	-	-	-
Michelow (1995) (as cited in Vankalakunti et al. [6])	N/M	N/M	Uterus	Thyroid nodular swelling	N/M	-	-	-	-	-	-	-	-	-
Nakhiavani (1997) (as cited in Vankalakunti et al. [6])	N/M	N/M	Uterus	N/M	N/M	-	-	-	-	-	-	-	-	-
Wang et al. (1998) [8]	63	F	Left leg	Rapidly progressive enlargement of the neck	N/M	-	-	-	-	-	-	-	-	-
Chen et al. 1999 [9]	N/M	N/M	Stomach	N/M	Unilateral	Anaplastic, malignant spindle cell tumor	N/D	-	-	-	-	-	-	-
Leath et al. (2002) [10]	5th decade	F	Uterus	Postmenopausal bleeding	Diffuse and numerous/ up to 2.9 cm	N/D	Smooth muscle cells with atypia and mitotic figures	N/D	Strong, positive	Focal, positive	N/D	N/D	N/D	N/D
D'Andrea et al. (2003) [11]	60	F	Pulmonary artery	Dyspnea and hemoptysis	Both thyroid/ up to 4.7 cm	N/D	N/D	-	-	-	-	-	-	-
Deng et al. (2005) [12]	N/M	N/M	Leg	N/M	N/M	-	-	-	-	-	-	-	-	-
Giamnikaki et al. (2006) [13]	54	F	Uterus	Single "cold" nodule in the right thyroid	Right thyroid/0.12 cm co-existing with PTC	N/D	Spindle cells with prominent nuclear atypia and mitoses	N/D	Positive	Positive	N/D	N/D	Negative	N/D
Eloy et al. (2007) [14]	54	F	Uterus	Rapidly enlarging and painful left neck mass	Left thyroid/ 2.5 cm	Consistent with a sarcomatous lesion	Large cells with hypercellularity, nuclear atypia, and pleomorphism with atypical mitoses	Positive	Negative	Negative	N/D	Negative	Negative	Negative
Nemenoqari et al. (2010) [1]	86	F	Pelvic soft tissue	Right thyroid swelling	Right thyroid	Hypercellular spindle cell proliferation arranged in sheets mixed with stroma; marked pleomorphism; large hyperchromatic nuclei; numerous mitoses	Numerous mitoses and bizarre nuclei	Positive	Negative	Positive	Negative	Negative	Negative	Negative

(Continued to the next page)

Table 1. Continued

Author	Age (yr)	Sex	Origin	Chief complaint	Location/size	Cytology	Pathology	Vimentin	Desmin	SMA	CD34	S100	Cytokeratin	Thyroglobulin
Young et al. (2011) [15]	55	F	Lung	Cough	N/M	N/D	Fascicular pattern of spindle-shaped cells with increased cellularity and hyperchromatic, bizarre, malformed, and megakaryocytic nuclei	Positive	Focal positive	Positive	Negative	Negative	N/D	N/D
Gauthier et al. (2017) [16]	47	F	Uterus	Fast growing thyroid nodule	N/M	N/D	N/D	N/D	N/D	N/D	N/D	N/D	N/D	N/D
Golovko et al. (2020) [17]	65	F	Vagina	Multinodular toxic goiter	Right thyroid	Suggestive of the benign thyroid lesion	Consistent with metastatic vaginal leiomyosarcoma	N/D	N/D	N/D	N/D	N/D	N/D	N/D
Inzary-Villafane et al. (2020) [18]	47	F	Uterus	Neck discomfort	Left upper lobe/2.4 cm	Marked cellularity of atypical spindle cells, dyscohesive, and in tissue aggregates with some binucleated cells	Spindle cell tumor with frequent mitotic figures	N/D	Positive	Positive	N/D	N/D	Negative	Negative

SMA, smooth muscle actin; M, male; F, female; N/M, not mentioned; N/D, not done.

[19]. Osteoclast-like giant cells, necrosis, and mitotic figures are a common feature, and in more than half of the case, anaplastic carcinomas are positive for cytokeratin. PAX8 is positive in about 80% of anaplastic carcinomas.

MPNST can present as highly cellular clusters of spindle cells showing wavy, elongated nuclei with tapered ends [20]. The cytologic features of synovial sarcoma include hypercellular and uniform oval-to-spindle cells without nuclear pleomorphism or necrosis. Despite its biphasic nature, the epithelial component is rarely observed in the FNA specimen.

Although there are differences between the differential diagnoses as described above, it is nearly impossible to conclusively diagnose leiomyosarcoma in FNA slides with only histologic observation of the cells in cytologic smears. Immunohistochemistry is crucial for a precise diagnosis. Leiomyosarcoma is positive for vimentin, SMA, muscle-specific actin, desmin and h-caldesmon and negative for cytokeratin, thyroglobulin, calcitonin, and S-100 protein. In our case, we diagnosed leiomyosarcoma by confirming that the resected scalp mass was positive for SMA and desmin and negative for S-100 protein, CD34, MDM2, c-Kit, and anaplastic lymphoma kinase. It is difficult to make a distinction between primary and metastatic leiomyosarcoma cytologically. Metastases to the thyroid gland occur more frequently than is generally appreciated and can be easily misdiagnosed as a primary thyroid tumor. Given the rarity of thyroid primary sarcoma, pathologists should be alert to the possibility of metastatic tumor, especially when benign follicular cells are identified within or around malignant cells.

Ethics Statement

This study was approved by the Institutional Review Board of Samsung Medical Center with a waiver of informed consent (IRB No. 2021-03-125).

Availability of Data and Material

The datasets generated or analyzed during the study are available from the corresponding author on reasonable request.

Code Availability

Not applicable.

ORCID

- Jiyeon Lee <https://orcid.org/0000-0002-4457-7499>
- Yunjoo Cho <https://orcid.org/0000-0003-1309-2015>
- Kyue Hee Choi <https://orcid.org/0000-0001-8386-5349>
- Inwoo Hwang <https://orcid.org/0000-0002-7749-3929>
- Young Lyun Oh <https://orcid.org/0000-0002-9127-4642>

Author Contributions

Conceptualization: YLO. Data curation: JL. Formal analysis: JL. Investigation: JL, YC, IH, KHC, YLO. Methodology: JL, YC. Resources: YLO. Super-

vision: YLO. Validation: YLO, JL. Visualization: JL, YC. Writing—original draft: JL. Writing—review & editing: YLO, YC. Approval of final manuscript: all authors.

Conflicts of Interest

The authors declare that they have no potential conflicts of interest.

Funding Statement

No funding to declare.

References

1. Nemenqani D, Yaqoob N, Khoja H. Leiomyosarcoma metastatic to the thyroid diagnosed by fine needle aspiration cytology. *J Pak Med Assoc* 2010; 60: 307-9.
2. Gattuso P, Castelli MJ, Reyes CV. Fine needle aspiration cytology of metastatic sarcoma involving the thyroid. *South Med J* 1989; 82: 1158-60.
3. Michelow PM, Leiman G. Metastases to the thyroid gland: diagnosis by aspiration cytology. *Diagn Cytopathol* 1995; 13: 209-13.
4. Tong GX, Hamele-Bena D, Wei XJ, O'Toole K. Fine-needle aspiration biopsy of monophasic variant of spindle epithelial tumor with thymus-like differentiation of the thyroid: report of one case and review of the literature. *Diagn Cytopathol* 2007; 35: 113-9.
5. Gross E, Horton MA. Leiomyosarcoma of the saphenous vein. *J Pathol* 1975; 116: 37-41.
6. Vankalakunti M, Kaur J, Srinivasan R. Cytology of sarcoma metastasizing to the thyroid: a case report. *Acta Cytol* 2008; 52: 729-32.
7. Bode-Lesniewska B, Schroder S, Gemenjager E, Staubli M, Pfaltz M. Leiomyosarcoma in the thyroid gland: primary tumor or metastasis?. *Pathologie* 1994; 15: 303-7.
8. Wang TY, Lee CH, Yang AH, P'Eng FK, Lui WY. Metastatic leiomyosarcoma of the thyroid: a case report. *Zhonghua Yi Xue Za Zhi (Taipei)* 1998; 61: 353-7.
9. Chen H, Nicol TL, Udelsman R. Clinically significant, isolated metastatic disease to the thyroid gland. *World J Surg* 1999; 23: 177-80.
10. Leath CA 3rd, Huh WK, Straughn JM Jr, Conner MG. Uterine leiomyosarcoma metastatic to the thyroid. *Obstet Gynecol* 2002; 100: 1122-4.
11. D'Andrea N, Romano V, Mattioli E, et al. Pulmonary artery leiomyosarcoma with thyroid metastases. *Monaldi Arch Chest Dis* 2003; 59: 304-7.
12. Deng XR, Wang G, Kuang CJ, Peng GZ, Chen RS. Metastasis of leiomyosarcoma to the thyroid. *Chin Med J (Engl)* 2005; 118: 174-6.
13. Giannikaki E, Mantadakis E, Mamalaki E, Delides G, Samonis G. Metastatic uterine leiomyosarcoma coexisting with papillary carcinoma of the thyroid gland. *Int J Gynecol Cancer* 2006; 16: 442-5.
14. Eloy JA, Mortensen M, Gupta S, Lewis MS, Brett EM, Genden EM. Metastasis of uterine leiomyosarcoma to the thyroid gland: case report and review of the literature. *Thyroid* 2007; 17: 1295-7.
15. Woo Young K, Young Ran K, Sang Uk W, Jae Bok L. Pulmonary leiomyosarcoma metastatic to the thyroid gland: case report and review of the literature. *Ann Endocrinol (Paris)* 2011; 72: 314-6.
16. Gauthe M, Testart Dardel N, Nascimento C, Trassard M, Banal A, Alberini JL. Uterine leiomyosarcoma metastatic to thyroid shown by (18)F-FDG PET/CT imaging. *Rev Esp Med Nucl Imagen Mol* 2017; 36: 113-5.
17. Golovko A, Kuryk O, Tkachenko R, Mendel N. Thyroid metastasis of vaginal leiomyosarcoma: a case report and review of the literature. *Exp Oncol* 2020; 42: 242-4.
18. Irizarry-Villafane G, Rivera-Santana N, Mangual-Garcia M, et al. A rare case of uterine leiomyosarcoma with metastasis to the thyroid gland. *Case Rep Endocrinol* 2020; 2020: 8889843.
19. Papi G, Corrado S, LiVolsi VA. Primary spindle cell lesions of the thyroid gland: an overview. *Am J Clin Pathol* 2006; 125 Suppl: S95-123.
20. Sanchez B, Dutra J, Nayar R, Lin X. Metastatic malignant peripheral nerve sheath tumor to the thyroid. *J Thyroid Cancer* 2015; 1: 18-23.



PathologyOutlines.com

What's new in gynecologic pathology 2021: ovary and fallopian tube

Gulisa Turashvili¹ and Ricardo Lastra²

¹Department of Pathology and Laboratory Medicine, Sinai Health System and University of Toronto, Toronto, ON, Canada

²Department of Pathology, University of Chicago Medical Center, Chicago, IL, USA

Received: July 26, 2021 Accepted: July 28, 2021
 Corresponding Author: Gulisa Turashvili, MD, PhD
 Department of Pathology and Laboratory Medicine
 Sinai Health System and University of Toronto
 Toronto, Ontario, Canada
 E-mail: Gulisa.Turashvili@sinaihealth.ca

ORCID

Gulisa Turashvili
<https://orcid.org/0000-0001-6125-5865>

Ricardo Lastra
<https://orcid.org/0000-0003-0691-5685>

This article has been published jointly, with consent, in both Journal of Pathology and Translational Medicine and PathologyOutlines.com.

Abstract

The 5th edition of the World Health Organization (WHO) Classification of Female Genital Tumors was published in 2020. Although the classification of ovarian and fallopian tube neoplasms is largely unchanged from the prior (4th) edition, this newsletter compiles the most important refinements in these organ sites, including serous and non-serous epithelial tumors, and sex cord-stromal tumors.

SEROUS NEOPLASMS

- The 4th edition divided serous carcinoma into low grade (LGSC) and high grade (HGSC) variants.
- LGSC and HGSC are best considered two fundamentally different tumors based on their distinct biology, rather than variants of the same neoplasm.
- Nearly all LGSCs arise in a background of ovarian benign or borderline serous tumors.
- Most HGSCs are believed to arise from a precursor lesion, STIC (serous tubal intraepithelial carcinoma), in the tubal fimbriae.
- New criteria for primary site assignment in

HGSC include:

- Fallopian tube: STIC present, or mucosal HGSC present, or part or all of the fallopian tube is inseparable from tubo-ovarian mass.
- Ovary: both fallopian tubes are separate from ovarian mass, and no STIC or mucosal HGSC present in either fallopian tube.
- Tubo-ovarian: fallopian tubes and ovaries are unavailable for complete examination, and pathologic findings are consistent with extrauterine HGSC.
- Peritoneal (exceedingly rare): both fallopian tubes and ovaries are fully examined using a SEE-FIM (Sectioning and Extensively Examining the FIMbriated end) protocol, and no gross or microscopic evidence of STIC or HGSC present in either fallopian tube or ovary.
- These criteria classify approximately 80% of HGSCs as primary tubal.
- Serous borderline tumor is the sole recommended term:
 - Obsolete terminology no longer recommended includes atypical proliferative serous tumor, serous tumor of low malignant potential, semimalignant serous tumor and non-invasive LGSC / micropapillary serous borderline tumor (the latter no longer considered definitionally synonymous with non-invasive LGSC).

NON-SEROUS EPITHELIAL TUMORS

- The following terminology is no longer recommended:
 - Atypical proliferative tumor or tumor of low malignant potential for all epithelial tumors (mucinous, endometrioid, seromucinous, clear cell, Brenner).

SEROMUCINOUS CARCINOMA

- Previously defined as a carcinoma composed predominantly of serous and endocervical-type mucinous epithelium, often with foci showing clear cells, endometrioid or squamous differentiation.
- Now considered a subtype of endometrioid adenocarcinoma with mucinous differentiation (Fig. 1).

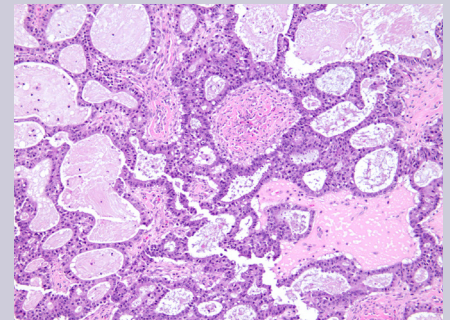


Fig. 1. Endometrioid adenocarcinoma with mucinous differentiation.

NEW VARIANTS OF EPITHELIAL TUMORS

- Mesonephric-like adenocarcinoma:
 - Composed of multiple architectural patterns (tubular, glandular/pseudoendometrioid, ductal, papillary, solid), intraluminal eosinophilic colloid-like material, dense or vesicular chromatin, inconspicuous nucleoli and nuclear crowding, and lacking squamous or mucinous differentiation.
 - Positive for GATA3, TTF1, CD10 (luminal) and PAX8, and negative for hormone receptors and WT1, with wild-type p53 expression.
 - Usually unilateral and diagnosed at stage I in postmenopausal women.

- May arise from paraovarian mesonephric remnants or Müllerian carcinomas displaying secondary mesonephric transdifferentiation.
- May be associated with endometriosis, cystadenomas, adenofibromas, borderline tumors and LGSC.
- The most common molecular alterations include *KRAS* mutations, 1p loss and 1q gain, while *NRAS* or *PIK3CA* mutations are rare.
- Tumors with coexisting serous neoplasms show shared molecular alterations (*KRAS* or *NRAS* mutations).
- Clinical outcome is unknown due to rarity.
- Dedifferentiated carcinoma:
 - A biphasic tumor composed of an undifferentiated carcinoma (sheet-like growth of monotonous, discohesive, round, rhabdoid to spindle cells with brisk mitoses, often necrosis and abundant tumor-infiltrating lymphocytes) and a differentiated (usually low grade endometrioid adenocarcinoma, rarely serous carcinoma) component, often with abrupt interface in between (Fig. 2).
 - Undifferentiated areas are focally positive for EMA, pan-keratin and CK18, focally positive to negative for PAX8, and negative for hormone receptors and E-cadherin, with common loss of *SMARCA4* (*BRG1*), *SMARCA2* (*BRM*), *SMARCB1* (*INI1*) or *ARID1A*, DNA mismatch repair deficiency in one-third of cases and typically wild-type p53 expression.
 - Usually diagnosed at advanced stages, with pelvic and para-aortic lymph node involvement and poor prognosis.

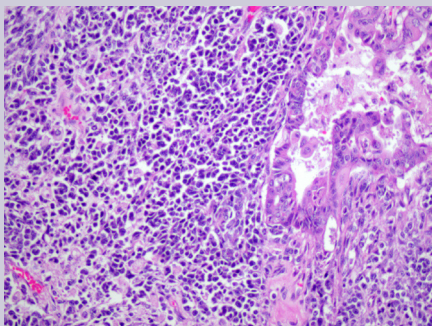


Fig. 2. Dedifferentiated carcinoma composed of undifferentiated carcinoma and low-grade endometrioid adenocarcinoma.

- Carcinosarcoma:
 - A biphasic neoplasm composed of high grade carcinomatous and sarcomatous elements.
 - Now considered a variant of carcinoma rather than a true mixed epithelial-mesenchymal tumor.
- Mixed carcinoma:
 - True mixed carcinomas are uncommon.
 - Should only be diagnosed when at least two tumor types are clearly recognizable on hematoxylin-eosin-stained sections, with distinct morphologic and preferably immunophenotypic differences.

- Each histotype with their percentages should be reported (no minimum percentage requirement).
- Endometriosis-associated histotypes are most common, e.g. endometrioid and clear cell carcinomas (Fig. 3).

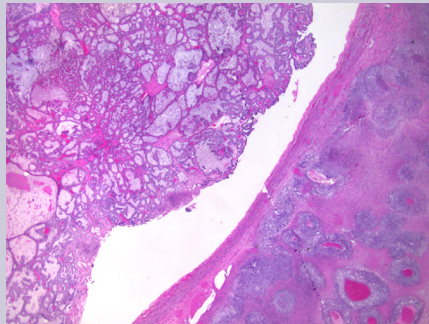


Fig. 3. Mixed carcinoma composed of clear cell carcinoma and endometrioid adenocarcinoma.

ANCILLARY TESTING

- Aberrant p53 expression refers to three immunostaining patterns associated with *TP53* mutation:
 - Overexpression (strong nuclear expression in >80% of tumor cells).
 - Complete absence of nuclear staining (with satisfactory controls).
 - Unequivocal cytoplasmic expression.

SEX CORD-STROMAL TUMORS

- Most (>90%) adult-type granulosa cell tumors (GCTs) exhibit somatic *FOXL2* mutations.
- Sertoli-Leydig cell tumors (SLCTs) may harbor *DICER1* or *FOXL2* mutations and are now classified into three molecular subtypes:
 - *DICER1*-mutant tumors show somatic (~50%) or germline (69%) hotspot mutations in the RNase IIIb domain of *DICER1*, an endoribonuclease involved in microRNA processing and gene expression regulation.
 - Occur in younger patients and induce androgenic symptoms.
 - Moderately or poorly differentiated with retiform or heterologous elements (the latter two predict *DICER1* mutations) (Fig. 4).

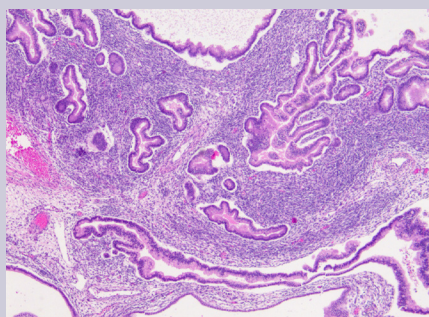


Fig. 4. Moderately differentiated Sertoli-Leydig cell tumor with heterologous elements (intestinal-type glands) and somatic *DICER1* mutation.

- *FOXL2*-mutant tumors show c.402C>G (p.Cys134Trp) mutations that upregulate *CYP19A1* encoding aromatase.
 - Occur in postmenopausal patients and induce estrogenic symptoms.
 - Moderately or poorly differentiated lacking retiform or heterologous elements.
 - Reported in 0-22% of cases.
 - *FOXL2* and *DICER1* mutations are mutually exclusive.
- *DICER1*-*FOXL2* wild-type tumors:
 - Occur in patients with intermediate age.
 - Well-differentiated lacking retiform or heterologous elements.
- Microcystic stromal tumors exhibit *CTNNB1* or, less frequently, *APC* mutations and may represent an extracolonic manifestation of familial adenomatous polyposis.
- Small cell carcinomas of hypercalcemic type exhibit deleterious germline or somatic mutations in *SMARCA4*, part of the SWI/SNF complex, resulting in loss of *SMARCA4* protein expression.
- Gynandroblastoma has been reintroduced (Fig. 5).
 - Defined as a sex cord-stromal tumor with an admixture of female (adult-type or juvenile GCT) and male (Sertoli cell tumor or SLCT) elements.
 - Most commonly composed of a predominant SLCT component and a smaller component of juvenile GCT, both expressing sex cord-stromal markers, sometimes with shared *DICER1* mutations.

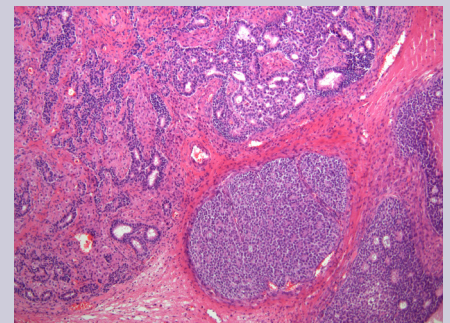


Fig. 5. Gynandroblastoma composed of Sertoli-Leydig cell tumor and adult-type granulosa cell tumor.

Meet the Authors

Dr. Turashvili has been part of the Pathology Outlines editorial board since 2020. She is originally from Georgia and pursued her pathology training in Canada and USA. She is currently affiliated with Mount Sinai Hospital and the University of Toronto as a gynecologic and breast pathologist and Assistant Professor.

Dr. Lastra has been part of the Pathology Outlines editorial board since 2020. He is currently an Associate Professor of pathology at the University of Chicago Medical Center, where he also serves as the gynecologic pathology fellowship program director.

